TYPE 2B VON HIPPEL-LINDAU DISEASE: MOLECULAR BIOLOGY, TUMOR GROWTH, AND DEVELOPMENT

Caroline Martz Lee

A dissertation submitted to the faculty of the University of North Carolina at Chapel Hill in partial fulfillment of the requirements for the degree of Doctor of Philosophy in the Curriculum of Genetics and Molecular Biology.

Chapel Hill
2009

Approved by:

W. Kimryn Rathmell

William Kim

Terry Magnuson

Norman Sharpless

David Threadgill

Terry van Dyke

ABSTRACT

CAROLINE MARTZ LEE: Type 2B von Hippel-Lindau Disease: Molecular Biology, Tumor Growth, and Development
(Under the direction of W. Kimryn Rathmell)

Von Hippel-Lindau (VHL) disease is caused by germline mutations in the *VHL* tumor suppressor gene, with Type 2B missense *VHL* mutations predisposing to renal cell carcinoma, hemangioblastoma, and pheochromocytoma. Type 2B mutant pVHL is predicted to be defective in hypoxia inducible factor (HIF)-α regulation. Interaction analysis in *VHL* –transgenic murine embryonic stem (ES) and renal cell carcionoma-derived cell lines supported previous observations that VHL Type 2B mutations disrupt the interaction between pVHL and Elongin C but maintain partial regulation of HIF-α, most likely via a remnant complex containing ROC1 and Cullin-2 and reduced or absent Elongin C. Murine embryonic stem (ES) cells in which the endogenous wild-type *Vhl* gene was replaced with the representative Type 2B *VHL* hotspot mutation R167Q ($Vhl^{2B/2B}$) likewise displayed preserved physiologic regulation of both HIF factors with slightly more normoxic dysregulation of HIF-2α. Differentiated $Vhl^{2B/2B}$-derived teratomas over-expressed the joint HIF targets *Vegf* and *EglN3* but not the HIF-1α-specific target *Pfk1* and displayed a growth advantage over $Vhl^{-/-}$-derived teratomas, suggestive of a tight connection between perturbations in the degree and ratio of HIF-1α and

HIF-2α stabilization and cell growth. *Vhl*$^{2B/2B}$ mice displayed mid-gestational embryonic lethality, while adult *Vhl*$^{2B/+}$ mice exhibited susceptibility to carcinogen-promoted renal neoplasia compared with wild-type littermates at twelve months. Our experiments support a model in which the representative Type 2B R167Q mutant pVhl retains intermediate HIF-α suppression via formation of a remnant ubiquitin ligase complex, thereby producing a unique profile of HIF-α dysregulation with tissue-specific effects on cell growth, development, and tumor predisposition.

To George Ames, Joseph Brian, and Jon Martin Martz

ACKNOWLEDGEMENTS

This dissertation is the culmination not only of four years' work in graduate school but also of a lifetime of support and encouragement from family, friends, and mentors. First, I thank my parents and sister. Thank you, Mom and Dad, for nurturing my academic interests, for telling me that I could do whatever I wanted to do when I "grew up" and genuinely meaning it, and for leading me in my personal and professional journeys by your excellent examples. Thank you, too, to my sister Brigid. Knowing that you look up to me makes me proud and keeps me honest, and I want you to know that I look up to you not only as a sister and a friend but also as a beautiful young woman.

Next, I thank my own little family. My personal life blossomed during my four years in graduate school: I married my very best friend Jason and gave birth to our first child Carson. Thank you, Jason, for being my closest friend and confidante, a supportive husband, and a loving father. Thank you, Carson, for enriching our lives with joy and laughter and introducing us to the fierce love and commitment only parents can understand.

Thank you to all of my friends but particularly to Yolanda, my fellow M.D./Ph.D. student. I am so lucky to have shared these past six years with you, both bad times and very good times. You are sweet and kind-hearted, and the

value of having such a friend who understands this arduous career path cannot be measured.

Finally, thank you to the Rathmell Lab. In particular, I thank Kim for being an excellent mentor in every sense of the word. Thank you for giving me the confidence to become increasingly independent in my work and my writing, for making the lab an environment conducive to practicing science, and providing me with a real-life example of navigating a clinical and research career with a family at your side. Thank you to my fellow graduate students in the lab, especially Tricia and Rose. Of course, none of the work in this dissertation would have been possible without our hard-working, conscientious laboratory technicians, past and present: Christie, Courtney, Kate, and Leslie.

TABLE OF CONTENTS

LIST OF TABLES

Table

LIST OF FIGURES

Figure

LIST OF ABBREVIATIONS

AMP, adenosine monophosphate

AMPK, adenosine monophosphate kinase

ARNT, aryl hydrocarbon receptor nuclear translocator

aPKC, atypical protein kinase C

ATP, adenosine triphosphate

BHD, Birt-Hogg-Dube

bHLH, basic helix-loop-helix

ccRCC, clear cell renal cell carcinoma

CDC, collecting duct carcinoma

Cdh5, VE (vascular endothelial)-cadherin

CI, confidence interval

CK, casein kinase

CNS, central nervous system

$CoCl_2$, cobalt chloride

COX-2, cyclooxygenase-2

CP, Chuvash Polycythemia

CreER, cre-recombinase oestrogen receptor fusion transgene

CT, computed tomography

CTAD, C-terminal activation domain

CUL2, cullin-2

DOPS, D,L-threo-3,4-dihydroxyphenylserine

dPA, double proline→alanine

E, embryonic day

ECOG, Eastern Cooperative Oncology Group

EglN3, prolyl hydroxylase 3

El B, Elongin B

El C, Elongin C

Eng, endoglin

ENU, N-ethyl-N-nitrosourea

EPO, erythropoietin

ER, endoplasmic reticulum

ES, embryonic stem

FDA, Food and Drug Administration

FH, fumarate hydratase

FIH, factor inhibiting hypoxia inducible factor

FLCN, folliculin

FN, fibronectin

FNIP, folliculin-interacting protein

Glut1, glucose transporter 1

GTP, guanosine triphosphate

HA, hemagglutinin tag

H&E, hematoxylin & eosin stain

HGF/SF, hepatocyte growth factor/scatter factor

HIF, hypoxia inducible factor

HLRCC, hereditary leiomyomatosis and renal cell cancer

HPGL, hereditary paraganglioma syndrome

HPRC, hereditary papillary renal cancer

HR, hazard ratio

HRE, hypoxia-responsive element

IFN, interferon

IFT, intra-flagellar transport

IL-2, interleukin-2

IP, immunoprecipitation

Kdr/Flk-1, Vegf receptor 2

K_m, Michaelis constant

LOH, loss of heterozygosity

lsl, loxP-stop-loxP

MEF, mouse embryonic fibroblast

MET, multiple endocrine tumor

MRI, magnetic resonance imaging

MTOC, microtubule organizing center

mTOR, mammalian target of rapamycin

mTORC, mammalian target of rapamycin complex

MUGA, multigated acquisition scan

MVD, microvascular density

Myc, myc tag

NCAM, neural cell adhesion molecule

NGF, nerve growth factor

Nrp1, neuropilin 1

ODDD, oxygen-dependent degradation domain

OR, overall response

OS, overall survival

PAS, Per Arnt Sims

PCR, polymerase chain reaction

PDGF, platelet-derived growth factor

PDK, pyruvate dehydrogenase kinase

PECAM, platelet/endothelial cell adhesion molecule

PEPCK, phosphoenolpyruvate carboxykinase

Pfk1, phosphofructokinase-1

PFS, progression free survival

PHD, prolyl hydroxylase domain

PI3K, phosphoinositide 3-kinase

PIP, phosphatidylinositol phosphate

PL, placental lactogen

PTEN, phosphatase and tensin homolog

pVHL, von-Hippel Lindau protein

qRT, quantitative reverse transcriptase

RCC, renal cell carcinoma

RDS, respiratory distress syndrome

RECIST, response evaluation criteria in solid tumors

ROC1/Rbx1, regulator of cullins-1 / RING box protein-1

RPTEC, renal proximal tubule epithelial cell

RTK, receptor tyrosine kinase

SABG, senescence-associated β galactosidase

SCF, Skp1/Cul1/F-box complex

SDH, succinate dehydrogenase

TAM, tamoxifen

TNT, *in vitro* transcribed

TSC, tuberous sclerosis protein

VBC, complex of pVHL, Elongin B, and Elongin C

VDU, VHL-interacting deubiquitinating enzyme

VEGF, vascular endothelial growth factor

VHL, von Hippel-Lindau

WT, wild-type

CHAPTER ONE

Introduction

Framing the clinical problem: renal cell carcinoma

An estimated 54,390 new cases of renal cell carcinoma (RCC) were diagnosed in the United States in 2008(1). Alarmingly, the incidence of RCC in the United States has been rising by approximately two percent per year since 1975(2). While the five-year survival for individuals with localized disease at diagnosis approaches 90%, 20-30% of patients present with distant metastases and face a five-year survival of <10%. In 2008, and estimated 13,010 people died from RCC in the United States. RCC is two times more common in men than in women. Other known risk factors for RCC include smoking, overweight and obesity, hypertension, kidney transplant and dialysis, and occupational exposure to organic solvents such as trichloroethylene(1, 3, 4).

RCC is a heterogeneous disease. According to the Heidelberg classification system, RCC can be divided into the following histological subtypes: clear cell (cc) RCC (75%), papillary Type I and Type II (15%), chromophobe (4%), and oncocytoma (benign, 4%) (5, 6)(Figure 1.1). Clear cell RCC tumors are highly vascular and glycolytic and contain cells with abundant

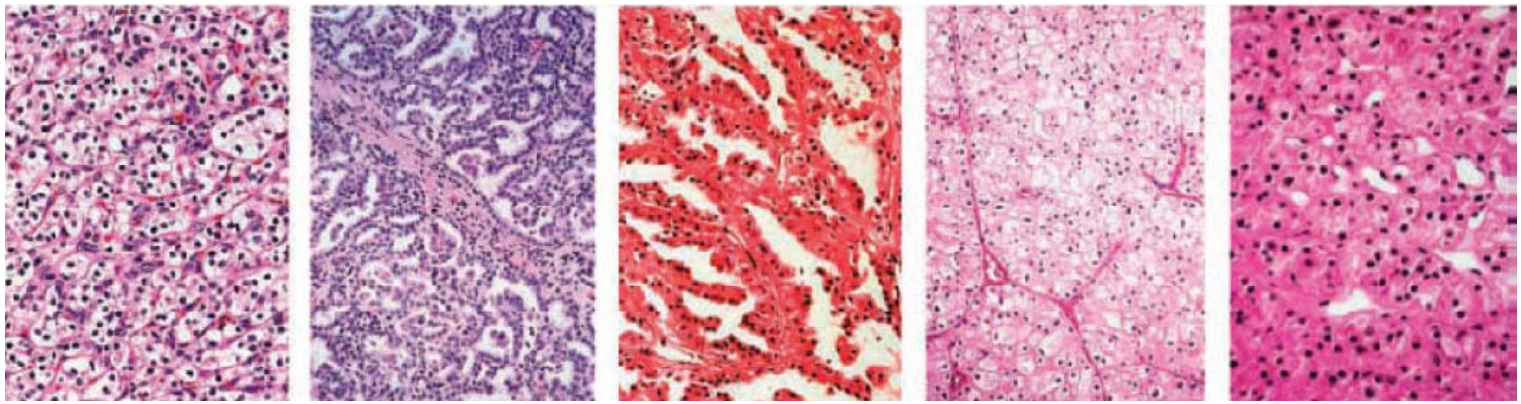

Histology	Clear cell	Papillary, Type 1	Papillary, Type 2	Chromophobe	Oncocytoma
% of total	75-80%	5%	10%	4%	4%
Syndromic	*VHL*	*MET*	*FH*	*BHD*	*BHD*
Sporadic	*VHL* , - 3p	*MET*, + 7, + 17, - Y		- 1, - 2, - 6, - 10, - 13, - 17	

Figure 1.1. Human renal epithelial neoplasms. Representative histological images for each renal cell carcinoma type with corresponding genetic lesions associated with syndromic and sporadic forms. Modified from Linehan WM *et al.* 2003(7).

clear lipid and glycogen-containing cytoplasm. The vast majority of sporadic ccRCC at all tumor stages feature mutation or silencing of the *von Hippel-Lindau* (*VHL*) tumor suppressor gene, loss of the short arm of chromosome 3, or LOH (LOH) at the *VHL* locus, implicating loss of wild-type *VHL* as an early or initiating event in ccRCC(8). Broadly, the architecture of papillary RCC consists of finger-like projections called papillae. The papillae of Type 1 papillary RCC tumors are composed of small, pale cells with small nuclei, while the papillae of Type 2 papillary RCC tumors are composed of large eosinophilc cells with large nuclei, distinct nucleoli, and a pseudostratified appearance. Sporadic Type 1 papillary RCC is strongly associated trisomy 7 and 17 and loss of the Y chromosome in men (9)and more rarely with activating mutations in the *MET* proto-oncogene (7q31-34)(10-12). Chromophobe RCC features sheets of cells with abundant clear, reticulated cytoplasm, irregular nuclei with perinuclear halo, and prominent cell membranes. Sporadic chromophobe RCC tumors tend to have multiple chromosomal losses, typically of chromosomes 1, 2, 6, 10, and 17(13-15). Other types of adult kidney cancer, histologically and/or` mechanistically distinct from renal cell carcinoma, include collecting duct carcinoma, *TFE3* translocation carcinoma, medullary carcinoma, and urothelial carcinoma. The most common pediatric kidney cancer is Wilm's tumor. This dissertation will focus on ccRCC, the histological subtype responsible for the greatest burden of kidney cancer morbidity and mortality in the adult population.

Surgical treatment is the standard-of-care for both local and metastatic RCC (16). RCC is highly resistant to standard chemotherapeutic agents, and

only a handful of drugs have been approved by the Food and Drug Administration (FDA) for the treatment of advanced RCC: the immunomodulatory drug interleukin (IL)-2 (high-dose), the mammalian target of rapamycin (mTOR) inhibitors temsirolimus and everolimus, and the small molecule receptor tyrosine kinase (RTK) inhibitors sorafenib and sunitinib. Sorafenib and sunitinib target multiple RTKs, including vascular endothelial growth factor (VEGF)-receptor and platelet-derived growth factor (PDGF)-receptor families, thought to be expressed on the tumor-supporting cells rather than the tumor cells themselves. Both mTOR inhibitors(17, 18) and RTK inhibitors (19, 20) roughly double progression-free survival (PFS) in highly selected populations but tend to stabilize disease rather than induce remissions and thereby fail to impact overall survival. The relative paucity of effective adjuvant therapies for RCC reflects a need for greater understanding of the molecular mechanisms underlying the initiation and progression of renal tumorigenesis.

The VHL tumor suppressor gene and VHL Disease

The *VHL* tumor suppressor gene (3p25) was isolated in 1993 by positional cloning (21). *VHL* contains three exons and encodes a 24-30 kDa protein $pVHL_{30}$. An internal transcriptional start site in the *VHL* gene also yields $pVHL_{19}$, a shorter 19 kDa isoform with overlapping or identical function (22, 23). Hereafter, "pVHL" will be used when both isoforms are indicated. The VHL protein is ubiquitously expressed in human fetal and adult tissues (24-26).

Germline mutations in *VHL* result in VHL Disease. VHL Disease has an incidence of approximately 1:36,000 live births and is 90% penetrant by age 65

(27, 28). Approximately 20% of VHL Disease kindreds arise from new mutations (29). VHL Disease predisposes to benign and malignant tumors in several, but not all, pVHL-expressing tissues: hemangioblastomas of the retina, brainstem, cerebellum, and spinal cord; tumors of the endolymphatic sac; adrenal gland pheochromocytomas and extra-adrenal paraganglinomas; renal cysts and ccRCC; pancreatic cysts, neuroendocrine tumors and cystadenomas; and cystadenomas of the epididymis (in males) and broad ligament (in females). Retinal and CNS hemangioblastomas, pheochromocytomas, and RCC are responsible for the majority of VHL Disease-associated morbidity and mortality (reviewed in (30)).

Hemangioblastomas are the most common VHL Disease-associated lesion, occurring in 60-80% of VHL Disease patients (31, 32). The mean age at diagnosis is 25 years for retinal (33) and 33 years for craniospinal lesions (32). Hemangioblastomas most commonly develop in the cerebellum and the spinal cord (34). Hemangioblastomas consist of a *VHL*-deficient neoplastic stromal mass associated with an abnormal, dense vascular network (35). Though histologically benign, CNS hemangioblastomas and associated peritumoral edema and cysts cause substantial neurological morbidity by mass effect. Cerebellar hemangioblastomas, for example, may cause gait ataxia, dysmetria, headache, diplopia, and nausea and vomiting, while spinal hemangioblastomas may be associated with segmental hypaesthesia, weakness, and pain, hyper-reflexia, gait ataxia, and incontinence (32). Retinal hemangioblastomas may cause visual disability or blindness. Hemangioblastomas also carry the risk of

bleeding or hemorrhage. Treatment of hemangioblastomas typically consists of surgical excision of the solid component with collapse of any associated cysts and resolution of edema following naturally (36). Clinical trials are underway, however, studying the use of targeted anti-angiogenesis therapy in the neoadjuvant or preventative setting in VHL Disease patients. Longitudinal radiographic studies of natural history suggest that most VHL Disease-associated hemangioblastomas grow in a salutatory manner, with quiescent periods interspersed between intervals of rapid growth (32, 34). Given that VHL Disease patients often develop multiple asynchronous lesions over the course of a lifetime, the decision to treat surgically must balance radiographic evidence of progression and clinical evidence of morbidity against the morbidity associated with multiple surgical procedures.

Pheochromocytomas occur in 10-20% of all VHL Disease patients, with greater penetrance in selected groups (described below), and are malignant in 5% of cases. The median age of onset for pheochromocytoma is 30 years of age (range 5-58 years) (37). Pheochromocytomas arise from chromaffin cells in the adrenal medulla and may secrete epinephrine and/or norepinephrine in a continuous or episodic fashion. Though 1/3rd of VHL Disease patients with pheochromocytoma are asymptomatic, the remaining 2/3rd show signs and symptoms of catecholamine secretion such as palpitations, diaphoresis, and hypertension (37). VHL Disease patients may also present with extra-adrenal pheochromocytomas or paragangliomas, for example in the jugular glomus, carotid body, or periaortic ganglia. Pheochromocytomas are usually treated by

adrenalectomy or enucleation with the goal of preserving adrenal cortical function (38, 39). In the case of disseminated or metastatic pheochromocytoma when surgical excision is not possible, α-adrenergic blocking drugs are used to prevent hypertensive crisis associated with secretion of norepinephrine and/or epinephrine. *VHL* loss is not commonly observed in sporadic pheochromocytomas (40).

Finally, renal cysts and/or ccRCC occur in 60% of VHL Disease individuals (41, 42) and contribute to the bulk of VHL Disease-associated mortality. Renal cysts are thought to be the precursor lesion for most or all ccRCC tumors associated with VHL Disease. Histological examination of grossly normal VHL Disease kidney tissue reveals hundreds of renal cysts and small tumors (43) as well as VHL inactivation in morphologically single cells (44). Statistically, the chance of a single cyst or small tumor out of hundreds progressing to a malignancy is substantial (45). RCC associated with VHL Disease displays clear cell histology and tends to be small and low-grade at the time of diagnosis (43). Surgical management of VHL Disease-associated RCC tends towards nephron-sparing partial nephrectomy in an effort to preserve renal function (46).

Endolymphatic sac tumors are less common (10% of VHL Disease patients) than hemangioblastoms, pheochromocytomas, and ccRCC, but are associated with substantial morbidity (47). Endolymphatic sac tumors uniformly present with partial or complete hearing loss and may additionally be associated with tinnitus and vertigo. Resection of endolymphatic sac tumors is curative and

usually maintains pre-operative hearing capacity but carries a risk of auditory or facial nerve damage.

VHL Disease patients adhere to a strict schedule of radiographic and clinical examinations and laboratory tests in order to identify new and monitor progression of established lesions and to minimize morbidity and mortality (30). Retinal hemangioblastomas and pheochromocytomas have been discovered in children with VHL Disease, so retinal exams are encouraged yearly beginning in infancy and yearly plasma or 24-hour urine catecholamine and metanephrine levels are suggested beginning at age two or with onset of hypertension. Screening for CNS hemangioblastomas begins at age eleven with magnetic resonance imaging (MRI) scan of the craniospinal axis. Finally, radiographic screening for visceral lesions such as pheochromocytoma, renal cysts and RCC, and pancreatic cysts and tumors, begins at age eight with yearly abdominal ultrasounds and at age eighteen with yearly abdominal computed tomography (CT) scans. MRI and CT scans of the auditory canal and audiometric testing are reserved until signs or symptoms of an endolymphatic sac tumor, such as vertigo, tinnitus, or hearing loss, arise. Lesions displaying radiographic evidence of progression and/or associated with clinical signs or symptoms of morbidity prompt more frequent examination.

VHL mutations fall into distinct classes with unique spectrums of clinical disease (48, 49). Type 1 patients (deletion/truncation mutations) have high ccRCC and low pheochromocytoma incidence (50). Type 2 patients (missense mutations) all have high risk of pheochromocytoma, either alone (2C) or in

addition to hemangioblastoma and low (2A) or high (2B) risk of ccRCC (51). Homozygosity for the VHL R200W mutation results in Chuvash Polycythemia, associated with polycythemia and elevated risk for thrombotic events but no increased cancer risk(52-54). This dissertation focuses on the VHL 2B subtype.

VHL protein structure and function

Structure of pVHL and VBC complex. The VHL protein acts as the recognition component of a complex with ubiquitin ligase activity. pVHL consists of an α domain and a β domain. The pVHL α domain consists of three α helices (H1-3, residues 155-192) which coordinate with a fourth α helix from Elongin C to generate an intermolecular four-helix bundle (55). The H1 α helix overlaps with the Elongin C binding domain (residues 157-171) determined empirically in earlier biochemical studies (56, 57). The pVHL α domain interacts directly with Elongin C, which in turn recruits the co-adaptor Elongin B, the scaffolding protein cullin-2 (CUL2) (58, 59), and the RING domain protein RBX1/ROC1(60). The pVHL β domain consists of a seven-strand β sandwich (residues 63-154) and an N-terminal α helix (H4, residues 193-204) (55). The complex of pVHL with Elongins B and C is referred to as the VBC complex.

The VBC complex with CUL2 shares similarities with the yeast Skp1/Cul1/F-box (SCF) complex: Elongin C and CUL2 share sequence identity with Skp1 and Cul1, respectively, and the pVHL α domain shows a similar hydrophobicity profile and structural similarity with F-box protein (55). Analogous to F-box function in yeast SCF, the pVHL β domain targets specific proteins to VBC ubiquitin ligase activity (61, 62). Known and putative targets of pVHL

ubiquitin ligase activity include the hypoxia-inducible factors (HIF)-1α and -2α (63-66), atypical protein kinase C (aPKC) isotypes (67), VHL-interacting deubiquitinating enzymes (VDU)-1 and -2 (68), and two subunits of RNA polymerase II Rpb7(69) and Rpb1(70).

HIF-1α and HIF-2α are the most well-described substrates for pVHL ubiquitin ligase activity. HIF-1α and HIF-2α are basic helix-loop-helix (bHLH) – Per Arnt Sims (PAS) transcription factors. Briefly, under normal oxygen conditions, specific prolyl residues in the oxygen-dependent degradation domain (ODDD) of hypoxia-inducible factor (HIF)-1α and -2α are hydroxylated. The pVHL β domain binds and targets prolyl hydroxylated HIF-α for ubiquitination and degradation by the 26S proteasome. Under hypoxic conditions, the ODDD is not hydroxylated, precluding targeting by pVHL (71-75). Stabilized HIF-α then accumulates, translocates to the nucleus, and heterodimerizes with aryl hydrocarbon receptor nuclear transferase (ARNT)/HIF-1β (76), and binds and activates transcription at consensus hypoxia-responsive elements (HRE, CGTG) (77, 78). HIF-1α and HIF-2α target gene repertoires are overlapping but distinct (79). Joint HIF-1α/HIF-2α targets include VEGF, GLUT-1, EGLN3, and ADM (80-83). The highly evolutionarily conserved HIF-1α uniquely activates such genes as those encoding the glycolytic pathway(83), pyruvate dehydrogenase kinase (PDK) 1 (84), and BNIP-3 (85). Finally, HIF-2α regulates a diverse set of genes, including OCT-4 (86), cyclin D1 (87), TWIST (88), TGFα (89), and EPO (90).

Non-ubiquitin ligase activities. Known non-ubiquitin ligase activities of pVHL include promotion of cellular senescence (91), assembly and maintenance

of cytoskeletal components (92, 93) and proper deposition of extracellular matrix proteins (94, 95). Acute inactivation of *Vhl* in mouse embryonic fibroblasts (MEF) results in persistant growth arrest and features of senescence, including flattened morphology, expression of senescence-associated β galactosidase (SABG), and formation of heterochromatic foci. Surprisingly, senescence in *Vhl*-deficient MEFs is independent of HIF and p53 and but dependent on activated (hypophosphorylated) Rb. *Vhl* loss in MEFs results in post-transcriptional reduction in the chromatin remodeling factor p400, directly or indirectly promoting post-transcriptional reduction in Skp2, the ubiquitin ligase for the cyclin-dependent kinase inhibitor p27Kip1. Stabilized p27Kip1 then activates Rb. Activated Rb is both necessary and sufficient for senescence in *Vhl*-deficient MEFs. Acute somatic inactivation of *Vhl* in the mouse is also associated with SABG-positivity and p27 stabilization in the kidney, providing a possible mechanistic explanation for the refractoriness of the murine kidney to renal tumorigenesis. Relevance of this function of VHL in human disease is uncertain, as VHL loss in human cell lines reduces proliferation but does not cause senescence or stabilize p27 (91), and p400-mediated senescence in human cells is p53-dependent and Rb-independent (96).

The VHL protein regulates the deposition of extra-cellular matrix via direct interactions with fibronectin(95), an integrin-binding protein, and collegen IV(97, 98). The direct interaction of pVHL with fibronectin requires conjugation of NEDD8 to K159 (95), a modification that simultaneously hinders pVHL association with CUL2 (99). pVHL-FN associates with the membrane fraction,

most likely with the endoplasmic reticulum (ER) and Golgi. The VHL-fibronectin interaction is required for the secretion and deposition of fibronectin in extracellular fibrillar arrays (95). The VHL protein also directly interacts with a component of collegen IV, specifically hydroxylated collagen IVa2(97, 98). Hydroxylated collagen IVa2 binds the pVHL β domain via one of its HIF-α hydroxylprolyl binding pockets in a presumably mutually exclusive interaction (98). VHL protein is required for deposition of a collagen IV matrix in the basement membrane both *in vitro* in cell culture and in xenografts. All Type 1, 2A, 2B, and 2C VHL mutants tested thus far are defective for fibronectin deposition (51, 95, 100), while the Type 2C but not 1, 2A, or 2B VHL mutants tested retain a small degree of collagen IVa2 capture (97).

Finally, pVHL binds cytoplasmic microtubules and, in a tightly related function, contributes to the maintenance of the primary cilium. VHL_{30} but not VHL_{19} binds directly to microtubules, partitioning to the cytoplasm at the microtubule organizing center (MTOC) and at the cell periphery. VHL protects microtubules from depolymerization by nocodozole(93) and additionally appears to control or assist in proper microtubule orientation. In *VHL* wild-type cells, microtubules orient towards the cell periphery, while microtubule orientation is haphazard in *VHL*-deficient cells(101).

The primary cilium is a single organelle extending from the apical cell membrane (reviewed in (102, 103)). The structure of the primary cilium consists of microtubules in a 9 + 0 arrangement arising from the centriole, variously known as the basal body or as the MTOC during mitosis. The general function of

the primary cilium is to interpret sensory information such as air or fluid flow and to transduce extracellular signals. The VHL protein is dispensible for the initial formation of the primary cilium but contributes, along with GSK3β, to its maintenance(104). In conditions under which GSK3β is active, GSK3β phosphorylates pVHL on a specific serine residue, rendering pVHL capable of binding but not stabilizing microtubules(105), and independently maintains the integrity of the primary cilium (104). When GSK3β is inactive or deficient, for example due to growth factor signaling, primary cilium maintenance falls to pVHL. VHL mutants that fail to bind cytoplasmic microtubules are likewise deficient in primary cilium maintenance (104). The role of the primary cilium in renal cyst formation will be discussed in more detail below.

In Vitro Models of VHL Disease

The distinct genotype-phenotype correlations of VHL disease suggest that disruption of wild-type or introduction of novel pVHL functions contribute to VHL Disease tissue specificity. *In vitro* transgenic models of VHL Disease in both RCC-derived and murine embryonic stem (ES) cell lines show disconnection between Elongin C and HIF-α binding and RCC predisposition. *VHL*-null RCC and ES cells cannot target HIF-α for degradation, resulting in abnormal normoxic accumulation of HIF-α and its target gene products. Complementation with wild-type *VHL* restores HIF-α regulation in these models. Complementation of RCC cells with 2A and 2B *VHL* mutants results in impaired HIF-α binding, while 2B *VHL* mutants additionally fail to recruit Elongin C (51, 106). In xenograft assays using RCC cells, *VHL*-null cells enhance tumor growth, while wild-type *VHL* and

all mutants except 2A suppress tumor growth. In ES cell teratoma assays, however, *Vhl*-null cells display suppressed growth compared to wild-type *VHL*-expressing cells. While type 2B *VHL* expression restores wild-type growth, 2A mutants retain the growth-suppressive phenotype (106, 107). Combined with recent evidence that HIF-2α can act as a tumor suppressor (108), the teratoma data weakens the assumption of a direct relationship between HIF dysregulation and RCC predisposition. Pheochromocytoma predisposition also appears to be HIF-independent, instead related to impaired c-Jun-dependent developmental culling of sympathetic neuronal precursors in response to nerve growth factor (NGF) withdrawal (109).

In Vivo Models of VHL Disease

Genetically engineered mouse models of human cancer are useful for understanding cancer biology and preclinical development and testing of therapeutic drugs. The majority of models of human VHL Disease currently in existence utilize null and conditional *Vhl* alleles, often in combination with tissue-specific promoter-driven and inducible cre recombinase activity. Though such conditional models of *Vhl* loss circumvent the mid-gestational lethality associated with germline nullizygosity for *Vhl* (110, 111), they assume a specific cell type of origin and/or temporal window of susceptibility to tumor initiation. Use of a null or conditional null allele of *Vhl* also fails to capture and take advantage of the strict genotype-phenotype correlations observed in VHL Disease and ideal for separating and defining *Vhl* functions. To that end, an endogenous gene replacement model of Chuvash Polycythemia has been generated recently which

recapitulates the human disease(112). The developmental and tumor predisposition phenotypes of germline and mosaic knock-out models of *Vhl* and pertinent *HIF* axis members will be discussed first, followed by tissue-specific *Vhl* models with or without *HIF* rescue (summarized in Table 1.1).

Germline and mosaic loss of murine Vhl. Three independent mouse lines utilizing null or conditional null alleles of *Vhl* have been developed and characterized. In 1997, Gnarra *et al*. published the first mouse model of VHL Disease(110). Mice heterozygous for a null *Vhl* allele ($Vhl^{+/-}$) were generated in a mixed C57BL/6 genetic background. $Vhl^{+/-}$ mice were aged to 15 months and did not display evidence of neoplasia. Inter-heterozygous matings revealed a 2:1 ratio of $Vhl^{+/-}$ to $Vhl^{+/+}$ mice and an absence of live-born $Vhl^{-/-}$ progeny, and timed mating analysis pinpointed the window of embryonic demise to embryonic day (E) 10.5-12.5. Because mouse embryos transfer dependency from the yolk sac to the placenta around E9.5-10.5 and $Vhl^{-/-}$ embryos were grossly and morphologically normal until E10.5, the time point of $Vhl^{-/-}$ embryonic demise was suggestive of placental failure.

The murine placenta consists of three layers: the labyrinth, spongiotrophoblast, and maternal decidua (reviewed in (113, 114)). The labrythine layer consists of highly branched embryonic-origin allantoic vessels surrounded by sheets of chorionic trophectoderm-origin syncitiotrophoblasts and bathed in maternal blood. The labyrinthine layer provides a vital transport function, providing oxygen and nutrients across the thin syncitiotrophoblast layer

Table 1.1. Mouse models of von Hippel-Lindau Disease

References	*Vhl* allele	Cre	Tissue (cell type)	Mouse strain	Phenotype
Gnarra *et al*.	Null	-		C57BL/6	$Vhl^{-/-}$: embryonic lethality at E10.5-12.5. Normal embryo. Absence of embryonic vessels in placental labyrinth at E10.5. $Vhl^{+/-}$: no evidence of disease by age 15 months.
Haase *et al*.	Floxed (f), Deleted (d)	-	-	Balb/c	$Vhl^{d/d}$: embryonic lethality at E9-11. $Vhl^{d/+}$: hepatic angiomas (90% at 12-17 months), rare renal cysts (3%). Normal serum Epo and red blood cell count.
and Rankin *et al*. MCB		Albumin-cre	Liver (hepatocytes)		*Albumin*-cre;$Vhl^{f/f}$: hepatomegaly and runting. Small hepatic angiomas and hepatic steatosis. Elevated serum Epo with erythrocytosis. Death at 6-12 weeks. Genetic rescue by $Arnt^{-/-}$ but not $Hif1a^{-/-}$.
Ma *et al*.	Floxed (f), Deleted (d)	β-actin-cre	Mosaic	C57BL/6	*β-actin-cre*;$Vhl^{f/d}$: hepatic angiomas (100%, 4-12 months), renal angiectasis, male infertility. $Vhl^{d/f}$: hepatic angiomas (18% at 12 months). $Vhl^{d/+}$: hepatic angiomas (88% at 18 months). $Vhl^{d/+}$: hepatic angiomas (67% at 18 months).
Kleymenova *et al*.	Null (Gnarra *et al*.)	-		C57BL/6	Untreated $Vhl^{+/-}$: hepatic angiomas (23% at 14-18 months). $Vhl^{+/-}$ + streptozotocin: enhanced hepatic angiomas (33-46%) relative to treated $Vhl^{+/+}$ (7-15%) at 14-15 months.

References	*Vhl* allele	Cre	Tissue (cell type)	Mouse strain	Phenotype
Hong *et al*.	Floxed (f), Deleted (d) (Ma *et al*.)	CreER^{TM}	Mosaic	C57BL/6	*CreER^{TM};Vhl$^{d/f}$* + TAM at E10.5: embryonic lethality at E13.5-15.5. Dilated and leaky embryonic blood vessels and focal liver necrosis. Placenta normal at E14.5. Decreased placental labyrinth thickness with dilated labyrinthine blood vessels at E16.5.
Rankin *et al*. Cancer Res	Floxed (f) (Haase *et al*.)	PEPCK-cre	Kidney (PT) and liver (periportal hepatocytes)	Balb/c	*PEPCK-cre*;*Vhl$^{f/f}$*: macroscopic (18%) and microscopic glomerular (35%) and tubular (25%) renal cysts at 12-25 months. Tubular microcysts: confirmed *Vhl* loss, positive for markers of dedifferentiation (35% of cysts) and distal tubule (>50% of cysts) but not proximal tubule markers. Genetic rescue by *Arnt$^{-/-}$* but not *Hif1a$^{-/-}$*.
Rankin *et al*. Oncogene and MCB					*PEPCK-cre;Vhl$^{f/f}$*: hepatic angiomas (35%) and microscopic vascular lesions (80%) at > 6 months. Genetic rescue by *Arnt$^{-/-}$* and *Hif2a$^{-/-}$* but not *Hif1a$^{-/-}$*.
Tang *et al*.	Floxed (f) (Haase *et al*.)	Tie2-cre	Endothelial cells	Balb/c	*Tie2-cre*;*Vhl$^{f/f}$*: embryonic lethality at E12.5-13.5. Embryonic hemorrhage at E12.5. Yolk sac and embryonic vessel dilation and decreased branching and networking associated with decreased fibronectin deposition. Placental labyrinth thickness decreased and lacking fetal blood spaces. No genetic rescue with *Hif1a$^{-/-}$*.
		Mox2-cre	Embryonic lineages		*Mox2-cre*;*Vhl$^{f/f}$*: embryonic lethality at E12.5 with identical embryonic hemorrhage phenotype observed in *Tie2-cre*;*Vhl$^{f/f}$*. No genetic rescue with *Hif1a$^{-/-}$*.

References	*Vhl* allele	Cre	Tissue (cell type)	Mouse strain	Phenotype
Frew *et al*. EMBO	Floxed (f) (Haase *et al*.)	Ksp1.3-cre	Kidney (DT, LH, and CD)	Balb/c	*Ksp1.3-cre*;$Vhl^{f/f}$: hydronephrosis (100%). No renal cysts. *Ksp1.3-cre*;$Pten^{f/f}$: uroepithelial hyperplasia and hypertrophy in renal pelvis, ureter, and bladder. *Ksp1.3-cre*;$Vhl^{f/f}$;$Pten^{f/f}$: hydronephrosis and enhanced uroepithelial proliferation. Renal cysts (100%, 6 weeks – 6 months). Renal cysts positive for distal tubule and collecting duct but not proximal tubule markers.
Hickey *et al.*	R200W (CP) Gene replacement	-		C57BL/6	$Vhl^{CP/CP}$: Slightly reduced viability. Age-dependent increase in hematocrit, red blood cell count, and hemoglobin. Elevated serum and kidney but not liver Epo. Normal bone marrow architecture. Splenomegaly with expansion of red pulp and increased megakaryocyte population. Increased microvascular density in skin and liver.

to and fetal waste away from the fetal circulation. The labyrinth is supported by spongiotrophoblast cells, derived from the trophectoderm of the ectoplacental cone, and is separated from the maternal decidual uterine tissue by a layer of polyploid trophoblast giant cells. The murine placenta derives from the trophectoderm layer of the inner cell mass and the extra-embryonic mesoderm (allantois). At E8.5, the embryonic allantois fuses with the chorionic plate in a process called chorioallantoic attachment. After attachment, from E8.5-10.5, the chorionic plate folds into villi as the allantoic vessels migrate into the inter-villous spaces. In a mutual induction process, the allantoic vessels and chorionic plate villi undergo branching morphogenesis to form the maze-like labyrinth, and the chorionic trophoblasts adjacent to fetal blood vessels differentiate into syncitiotrophoblasts. The murine placental labyrinth is analogous in structure and function to human chorionic villi.

Vhl$^{-/-}$ placentas developed normally until E9.5, exhibiting proper chorioallantoic fusion and morphologically normal chorionic trophoblasts. At E10.5, however, no allantoic vessels had penetrated the chorionic plate, maintaining complete separation of maternal and fetal circulation. Between 11.5-12.5, *Vhl*$^{-/-}$ placental labyrinths became hemorrhagic and embryos became necrotic. Immunohistochemical studies demonstrated that wild-type placentas expressed pVhl in both extra-embryonic (labyrinthine trophoblasts and allantoic mesoderm) and embryonic (endothelial) tissues.

Several years later, the Gnarra *Vhl*$^{+/-}$ mouse line was used by another research group in mutagenesis studies(115). *Vhl*$^{+/-}$ and control *Vhl*$^{+/+}$ mice

received intraperitoneal (i.p.) injection of the renal mutagen streptozotocin (50, 100, 150, or 200 mg/kg) at 8 weeks of age. Streptozotocin induced renal cyst formation equally well in *Vhl*$^{+/-}$ and *Vhl*$^{+/+}$ mutagenized mice at 14-15 months. Interestingly, approximately 20% of untreated *Vhl*$^{+/-}$ mice aged 14-17 months developed hepatic angiomas, vascular liver tumors uncommon in human VHL Disease and not observed in the original study of this mouse line. Streptozotocin significantly enhanced hepatic angioma formation in *Vhl*$^{+/-}$ mice relative to untreated *Vhl+/-* mice and mutagenized *Vhl*$^{+/+}$ controls, increasing penetrance from ~20% to 33% at 150 mg/kg and 46% at 200 mg/kg at 14-15 months.

In 2001, Haase *et al*. published a second mouse model of VHL Disease utilizing a *Vhl* allele flanked by loxP sites (floxed, f) and the corresponding recombined *Vhl*-deleted (d) allele in a mixed Balb/c background(111). *Vhl*$^{d/d}$ embryos died at E9-11 with a placental phenotype identical to that observed in the Gnarra *et al*. *Vhl*$^{-/-}$ model. In a significant departure from the original Gnarra *et al. Vhl*$^{+/-}$ model, *Vhl*$^{d/+}$ mice developed hepatic angiomas in an age-dependent fashion. Approximately 50% of *Vhl*$^{d/+}$ mice aged to 3-11 months and more than 90% of *Vhl*$^{d/+}$ mice aged 12-17 months developed large hepatic vascular cavities associated with steatosis and small vessel proliferation. Only 1/30 *Vhl*$^{d/+}$ mice developed a renal microcyst (3%), the presumptive precursor lesion to RCC, and none developed pheochromocytoma.

Ma *et al*. independently derived a third VHL Disease mouse model utilizing floxed or deleted *Vhl* on a C57BL/6 background alone or in combination with mosaic promoter-driven cre recombinase (116) and with tamoxifen-inducible cre

recombinase (117). In an effort to circumvent embryonic lethality and mimic stochastic loss of heterozygosity (LOH) in VHL Disease patients, Ma *et al.* first characterized the floxed *Vhl* allele using a human β-actin- cre transgenic mouse line(116). The particular β-actin-cre mouse line used was chosen for its stochastic expression in early embryonic development, resulting in mosaic *Vhl* LOH in adult tissues, and minimal expression in placental tissues. β-actin-cre;$Vhl^{f/d}$ mice were viable and developed hepatic angiomas with complete penetrance at time points ranging from 4-12 months. β-actin-cre;$Vhl^{f/d}$ mice also developed renal, pancreatic, and hepatic angiectasis (enlarged blood vessels) and male infertility due to defective spermatogenesis. In light of the large variation in hepatic angioma penetrance between the Gnarra *et al.* $Vhl^{+/-}$ (C57BL/6, 0-20% at 15 months) mouse line and the Haase *et al.* $Vhl^{d/+}$ (Balb/c, >90% at 12-17 months), Ma *et al*. also back-crossed the *Vhl*-deleted allele to two additional genetic backgrounds. $Vhl^{f/d}$ mice on the original mixed C57BL/6 background displayed 18% penetrance of hepatic angiomas at 12 months, while hepatic angiomas were 88% penetrant in $Vhl^{d/+}$ mice on Balb/c and 67% penetrant in $Vhl^{d/+}$ mice on A/J at 18 months.

Hong *et al*. used a tamoxifen-inducible cre recombinase-oestrogen receptor fusion receptor fusion transgene (CreER^{TM}) system as a second approach to circumvent embryonic lethality in the Ma *Vhl* model (117). CreER is sequestered and inactive in the absence of estrogens. Ingestion of tamoxifen (TAM) by mature animals with subsequent binding of TAM to CreER results in nuclear translocation and functional activation of cre recombinase to mediate

recombination between loxP sites in affected cells. CreER^{TM};*Vhl*$^{d/+}$ mice were crossed to *Vhl*$^{f/f}$ mice, and pregnant dams were injected with 2-4 mg TAM at E10.5. Acute *Vhl* loss at E10.5 delayed embryonic lethality until E13.5-15.5. CreER^{TM};*Vhl*$^{d/f}$ + TAM embryos during this window displayed gross dorsolateral hemorrhage and body necrosis, associated with dilated, leaky vessels and focal liver necrosis on histological examination. The CreER^{TM};*Vhl*$^{d/f}$ + TAM placentas were morphologically normal at E14.5 but displayed a mild decrease in labyrinthine layer thickness with dilated blood vessels and mislocalized spongiotrophoblast cells at E16.5, suggestive of a greatly reduced or delayed placental phenotype.

Altogether, *Vhl* null and mosaic null mouse models exhibit a requirement for murine placental and embryonic development in mid-gestation and a predisposition to hepatic angioma but not renal cysts or RCC.

Germline loss of hypoxia-inducible factor and related genes. In 1998, Iyer *et al*. published a mouse model utilizing a null allele for *Hif1a* (118). Nullizygosity for *Hif1a* conferred embryonic lethality at E10-11 on both C57BL/6 and 129 genetic backgrounds. *Hif1a*$^{-/-}$ lethality was preceded by developmental arrest (reduced somite number) at E8 and morphological changes at E9. E9 *Hif1a*$^{-/-}$ embryos displayed neural tube defects associated with replacement of cephalic mesenchyme by dilated vessels; abnormal vasculature including the branchial arch, dorsal aorta, and intersomitic vessels; and myocardial hyperplasia with pericardial effusion.

Three independent models of *Hif2a* loss were developed with drastically different phenotypes (81, 119, 120). The *Hif2a* knock-out model developed by Tian *et al.* exhibited embryonic lethality at E12.5-16.5 (120). *Hif2a*$^{-/-}$ embryos did not display vascular defects and possessed a histologically normal placenta, suggestive of a physiological cause of lethality. *Hif2a*$^{-/-}$ mice were determined to have bradycardia and low norepinephrine levels, postulated to result from a requirement for *Hif2a* in catecholamine biosynthesis in adrenal chromaffin cells. Embryonic lethality was partially rescued by treating pregnant dams with D,L-threo-3,4-dihydroxyphenylserine (DOPS), which could be directly converted to norepinephrine by decarboxylase activity *in utero*. Surviving *Hif2a*$^{-/-}$ mice died within 24 hours.

Hif2a$^{-/-}$ mice developed by Peng *et al*. displayed vascular defects with variable penetrance(119). One third of *Hif2a*$^{-/-}$ mice on an outbred 129Sv/ICR background were viable for several weeks, while the remaining two thirds displayed embryonic lethality at E9.5-13.5. Death *in utero* was associated with subtle defects in vascular remodeling especially apparent in the yolk sac and only rarely observed in the embryo and variably associated with embryonic hemorrhage. *Hif2a*$^{-/-}$ embryonic lethality was partially rescued by DOPS treatment, with rescued animals surviving for less than 24 hours, suggesting that reduced catecholamine biosynthesis featured in embryonic demise. *Hif2a*$^{-/-}$ mice on a congenic 129Sv background uniformly displayed embryonic lethality at E9.5-12.5, associated with defective vascular remodeling in both the yolk sac and the embryo proper.

In a third model by Compernolle *et al.*, 50% of *Hif2a*$^{-/-}$ mice on a mixed 129Sv/Swiss genetic background died at E13.5 due to cardiac failure, while the remaining 50% died two-three hours post-natally (81). Post-natal death was due to respiratory distress syndrome (RDS) due to a maturation defect in the surfactant-producing Type II pneumocytes. The lungs of surviving *Hif2a*$^{-/-}$ neonates also subtle vascular defects. Neither embryonic nor post-natal lethality was rescued by DOPS treatment *in utero*.

Two independent models of *Arnt* loss have also been developed and characterized (121-124). *Arnt* is the heterodimerization partner for HIF-α subunits and is required for HIF-α transcriptional activity. *Arnt*$^{-/-}$ mice on a mixed 129SvJ/C57BL/6 background display embryonic lethality at E9.5-10.5 (124). At E9.5-10.5, *Arnt*$^{-/-}$ yolk sacs were essentially avascular but embryonic vasculaturization was normal except for a mild defect in capillary formation in solid organs(124). Preceding embryonic lethality at E8.5, the *Arnt*$^{-/-}$ placenta contained all the proper cell lineages, including 4311-positive spongiotrophoblast cells and placental lactogen (PL)-1-positive trophoblast giant cells and an unidentified population of double-positive cells, but were slightly smaller than wild-type and *Arnt*$^{+/-}$ placentas. The E9.5 *Arnt*$^{-/-}$ placenta displayed an absence of fetal vessels in the labyrinth and evidence of shallow invasion of the maternal myometrium. Histologically, E9.5 *Arnt*$^{-/-}$ placentas contained very few 4311-positive spongiotrophoblasts and an expanded population of PL-1-positive trophoblast giant cells (121).

In order to determine whether the observed placental defect was embryonic or trophoblastic in origin, diploid *Arnt*$^{-/-}$ ES cells were aggregated with tetraploid wild-type morulas in a technique referred to as tetraploid aggregation(121). Tetraploid cell contribution is limited to the extra-embryonic lineages, resulting in an *Arnt*$^{-/-}$ embryo with a wild-type placenta (excluding the contribution of *Arnt*$^{-/-}$ embryonic-origin allantoic vessels to the labyrinth). Tetraploid aggregation slightly delayed embryonic lethality until E10.6 and rescued the placental defects, demonstrating that the defects in labyrinthine vascularization and altered trophoblast differentiation resulted from *Arnt* deficiency in the trophoblast lineage. Rescued embryos at E10.6 displayed severe cardiac hypoplasia, possibly the causative lesion for the absence of yolk sac vascularization(121).

In order to determine the relative contributions of *Hif1a* and *Hif2a* loss of function in *Arnt* models, Cowden *et al.* compared *Arnt*$^{-/-}$ development to *Hif1a* and *Hif2a* placental development singly and in combination(122). In their hands, 30% of E9.5 *Hif1a*$^{-/-}$ placentas failed chorio-allantoic attachment, while the remaining 70% fused properly but allantoic vessels failed to migrate into the chorionic plate. E9.5 *Hif1a*$^{-/-}$ labyrinths showed a 50% reduction in Tpbp-positive spongiotrophoblast cells but a normal number of PL-1-positive trophoblast giant cells. *Hif2a*$^{-/-}$ placentas at E9.5 displayed normal chorioallantoic fusions, allantoic vascularization of the chorionic plate, and spongiotrophoblast and giant cell populations. Double *Hif1a*$^{-/-}$*;Hif2a*$^{-/-}$ mutant placentas at E9.5 were identical to *Arnt*$^{-/-}$ placentas at E9.5, displaying complete failure of chorioallantoic

attachment, no vascular invasion of the chorion, an absence of spongiotrophoblast cells, and an expanded population of trophoblast giant cells. Indicating that HIF dosage is critical in placental development, *Hif1a*$^{-/-}$ in conjunction with heterozygosity for *Hif2a* loss resulted in a placental phenotype nearly as severe as the *Arnt*$^{-/-}$ phenotype.

Kozak *et al.* published a second independent mouse model of *Arnt* deficiency using a similar targeting strategy (replacement of the sequence encoding the Arnt bHLH domain) and a nominally similar genetic background (mixed 129SvJ/C57BL/6) to the mice derived by Maltepe *et al*. but with a more severe embryonic and less severe placental phenotypic outcome. Nullizygosity for *Arnt* conferred embryonic lethality at E9.5-10.5 (123). E9.5 *Arnt*$^{-/-}$ embryos were slightly growth-retarded. E10.5 *Arnt*$^{-/-}$ embryos were clearly developmentally delayed as evidenced by reduced somite number and were afflicted with neural tube defects and forebrain hypoplasia. E10.5 *Arnt*$^{-/-}$ embryos were associated with normal yolk sacs. The corresponding E10.5 *Arnt*$^{-/-}$ placentas were hemorrhagic and displayed reduced labyrinthine vascularization but uniformly succeeded in chorioallantoic fusion.

The preceding mouse models of *Hif1a*, *Hif2a*, and *Arnt* deficiency demonstrate a broad requirement for HIF-α activity in the murine placental trophoblast lineage as well as in development of the embryonic cardiovascular, nervous, and respiratory systems. The lack of embryonic models of constitutively stabilized *Hif1a* and *Hif2a* prevents direct analysis of the impact of over- or mis-expression of HIF-α on murine development. Takeda *et al.*, however, developed

mouse models of *proly hydroxlase domain* (*Phd*) *1*, *2*, and *3* deficiency (125). Phd proteins hydroxylate specific prolyl residues on the HIF-α ODD (71, 72, 74, 126-130), thereby targeting HIF-α to the pVhl β domain for ubiquitylation and proteasome mediated degradation (73, 75). Given that the embryo and placenta are hypoxic environments during development and that Phd activity is limited to normal oxygen conditions *in vitro* (127, 131), the impact of *Phd* deficiency, if any, on HIF stability and/or development was difficult to predict.

Indeed, *Phd1*$^{-/-}$ and *Phd3*$^{-/-}$ mice were viable and displayed no embryonic or placental defects. *Phd2*$^{-/-}$ mice died *in utero* between E12.5-14.5 due to cardiac failure(125). *Phd2*$^{-/-}$ yolk sacs and embryos displayed no gross defects in vessel patterning, but *Phd2*$^{-/-}$ embryos did display defective ventricular maturation by E11.5. *Phd2*$^{-/-}$ placentas appeared normal at E9.5 but showed reduced chorionic villus folding and with an equivalent reduction in fetal blood vessel content in the presumptive labyrinth at E12.5, suggestive of defective trophoblastic branching morphogenesis. E12.5 *Phd2*$^{-/-}$ placentas also contained an abnormal distribution of trophoblast giant cells and spongiotrophoblast cells. *Phd2*$^{-/-}$ embryos and placentas both demonstrated HIF-1α and HIF-2α stabilization relative to wild-type and *Phd2*$^{+/-}$, confirming that Phd2 does have activity towards HIF-α in these tissues but neither proving HIF-dependent nor ruling out HIF-independent components of the *Phd2*-null phenotype.

Tissue-specific and combinatorial mouse models of VHL Disease. As discussed above, *Vhl*-null germline and mosaic models are characterized by defects in placental vascularization, age- and genetic background-dependent

hepatic angiomas, and a lack of renal cysts and RCC. Tissue-specific promoter-driven cre recombinase systems have been used variously to determine cell type of origin, dependence on HIF-α, and to enhance or reveal VHL Disease-associated phenotypes.

Cell-of-origin for Vhl-dependent placental labyrinth phenotype. The requirement for *Vhl* in the embryonic vasculature was investigated using a *Tie2-cre* transgenic mouse line directing recombination in endothelial cells(132). *Tie2-cre;Vhl*$^{f/f}$ and *Tie2-cre;Vhl*$^{f/f}$*;Hif1a*$^{f/f}$ died *in utero* at E12.5-13.5, slightly later than germline *Vhl*-null mice but with an identical defect in labyrinthine vascularization. Use of a *Mox2-cre* transgenic mouse line, in which recombination is completely excluded from extra-embryonic and trophoblast lineages, recapitulated the *Tie2-cre* results, indicating that the requirement for *Vhl* in labyrinthine vascularization resides in the embryonic allantoic endothelium rather than the trophoblast compartment. In addition to placental defects, *Tie2-cre;Vhl*$^{f/f}$ and *Tie2-cre;Vhl*$^{f/f}$*;Hif1a*$^{f/f}$ embryos were associated with several other vascular defects, including gross embryonic hemorrhage, collapse of endocardial vessels, and dilation and decreased branching and network complexity in the yolk sac and cephalic and dorsal regions of the embryo.

Cell-of-origin and HIF-dependence of Vhl hepatic angiomas. Given that VHL Disease-associated hemangioblastomas arise secondary to *VHL* LOH in the stromal compartment (35), *Vhl*-associated hepatic angiomas were postulated to originate from hepatocytes. Two groups analyzed the repercussions of *Vhl* loss in the hepatocyte compartment using an albumin-cre transgenic mouse line in

which directs high-efficiency (60-80%), hepatocyte-specific recombination(111, 133). Both groups observed that *Albumin-cre;Vhl*$^{f/f}$ mice were runted and died at 6-12 weeks with gross hepatomegaly and severe hepatic steatosis, angiectasis or microscopic angiomas, and endothelial cell proliferation(111, 133). *Albumin-cre;Vhl*$^{f/f}$*;Hif1a*$^{f/f}$ mice developed an identical phenotype, but the livers of *Albumin-cre;Vhl*$^{f/f}$*;Arnt*$^{f/f}$ mice were grossly and microscopically normal(133).

In a complementary approach, Rankin *et al*. utilized a *PEPCK-cre* transgenic mouse line activity in the kidney and periportal hepatocytes (20-30% efficiency)(134). In contrast to *Albumin-cre;Vhl*$^{f/f}$ mice, *PEPCK-cre;Vhl*$^{f/f}$ mice survived past 15 months and developed high penetrance macroscopic or cavernous hemangiomas (35%) and microscopic heptic angiectasis, steatosis, and endothelial cell proliferation (80%) at age six months or older. *PEPCK-cre;Vhl*$^{f/f}$*;Hif1a*$^{f/f}$ mice developed identical macroscopic and microscopic hepatic vascular lesions with similar penetrance(133, 134). Furthermore, both *Arnt* (133) and *Hif2a* (134) knock-out rescued the hepatocytic *Vhl*-dependent hepatic angioma phenotype, confirming that the hepatic angioma phenotype observed in germline and mosaic *Vhl*-null animals arises from *Vhl* loss in the hepatocyte compartment and is dependent on HIF-2α.

A third approach solidified the connection between hepatocytic HIF-2α stabilization and hepatic angioma formation. Kim *et al*. studied the effects of stabilized HIF-1α and/or HIF-2α in hepatocytes using Albumin-cre and conditional loxP-stop-loxP (lsl) *HIF-α double proline→alanine* (*dPA*) mutants alleles knocked-in to the ubiquitously-expressed *Rosa26* locus (135). Cre

recombinase activity results in recombination between loxP sites, excising the stop cassette and permitting expression of the *HIF-α dPA* genes. HIF-1α dPA and HIF-2α lack the prolyl residues required for recognition by pVhl and are therefore consitutively stable. Similarly to *Albumin-cre;Vhl*$^{f/f}$ mice, *Albumin-cre;lsl-Hif1a-dPA;lsl-Hif2a-dPA* died at 6-8 weeks with hepatomegaly and microscopic hepatic angiomas and steatosis. *Albumin-cre;lsl-Hif2a-dPA* mice likewise died at 6-8 weeks with hepatomegaly and recapitulated the hepatic vascular phenotype. The livers of *Albumin-cre;lsl-Hif1a-dPA* mice were grossly normal and displayed minimal microscopic evidence of hepatic steatosis and no vascular lesions. These experiments show that hepatocytic HIF-2α stabilization is both necessary and sufficient for the formation of hepatic angiomas in mice.

Enhancement and HIF-dependence of Vhl renal cyst formation. Though approximately 60% of VHL Disease individuals develop renal cysts, germline *Vhl*$^{+/-}$ mice only rarely develop renal cysts (~3%)(111). The cell type of origin for VHL Disease-associated cysts is unknown, but evidence supporting both the proximal and distal tubule epithelium exists. Rankin *et al.* investigated the loss of *Vhl* in the proximal renal tubule using the same PEPCK-cre system discussed above (136). PEPCK-cre recombinase displays activity in the renal cortex and outer medulla, specifically in the proximal tubule epithelium, and in periportal hepatocytes. The kidneys of *PEPCK-cre;Vhl*$^{f/f}$ mice aged to <12 months were microscopically normal, but the kidneys of 12-25 month old *PEPCK-cre;Vhl*$^{f/f}$ mice contained macroscopic (18%) and microscopic tubular (25%) and glomerular (35%) renal cysts. Glomerular renal cysts are not a feature of human VHL

Disease. Using immunohistochemical analysis, the epithelial cells lining the tubular microcysts were discovered to express markers of the distal tubule (55% of cysts) and de-differentiation (vimentin, 35% of cysts) but not of the proximal tubule (<5% of cysts). These marker studies suggest that PEPCK-cre has undetectable or rare activity in the distal tubule or that proximal tubule-derived cystic epithelial cells undergo de- or trans-differentiation. *PEPCK-cre;Vhl$^{f/f}$;Hif1a$^{f/f}$* mice developed renal macrocysts and microcysts with similar appearance and penetrance. *PEPCK-cre;Vhl$^{f/f}$;Arnt$^{f/f}$* mice did not develop renal cysts, suggesting a dependence on HIF-2α.

Though a dramatic improvement over germline *Vhl$^{+/-}$* mice, the modest penetrance and delayed age-of-onset for renal cysts in the *PEPCK-cre;Vhl$^{f/f}$* model suggests that additional genetic events are required to make a *Vhl*-initiated renal cyst. Given that human ccRCC tumors display reduced expression or loss of *Pten* or activation of PI3K or AKT(137-139), Frew *et al.* studied the combination of *Vhl* and *Pten* loss using the distal tubule-specific Ksp1.3-cre recombinase system(140). *Ksp1.3-cre;Vhl$^{f/f}$* mice developed fully penetrant hydronephrosis, and *Ksp1.3-cre;Pten$^{f/f}$* mice developed uroepithelial hyperplasia and hypertrophy in the renal pelvis, ureters, and bladder. In addition to hydronephrosis and enhanced uroepitheial hyperplasia, 100% of double *Ksp1.3-cre;Vhl$^{f/f}$;Pten$^{f/f}$* mice aged 6 weeks – 6 months (n=14) developed renal cysts. Microscopically, the renal cysts displayed clear cell histology and predominantly simple epithelium. Atypical papillary changes were observed in 8% of cysts. Immunohistochemical analysis showed that the renal cyst epithelium expressed

markers of the distal tubule and collecting duct but not the proximal tubule. *Ksp1.3-Vhl$^{f/f}$;Pten$^{f/f}$* renal cysts also displayed activating phosphorylation of Akt and Erk enhanced relative to *Ksp1.3-Vhl$^{f/f}$* mice based on both immunohistochemical analysis and immunoblot analysis from whole-kidney lysates. These studies provide evidence that *Vhl*-initiated renal cysts arise from the distal tubular epithelium, are HIF-2α-dependent, and require additional genetic events.

A gene replacement model of Chuvash Polycythemia. Taking advantage of the genotype-phenotype correlations in VHL Disease, Hickey *et al*. recently published a gene replacement mouse model of human Chuvash Polycythemia (112). Humans homozygous for the R200W *VHL* mutation develop Chuvash Polycythemia, a benign polycythemia characterized by elevated hematocrit and hemoglobin levels, elevated serum Vegf and Epo, and thrombotic events(52-54). Mice homozygous for the Chuvash Polycythemia mutation (*Vhl$^{R/R}$*) are viable. *Vhl$^{R/R}$* mice gradually developed signs of polycythemia, including an age-dependent increase in hematocrit (to 55% by 26 weeks) accompanied by elevated red and white blood cell counts and hemoglobin levels. The erythrocytosis present in *Vhl$^{R/R}$* mice was associated with elevated Epo levels in the serum and kidney but not the liver. *Vhl$^{R/R}$* bone marrow was histologically normal, but the spleen showed evidence of extra-medullary erythropoiesis, including expansion of the red pulp with erythroid precursors, and an increased megakaryocyte population. *Vhl$^{R/R}$* mice displayed no evidence of tumor predisposition.

VHL and the Primary Cilium Hypothesis

Structure and function of the primary cilium. The primary cilium is a single apical extension of the cell membrane (reviewed in (102, 103)). The non-motile primary cilum acts like an antenna, tranducing molecular and sensory signals from the extracellular space. The primary cilium consists of microtubules in a 9+0 arrangement arising from the basal body or centriole. Most quiescent (G0) cells have a primary cilum. Upon entry into the cell cycle, the primary cilium is resorbed and the basal body acts as the microtubule organizing center (MTOC) for mitosis. Because the primary cilium does not contain ribosomes, all proteins required for structure and function must be transported from the cytoplasm by intra-flagellar transport (IFT) with molecular motors. Anterograde IFT proceeds by the action of the molecular motor kinesin-2, while retrograde IFT utilizes dynein-1b.The primary cilia of renal tubular epithelial cells extend into the tubular lumen and function as mechanosensors of urinary flow.

The Ciliary Hypothesis. According to the ciliary hypothesis, mutation or loss of genes required for primary cilium structure or function predisposes to renal cyst formation (141). Several inherited diseases featuring renal cyst formation have been linked to the primary cilium , including both autosomal dominant (142) and recessive (143) forms of Polycystic Kidney Disease and Bardet-Biedl Syndrome (144-146).

VHL and the Primary Cilium. VHL-deficient RCC-derived cells are only sparsely ciliated in culture, but transgenic rescue with wild-type *VHL* restores primary cilium prevalence(147). In primary cells such as MEFs, *Vhl* loss is

insufficient to lose cilia, indicating that *Vhl* is dispensible for primary cilium formation. *Vhl*-deficient MEFs lose their cilia, however, in the context of physiological (ie, by growth factor or serum stimulation) or pharmacological GSK3β inhibition or deficiency, confirming a role for pVHL in primary cilium maintenance(104). Phosphorylation of serine 72, likely by casein kinase (CK)-1, primes VHL_{30} for phosphorylation on serine 68 by GSK3β. Phosphorylated VHL_{30} retains the capacity to bind microtubule but cannot stabilize cytoplasmic microtubules or maintain the primary cilium (105). pVHL mutants defective for cytoplasmic microtubule binding cannot maintain the primary cilium, suggesting that the two functions are intimately linked (104). These *in vitro* studies support a model in which GSK3β has both VHL-dependent and VHL-independent functions in maintaining the primary cilium. Active GSK3β independently maintains the primary cilium and inactivates the microtubule stabilizing function of VHL_{30} via S68 phosphorylation. In conditions when GSK3β is inactive or deficient, however, unphosphorylated VHL_{30} takes over responsibility for primary cilium maintenance(104). *VHL* deficiency or loss, then, would be predicted to sensitize cells to loss of the primary cilium.

Supporting the idea that *VHL* loss alone is insufficient for renal cyst formation, VHL Disease-associated renal cysts (n=33) display a three-fold reduction in ciliation and are associated with *VHL* deficiency (approximated by expression of the HIF target gene CA9) and inactive (phospho-) GSK3β, but only 46 out of 303 *VHL*-deficient single cells were concomitantly positive for displayed inactivated GSK3β (104). Sporadic ccRCC tumors (n=20) also display drastically

reduced ciliation (7.5%) relative to normal renal tubular epithelium (83.7%), and a subset (5/20) additionally display positivity for phospho-Ser9 GSK3β (148).

Deficiency in PTEN activity would be predicted to increase signaling through AKT, which in turn phosphorylates and inactivates GSK3β (149). Combination of *VHL* loss and *PTEN* loss, then, would be predicted to confer predisposition to renal cysts. In fact, distal tubule inactivation of both *Vhl* and *Pten*, but neither singly, results in a fully-penetrant renal cyst phenotype (140). While wild-type, single *Vhl*- or *Pten*-deficient, and morphologically normal double *Vhl*- and *Pten*-deficient distal tubules were 80-90% ciliated, cystic double *Vhl*- and *Pten*-deficient distal tubules were only 30% ciliated. *In vitro* MEF cultures derived from single and double *Vhl*- and *Pten*-deficient mice indicated that primary cilium loss in double mutants was mTOR-independent but both AKT- and ERK/MEK-dependent, the activation of the latter pathways most likely due to autocrine or paracrine growth factor stimulation resulting from HIF-α stabilization.

Indeed, while *Vhl* single kidneys displayed mild activation of AKT and ERK1/2 and inactivation of GSK3β, the addition of *Pten* loss markedly enhanced both AKT and ERK activation and GSK3β inactivation. Also, in addition to uniform inactivation of GSK3β, 25/33 human VHL Disease renal cysts additionally displayed ERK1/2 activation(140). Altogether, current data suggests that VHL Disease- and sporadic ccRCC-associated renal cysts result from primary cilium loss due to the combined loss of VHL function and signaling through AKT and ERK/MEK.

HIF and Renal Tumorigenesis

Regulation of HIF-α translation. HIF-1α and HIF-2α are constitutively and ubiquitously transcribed but are highly regulated at the level of translation, stability, and transcriptional activity. Normoxic translation of HIF-1α and HIF-2α mRNA is enhanced by activation of mammalian target of rapamycin (mTOR) kinase activity.

The mTOR pathway ties protein translation to nutrient availability and growth factor signaling (reviewed in (150, 151)). The serine/threonine kinase mTOR assembles into two distinct complexes, mTORC1 and mTORC2, with distinct targets. mTORC1 contains mTOR, raptor (152), mLST8, and PRAS40 and directs phosphorylation of the substrates p70S6K and 4EBP1 (153). mTORC1 phosphorylation activates p70S6K (154), resulting in the phosphorylation of the 40S ribosomal subunit S6 and thereby promoting translation of ribosomal and other pyrimidine tract-containing RNAs (155). mTORC1-phosphorylated 4EBP1 results dissociates from eIF4E, localized at the 5' end of select mRNAs. Released from 4EBP1, eIF4E is free to promote translational initiation of genes involved in cell proliferation including HIF-α, cyclin D1, c-myc, and VEGF(156, 157). mTORC2 consists of mTOR, rictor, protor, and sin1 and phosphorylates AKT on Ser473, contributing to AKT activation.

mTORC1 activity is activated by Rheb (158), a small G protein, the activity of which is in turn inhibited by the GTPase activity of TSC2 in complex with TSC1(159-161). TSC1/2 integrates nutrient and growth factor signaling to direct appropriate mTOR activity. Conditions of energy deficiency (decreased

ATP:AMP ratio) activate AMP kinase (AMPK) (162). Activated AMPK phosphorylates and activates TSC2, resulting in inhibition of mTORC1 activity and repression of translation(159-161). In contrast, growth factor signaling via receptor tyrosine kinases activates PI3K, responsible for phosphorylating PIP2 to generate PIP3 in a reaction antagonized by PTEN activity. The resulting PIP3 activates PDK phosphorylation and activation of AKT(163), and activated AKT directs inhibitory phosphorylation of TSC2(164, 165), effectively relieving mTORC1 inhibition. mTORC2 may be negatively regulated by Rheb, which would tend to shut down the feedback inhibition generated by mTORC2-mediated activating phosphorylation of AKT(166).

Regulation of HIF-α stability. HIF-α stability is primarily oxygen-dependent. In the presence of oxygen, the HIF prolyl hydroxylases (PHD) 1, 2, and 3 (74, 126, 127, 129), target two specific prolyl residues in the HIF-1α (residues 402 and 564) and HIF-2α (residues 405 and 531) oxygen-dependent degradation domains (ODDD) for hydroxylation(71, 72, 128, 130). The PHD enzymes, together with the co-factors Fe^{++} and ascorbate, utilizes the substrates molecular oxygen (O_2) and 2-oxoglutarate (2-OG) to convert prolyl residues to hydroxyprolyl residues, generating CO_2 and succinate as by-products(167). HIF-α hydroxyprolyl residues are recognized and bound by the pVHL β domain, resulting in HIF-α ubiquitylation by the VBC ubiquitin ligase complex and degradation by the 26S proteasome(73, 75). The Michaelis constant (K_M) of the PHD enzymes for O_2 is approximately 100 μM(168, 169), whereas most tissues achieve at most 10-30 μM O_2. As a result, PHD enzymatic activity is exquisitely

sensitive to changes in O_2 tension. Under anoxic conditions, PHD is inactive and HIF-α prolyl residues escape hydroxylation and recognition by pVHL. PHD2 is thought to be the primary HIF-α hydroxylase(170-172). HIF-α is also stabilized in an oxygen-independent manner by its association with the chaperone protein HSP90(173, 174).

Regulation of HIF-α transcriptional activity. The C-terminal activation domain (CTAD) directs HIF-1α and HIF-2α transcriptional activation. The CTAD is regulated in an oxygen-dependent manner analogous to the regulation of the HIF-α ODDD. Factor inhibiting HIF (FIH), an Fe(II)- and 2-OG-dependent dioxygenase related to the PHD enzymes, catalyzes the hydroxylation of a single asparaginyl residue in the HIF-α CTAD (residue 803 in HIF-1α and 851 in HIF-2α)(175-177). The asparaginyl hydroxylation reaction requires Fe^{++} and ascorbate as co-factors, utilizes O_2 and 2-OG as substrates, and generates CO_2 and succinate as by-products. Similar to PHD, the K_M of FIH for O_2 (~90 μM) far exceeds physiological oxygen levels(178), making FIH likewise very sensitive to slight changes in oxygen tension. Asparaginyl hydroxylation prevents the direct association of HIF-α CTAD with the transcriptional co-activators CBP and p300 (176) and the recruitment of additional co-activators(179). As a result of ODDD and CTAD hydroxylation, HIF-α subunits are both highly unstable ($t_{1/2}$ ~5 minutes(180)) and transcriptionally inactive under normal oxygen conditions.

Pseudohypoxia in renal tumorigenesis syndromes. In order to determine whether HIF-α stabilization is a common early molecular event in renal tumorigenesis, small renal cortical tumors (<2.0 cm in greatest diameter) from

patients with the inherited renal tumor predisposition syndromes Birt-Hogg-Dube (BHD), Hereditary Papillary Renal Cancer (HPRC), and VHL Disease (n=12 for each) were analyzed for HIF-1α and HIF-2α (181). As expected, VHL ccRCC tumors uniformly expressed HIF-2α and 10/12 additionally expressed HIF-1α. BHD chromophobe and hybrid chromophobe/oncocytic RCC tumors also strongly and uniformly expressed HIF-2α, with 6/12 additionally and more weakly expressing HIF-1α. Fifty percent of HPRC Type II papillary RCC tumors expressed HIF-2α, half of which expressed HIF-1α as well. Given the small size of these tumors, HIF-1α and HIF-2α stabilization in BHD and HPRC tumors is unlikely to reflect physiological hypoxia. Indeed, increasing evidence, discussed below, suggests that the genetic events predisposing to renal tumorigenesis have molecular links to the translation and post-translational stability of HIF-α. The renal and extra-renal manifestations of each syndrome are summarized in Table 1.2.

Tuberous Sclerosis**.** Tuberous sclerosis is an autosomal dominant disease caused by germline mutations in *TSC2* (encoding tuberin) and *TSC1* (15-30% of families, encoding hamartin) with an incidence of 1:6000 live births (reviewed in (182)). *TSC1*-associated tuberous sclerosis tends to have a milder clinical course than *TSC2*-associated tuberous sclerosis(183-186). The defining manifestation of tuberous sclerosis is the development of benign tumors (hamartomas or tubers) in multiple tissues. Tuberous sclerosis patients are also afflicted with renal angiomyolipomas (80%)(187), cysts (53%), and rarely ccRCC (2-3%)(188, 189).

The Eker rat model of renal adenoma features a spontaneous retroviral insertion in the rat *TSC2* gene(190, 191). Eker rats develop renal cysts, papillary cystadenomas, and solid adenomas with high penetrance. *Tsc2*$^{+/-}$ mice also develop high-penetrance papillary cystadenoma (>95% at 14 weeks – 6 months)(192). Two different murine Tsc1 models displayed drastically different, partly genetic background-dependent, phenotypes. The renal phenotype of *Tsc1*$^{+/-}$ mice ranged from altered tubules at 9-12 months on a mixed 129SvJ/C57BL/6 background (193) to fully penetrant microscopic cysts, cystadenomas, and frank carcinoma with lung metastases on a Balb/c background by 15-18 months (194). Like *Vhl*$^{+/-}$ mice, both *Tsc1*$^{+/-}$ and *Tsc2*$^{+/-}$ mice develop hepatic angiomas (20-80% at 15-18 months)(192-194).

Tuberous sclerosis has a clear link to HIF-α – as described in detail, TSC1 and TSC2 participate in the inhibition of mTOR. Loss of function in either TSC1 or TSC2, then, would be predicted to release mTOR from inhibition and enhance translation of HIF-α transcripts. Eker-derived renal tumor cell lines (Tsc2$^{-/-}$) and renal tumors over-express HIF-2α but not HIF-1α and over-express the joint HIF target gene VEGF. Over-expression of HIF-1α and VEGF in Tsc2$^{-/-}$ murine embryonic fibroblasts (MEF) was rescued by rapamycin, indicating mTOR-dependence(195).

Birt-Hogg-Dube Syndrome. Birt-Hogg-Dube Syndrome (BHDS) is an autosomal dominant disease associated with germline mutations in the *BHD* tumor suppressor gene located at 17p11.2(196). *BHD* mutations are almost exclusively frameshift and nonsense mutations predicted to result in C-terminal

Table 1.2. HIF-related renal tumor predisposition syndromes

Syndrome	Gene(s)	Renal tumor histology	Renal pentrance	Other manifestations
Birt-Hogg-Dube Syndrome (BHDS)	*FLCN*	Chromophobe RCC (33%), hybrid chromophobe-oncocytic RCC (50%), ccRCC (9%), oncocytoma (5%), papillary RCC (2%)	34%	Cutaneous fibrofolliculomas (90%), pulmonary cysts (84%) and spontaneous pneumothorax (38%)
Hereditary Leiomyomatosis and Renal Cell Carcinoma (HLRCC)	*FH*	Unilateral, solitary Type 2 papillary RCC or collecting duct carcinoma	20-35%	Cutaneous (85%) and uterine (98% of women) leiomyomas
Hereditary Papillary Renal Carcinoma (HPRC)	*MET*	Bilateral, multifocal Type 1 papillary RCC	Unknown	None
Hereditary Paraganglionoma (HPGL)	*SDHB*	Bilateral, multifocal chromophobe RCC, ccRCC, or Type 2 papillary RCC	3%	Pheochromocytoma (19%) and paraganglionomas (38%)
Tuberous Sclerosis	*TSC1, TSC2*	Bilateral, multifocal angiomyolipoma (80%), renal cysts (53%), ccRCC (4%)	61%	Hamartomas

truncation of the encoded protein, folliculin (FLCN)(196, 197). The defining clinical feature of BHDS is fibrofolliculoma (95%) and other cutaneous lesions. BHDS patients also develop lung cysts (84%) with spontaneous pneumothorax (38%) and kidney tumors (34%). While no specific genotype-phenotype correlations have been proven, RCC is present in 57% of BHDS individuals with family histories and only 23% of BHDS individuals without a family history of RCC(197). The diverse histologies of BHDS-associated renal tumors include hybrid oncocytic/chromophobe RCC (50%), chromophobe RCC (34%), ccRCC (9%), oncocytoma (5%), and papillary RCC (2%)(198).

The Nihon rat model of spontaneous RCC features a frameshift mutation in the rat *BHD* gene. Nihon rats develop ccRCC with complete penetrance by six months (199). In a germline mouse model, 45% and 8% of $Bhd^{+/-}$ mice had developed oncocytic renal cysts and oncocytoma or chromophobe RCC, respectively (200). In two independent models, loss of *Bhd* in the distal tubule (*Ksp1.3-cre*) resulted in death at three weeks from kidney failure, associated with gross bilateral polycystic kidneys and microscopic tubular dilatation (201, 202), hyperplasia, and cystic RCC(202) but no solid RCC.

Death due to renal failure was delayed in distal tubule *Bhd*-deficient mice by treatment with rapamycin (201, 202), and cystic $Bhd^{d/d}$ kidneys displayed enhanced phosphorylated, activated Akt, mTOR, and S6 levels relative to control kidneys. Furthermore, human BHD-associated (201) and sporadic (203) chromophobe and hybrid oncocytic/chromophobe RCC tumors display a mild increase in mTOR phosphorylation and activation relative to adjacent normal

tissue. *BHD* deficiency is clearly associated with mTOR with AKT/mTOR pathway activity, but the mechanism of such influence is still unclear. FLCN has been shown to interact with folliculin-interacting proteins (FNIP)1 (204) and/or FNIP2 (205, 206) directly via its C-terminus, and FNIP1/2 in turn binds to phosphorylated AMPK (204-206). As the majority of human BHDS mutations result in C-terminal truncations of FLCN which would be predicted to disrupt this interaction(197) and because both FNIP1/2 and FLCN are phosphorylated in an AMPK- and mTOR-dependent manner, the FLCN-FNIP1/2-AMPK interaction is likely to biologically significant. The influence of *BHD* status on mTOR activity, however, is highly context-dependent. Genetic knock-down of *BHD*, *FNIP1*, or *FNIP2* by siRNA in HeLa cells, for example, resulted in decreased phosphorylation and activation of mTOR (206). In contrast, inhibition of mTOR signaling by exogenous AMPK stimulation or rapamycin treatment or activation of mTOR by serum stimulation were unaffected by *BHD* status, while inhibition of mTOR activity by serum starvation was impaired and by amino acid deprivation was enhanced in a *BHD*-null ccRCC cell line relative to its *BHD*-rescued counterpart (204). Over-expression of HIF-α in BHDS renal tumors, then, may result from FLCN function upstream or downstream of mTOR, depending on the tumor's genetic history and microenviroment.

Hereditary Papillary Renal Carcinoma. Hereditary Papillary Renal Carcinoma (HPRC) is an autosomal dominant disorder with incomplete penetrance resulting from germline activating mutations in the *MET* proto-oncogene (7q)(207, 208). MET is the receptor tyrosine kinase (RTK) for

hepatocyte growth factor/scatter factor (HGF/SF)(209) and transduces signals for cell growth and motility via several signaling cascades, including MAPK/ERK and PI3K/AKT(210). HPRC *MET* mutations are typically missense mutations in the MET TK domain conferring constitutive phosphorylation and activation (10, 11, 207). HPRC individuals are at risk for multiple, bilateral Type I papillary RCC tumors but are not predisposed to any other benign or malignant neoplasms (211). Both HPRC-associated (10) and sporadic (12, 212) papillary RCC tumors commonly feature trisomy of chromosome 7, with selective duplication of the chromosome carrying the mutant *MET* allele.

A panel of mice expressing gene replacement alleles representative of several human HPRC *MET* missense mutations developed sarcomas, lymphomas, and rare carcinomas with genotype-specific associations (213). None of the *Met* mutant mice developed renal carcinoma. Cytogenetic analysis of mutant *Met* tumors, however, indicated that 97% contained cells with trisomy and 30% contained cells with tetrasomy for Chromosome 6 (the locus for murine *Met*). Less than 2% of cells in normal tissues displayed Chromosome 6 trisomy. Fifty percent of mutant *Met* tumors also contained cells with specific amplification of the *Met* locus, though such events were less frequent than whole-chromosome duplication. Despite being unable to recapitulate the tissue-specificity of human mutant MET activity, the mouse model validates *MET* amplification as a critical event in tumorigenesis.

No studies have directly addressed the mechanism by which oncogenic MET might directly increase HIF-α expression. Constitutively active MET may

signal through PI3K, resulting in AKT activation, TSC1/2 inhibition, and mTOR activation with an outcome of increased HIF-α translation. The possibility remains that HIF-α stabilization may be an independent event in the history of HPRC-associated and sporadic papillary RCC tumors. Interestingly, evidence exists linking *VHL* loss to MET activity (214). *VHL*-null RCC cell lines over-express phosphorylated, activated MET relative to normal renal proximal tubule epithelial cells (RPTEC). Suppression of MET signaling required both wild-type *VHL* and cell-cell contact.

*Hereditary Leiomyomatosis and Renal Cell Cancer and Hereditary Paraganglioma***.** Hereditary Leiomyomatosis and Renal Cell Cancer (HLRCC) is associated with germline mutations in the fumarate hydratase (*FH*) gene (215, 216). Fumarate hydratase catalyzes the conversion of fumarate to malate in the Krebs Cycle. Fibroblast cell lines derived from the cutaneous leiomyomas of HLRCC patients ($FH^{m/m}$) display a near-complete reduction in fumarate hydratase enzymatic activity (217). Cutaneous leimoyomas (100%) and uterine leiomyomas (98% of females), or fibroids, are highly penetrant features of HLRCC(216). Approximately 1/3rd of HLRCC individuals develop unilateral, solitary Type 2 papillary RCC or collecting duct carcinoma (CDC), often with an aggressive clinical course(218). HLRCC-associated Type 2 papillary RCC tumors display HIF-α over-expression (HIF-1α > HIF-2α) (217, 219).

Distal tubule-specific (*Ksp1.3-Cre*) deletion of *fumarate hydratase 1* (*Fh1*) in mice confers death from renal failure with complete penetrance at 8-15 months(220). Renal failure in *Ksp1.3-Cre;*$Fh1^{f/f}$ mice is associated with

development of bilateral renal macrocysts and over-expression of both HIF-1α and HIF-2α in the cyst epithelial lining (in 50% and 25% of nuclei, respectively).

Germline mutations in *succinate dehydrogenase* (*SDH*) subunits B, C, and D, are associated with Hereditary Paraganglioma (HPGL) syndrome (221-223). The HPGL syndromes were originally described as predisposing to head and neck paragangliomas and adrenal and extra-adrenal pheochromocytomas. Somatic mutations in *SDH* are also common in sporadic pheochromocytomas and paragangliomas (224). Recently, however, several families with germline *SDHB* mutations have been reported to develop early-onset RCC with (225, 226) or without (227) a family or personal history of paraganglioma or pheochromocytoma. Succinate dehydrogenase functions in the Krebs cycle, converting succinate to fumarate, the substrate of fumarate dehydrogenase.

FH and *SDHB* mutations contribute to HIF-α stabilization by a novel mechanism: direct competitive inhibition of PHD activity. As described above, hydroxylation of specific prolyl residues in the HIF-α ODDD utilizes prolyl, O_2, and 2-OG as substrates to generate hydroxyprolyl, CO_2, and succinate (167). *SDH* deficiency would be predicted to increase intracellular succinate levels, and *FH* deficiency would be predicted to increase both fumarate and, because the SDH reaction is reversible, succinate. Metabolomic analysis of human disease tissues indicates that HLRCC-derived fibroids do indeed have elevated intracellular levels of both succinate and fumarate, while HPGL (*SHDB*)-derived paragangliomas have elevated intracellular levels of succinate alone (217). Suggesting that the association between the genetic lesion and metabolic profile

is a causative relationship, knock-down of *FH* (219) or *SDHB* (228, 229) *in vitro* results in intracellular fumarate or succinate accumulation, respectively, and HIF-α stabilization (HIF-1α > HIF-2α). Isaacs *et al*. confirmed that both succinate and fumarate are direct competitive inhibitors of 2-OG for PHD2 activity, resulting in reduced HIF-α ODDD prolyl hydroxylation and recognition by VHL. Interestingly, fumarate (Km = 2.6 μM) was shown to be a better inhibitor of PHD2 activity than succinate (Km = 9 μM), possibly because the chemical structure of fumarate is similar to but more rigid than succinate (219). As proof of concept, exogenous 2-OG treatment rescues PHD activity in cells with artificially elevated succinate (230) or fumarate (219) levels. Though the HIF-α asparaginyl hydroxylation reaction catalyzed by FIH proceeds by a mechanism analogous to PHD-mediated prolyl hydroxylation, neither succinate nor fumarate were determined to inhibit FIH activity at physiologically-achievable intracellular concentrations (178).

The mechanisms by which each renal tumor predisposition syndrome affects HIF-α expression or stability is summarized in Figure 1.2.

Treatment of Renal Cell Carcinoma

Modified with permission from: Rathmell WK, Martz CA, and Rini B. Renal cell carcinoma. *Current Opinion in Oncology* 19(3): 234-40 (231).

Gene expression analysis of RCC. The development of rational treatment strategies for renal tumors necessitates a nuanced understanding of the shared

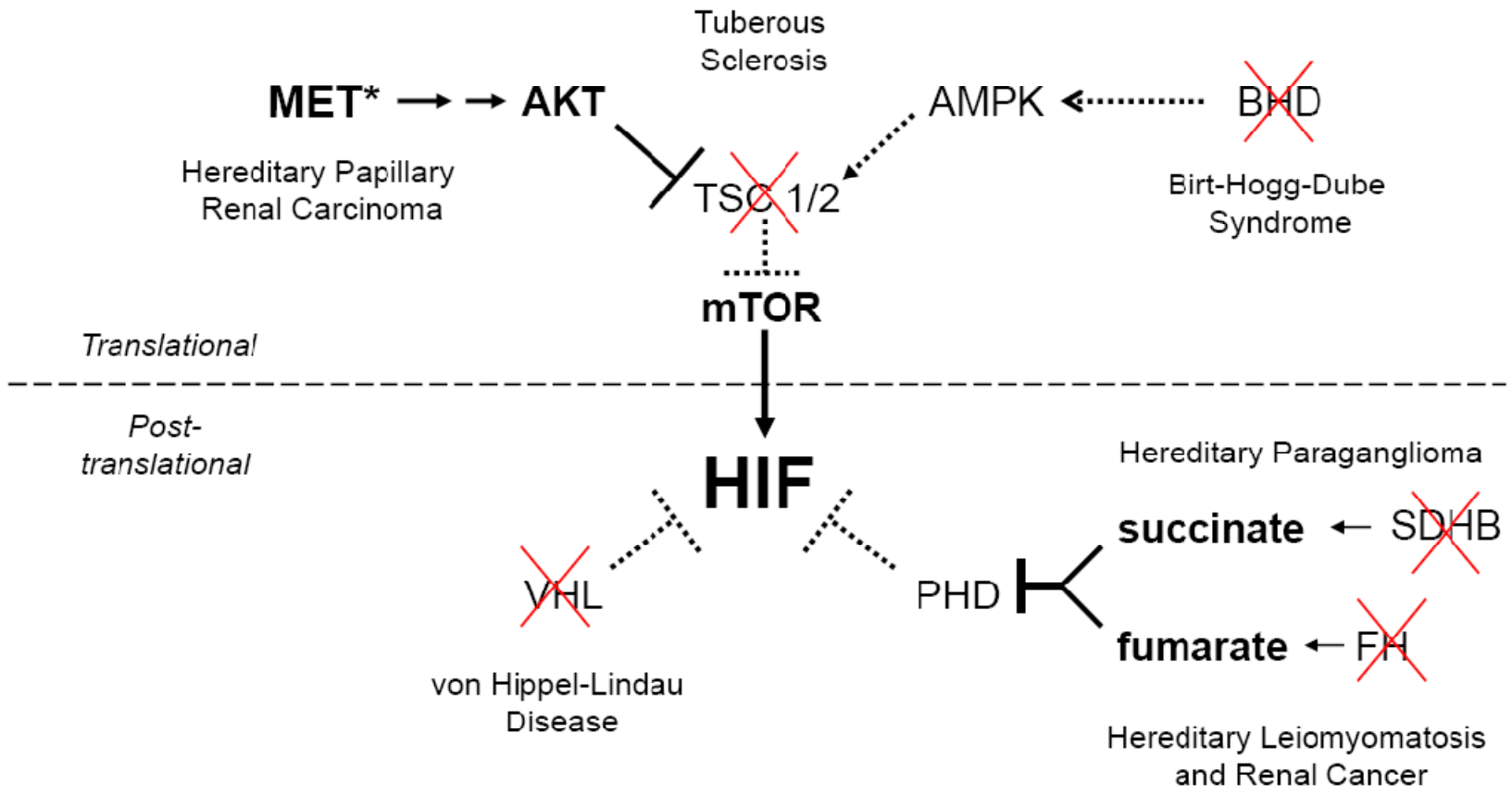

Figure 1.2. HIF expression is a common feature of familial renal tumor development. Germline inactivating mutations of *VHL*, *TSC1* or *TSC2*, *FH*, and *BHD* as well as germline activating mutations in *c-Met* predispose to differing histologic subtypes of RCC. However, renal tumors associated each germline mutation can have increased protein expression of one or both HIF factors and subsequent target gene expression within the renal tumors. Modified from Rathmell WK *et al.* 2004 (107).

and unique features of each RCC subtype. In addition to studying the shared molecular biology of renal tumors, as discussed above, the study of mixed RCC tumors by gene expression profiling has yielded remarkable insight into the biologies of individual RCC subtypes. Yang *et al*. found that histopathological review alone could not fully and accurately describe a chromophobe-oncocytoma hybrid and a high-grade clear cell tumor with an oncocytomatous component, but adding gene expression array analyses aided identification of these mixed tumors (232). Jones *et al*. studied the genetic histories of RCC tumors with both clear cell and sarcomatoid components. Clear cell and sarcomatoid components displayed identical X-inactivation patterns but different patterns of tumor suppressor loss, pointing towards origin from a common cell with subsequent genetic divergence (233). Finally, Skubitz *et al*. found clinically-relevant molecular and metabolic heterogeneity even within a group of morphologically homogeneous clear cell RCC tumors(234).

Even tumors with similar morphologies exhibit molecular heterogeneity. In a small study of sixteen RCC tumors classified as clear cell in histology, gene expression array analysis separated the ccRCC tumors into ccRCC-A and –B groups with different clinical and molecular profiles(234). Type B tumors tended to display higher nuclear grade and higher clinical stage, supporting a more clinically aggressive phenotype, in comparison to Type A tumors. Tumors with sarcomatoid features, historically associated with poor prognosis, grouped in the Type B cluster, and previously identified gene sets predictive of clinical outcome sorted the tumors into similar groups. The gene expression array analysis also

provided insight into underlying differences in tumor biology between Type A and Type B ccRCC. Type B tumors over-expressed extra-cellular matrix genes, including fibronectin and collagens, and adhesion genes, including NCAM and CD44, while Type B ccRCC tumors over-expressed genes in the glycolytic pathway.

DNA microarray analysis of a much larger set of 177 ccRCC tumor samples separated ccRCC tumors into five distinct subgroups (235) with prognostic significance. Subgroups one and two were very molecularly similar, differing mainly in the transcriptional regulator profiles, and displayed the best long-term survival after radical nephrectomy. Subgroup three tumors displayed relatively higher expression of proliferation-associated and collagen genes but not hypoxia-regulated genes and were associated with the worst long-term survival after surgery. Subgroup four tumors, featuring granular cytoplasm, were associated with over-expression of characteristic chromophobe RCC and oncocytic genes including c-KIT and mitochondrial genes. Finally, subgroup five tumors displayed decreased expression of membrane transporters and a subset over-expressed collagen genes. Tumor subgroup predicted long-term survival independently of grade, stage, or performance status, indicating that the subgroups reflect clinically-relevant and fundamental differences in tumor biology. These studies validate searches for shared RCC initiation pathways but simultaneously urge further study of the molecular changes responsible for specifying RCC subtype and determining clinical behavior and response to treatment.

Targeted Therapy. Recent years have witnessed a significant expansion of therapeutic options in metastatic RCC through the application of therapy targeted at specific proteins and cellular receptors, most notably directed against various components of the VEGF pathway. Data regarding several of these approaches has been updated recently (summarized in Table 1.3). A randomized phase II trial of bevacizumab monotherapy versus bevacizumab plus erlotinib was conducted to determine the value of the combination regimen, and the results provide further insight into the benefit of this agent in metastatic RCC. One hundred three patients with metastatic RCC and no prior systemic therapy were randomized. Bevacizumab monotherapy had a 13% objective response rate and an 8.5 month progression-free survival (PFS) (236). Of note, this trial failed to confirm a response rate or PFS advantage for combination bevacizumab/erlotinib therapy over bevacizumab monotherapy. This important data substantiates the benefit of bevacizumab in untreated RCC. The results also underscore the importance of randomized comparisons to determine the additive value of combinations over monotherapy.

Sunitinib is an oral inhibitor of VEGF and related receptors that was Food and Drug Administration (FDA) approved in January 2006 for the treatment of advanced RCC. The second of two phase II trials was published recently and contains a pooled analysis of patients on both phase II trials (237, 238). These trials were conducted in cytokine-refractory, metastatic RCC patients and demonstrated a RECIST-defined overall response rate (investigator-assessed) of 42%. The combined PFS was 8.2 months, and the median PFS of patients

Table 1.3. Summary of select phase II /III trials using targeted therapy in metastatic RCC*

Agent	Trial design	Results: PFS, ORR, OS	Major toxicities
Bevacizumab	Phase II Randomized double-blind Cytokine-refractory Low or high dose bevacizumab vs. placebo n=116	*PFS*:4.8 months with high dose (vs. 2.5 months with placebo); p=0.0001	Hypertension, proteinuria
	Phase II Randomized Previously untreated Bevacizumab/erlotinib vs. bevacizumab/placebo n=104	*PFS*: 8.5 months with bevacizumab monotherapy (vs. 9.9 months with combination; p=n.s.) *ORR*: 13% (vs.14% with bevacizumab + erlotinib)	Hypertension, rash, diarrhea, bleeding
Sunitinib	Phase II Two single arm trials n=63 and 106	*PFS*: 8.2 months, *ORR*:42%	Fatigue, hand foot syndrome, diarrhea, cytopenia, mucocitis
	Phase III Randomized trial Previously untreated Sunitinib vs. IFN n=750	*PFS*:11 months (vs.5 months with IFN); p<0.000001 *ORR*: 31% (vs.6% with IFN) p<0.000001	
Temsirolimus	Phase II Random assignment to 25, 75 or 250 mg temsirolimus IV weekly n=111	*PFS*: 5.8 months *ORR*: 7%	Rash, mucositis, asthenia, nausea hyperglycemia, hypo-phosphatemia, anemia, hyper-triglyceridemia
	Phase III Randomized three arm: temsirolimus + IFN vs. IFN alone vs. temsirolimus alone n=626	*PFS*: 3.7 months for monotherapy arm (vs.1.9 months for IFN α) *OS*: 10.9 months (vs. 7.3 months for IFN); p=0.0069	Asthenia, anemia, dyspnea
Everolimus	Phase III Randomized double-blind RTK refractory Everolimus (10 mg oral qd, n=272) vs. placebo (n=138)	*PFS*: 4 months (vs. 1.9 months for placebo), p<0.0001 *ORR*: 1% (vs. 0% for placebo)	Stomatitis, rash, asthenia, diarrhea

*Modified from Rathmell WK *et al.* 2007 (231)

achieving a PR was 14.8 months versus 7.9 months for patients with a best response of SD. Toxicity in the combined analysis of these trials included fatigue/asthenia (all grades 28%; grade 3: 11%), hypertension (16%, 6%), diarrhea (20%, 3%), stomatitis (13%, 5%) and hand-foot syndrome (15%, 7%). Neutropenia was observed in 42% (grade 3 or 4 in 16%) but there were no cases of neutropenic fever or sepsis. Five patients experienced a decline in cardiac ejection fraction as assessed by MUGA of 20% or more and to below the lower limit of normal, but no patient developed signs or symptoms of congestive heart failure. Baseline patient characteristics associated with response to sunitinib included a normal hemoglobin and ECOG performance status 0. Additional data regarding the association of tumor response/shrinkage and clinical outcome as well as discovery of factors predictive of response to sunitinib and similar agents is needed. A subsequent randomized phase III trial in untreated, metastatic RCC patients (n=750) of sunitinib versus interferon alpha was also recently reported (20). Sunitinib-treated patients demonstrated a significant advantage in objective response rate (31% versus 6%; $p<000001$) and PFS (11 months versus 5 months; $p<0.000001$). Data is not presently mature to permit assessment of possible overall survival benefit.

Temsirolimus is an inhibitor of mTOR, a molecule implicated in multiple tumor-promoting intracellular signaling pathways. Regulation of mTOR pathway activation is mediated through a series of complex signaling interactions linking growth factor receptor signaling, PI3Kinase activation, and activation of the Akt/PKB pathway which dictates changes in cellular metabolism, coordinated

with alterations in cell growth, mitogenesis and susceptibility to apoptosis. Akt causes mTOR activation via negative signals which disrupt the tonic inhibition of Rheb provided by the TSC1/TSC2 complex. This signaling pathway was recently comprehensively reviewed by Plas and Thompson (239). Mutations in either *TSC1* or *TSC2* cause constitutive activation of mTOR and subsequent enhanced translation of HIF-1α and increased susceptibility to the development of renal cell carcinoma (Figure 1.2).

Temisrolimus was initially tested in treatment-refractory, metastatic RCC randomized 111 patients to one of multiple dose levels (25 mg, 75 mg or 250 mg IV weekly). The overall response rate was 7%, with additional patients demonstrating minor responses. Retrospective assignment of risk criteria to patients in this study identified a poor-prognosis group (n=49). Temsirolimus-treated patients in this poor-prognosis group had a median overall survival (OS) of 8.2 months compared to 4.9 months for historical control IFNA treated patients (240). Additionally, a phase I trial investigated the safety of combination therapy with temsirolimus and IFNA and established the MTD to be temsirolimus 15 mg IV weekly and IFN 6 MU 3x/week, a dose which produced an objective partial response in 13% of patients (241).

A subsequent randomized phase III trial was conducted in patients with metastatic RCC and 3 or more adverse risk features as defined by existing prognostic schema (240, 242). Patients were randomized equally to receive IFNA 18 MU 3x/week, temsirolimus 25 mg IV weekly or temsirolimus 15 mg IV weekly + IFNA 6 MU 3x/week. The primary study endpoint was OS and the study

was powered to compare each of the temsirolimus arms to the IFNA arm. Patients treated with temsirolimus had a statistically longer overall survival than IFNA monotherapy patients (10.9 months vs. 7.3 months, p=.0069) (17).

A second related mTOR inhibitor, everolimus (RAD001), was tested in a double-blind randomized Phase III trial in patients with metastatic RCC with a clear cell component who had progressed on the VEGF RTK inhibitors sunitinib and/or sorafenib(18). Patients were randomized 2:1 to receive 10 mg oral everolimus daily plus best supportive care or placebo plus best supportive care. Treatment was administered in 28-day cycles until progression, death, unacceptable toxicity, or discontinuation. Patients who developed documented progression on placebo therapy were unblinded and permitted to cross-over to the everolimus arm. The primary endpoint for the study was progression-free survival (time from randomization to disease progression or any-cause death) as measured by RECIST criteria by blinded central review. Secondary endpoints included OS and OR. The trial was halted after the second interim analysis because its criterion of clinical significance, a 33% reduction in risk, had been reached.

Everolimus significantly prolonged PFS compared to placebo (HR 0.30, 95% CI 0.22-0.44, p<0.0001). The median PFS for patients randomized to receive everolimus was 4.0 months (95% CI 3.7-5.5), while the median PFS for patients randomized to receive placebo was 1.9 months (95% CI 1.8-1.9). One percent (three patients, all PR) achieved objective response on everolimus treatment and none in the placebo group, indicating that the prolonged PFS

observed in patients randomized to receive everolimus therapy was due to disease stabilization rather than disease regression. OS was not significantly different between patients randomized to receive everolimus and those randomized to receive placebo (median not reached versus 8.8 months, respectively). Any difference in OS was likely blunted by the conjunction of intention-to-treat analysis and heavy cross-over from the placebo to the everolimus arms. Based on these results, the FDA recently approved everolimus for the treatment of patients with advanced RCC who have failed on sunitinib or sorafenib. Additional trials studying everolimus in the neoadjuvant setting and in combination therapy are currently underway. The outcomes of the temsirolimus and everolimus clinical trials validate mTOR as a relevant therapeutic target in RCC, at least in a subset of patients with multiple adverse risk features.

It has become clear through further experience with targeted agents that the traditional methods to assess response and progression of disease employing CT scans and RECIST criteria may be inadequate. Some responding lesions may not change or even increase in size, but have a necrotic appearance to the center of the lesion consistent with an anti-tumor effect. Similarly, the 30% threshold of tumor burden shrinkage required for a RECIST-defined objective response is arbitrary and may not carry substantial weight in the evaluation of these agents. More precisely, lesser degrees of tumor shrinkage (1-29%) have been commonly observed with targeting agents and likely account for some of the PFS benefits observed in randomized trials. A recent publication adds to the literature regarding functional imaging of tumors for more precise evaluation of

drug effect (243). Twenty-four patients with RCC underwent a dynamic contrast-enhanced helical CT of the kidney prior to radical nephrectomy. Radiographic parameters of tumor enhancement were then compared to the histologic parameters of grade and microvessel density (MVD). Radiographic enhancement parameters were significantly correlated with MVD but not grade in this small series. This data supports that radiographic enhancement of RCC tumors is a reflection of the vascularity of RCC tumors and that this vascularity can potentially be quantified. The next step would then be to use these techniques to assess tumor vascularity pre- and post-VEGF targeted therapy to determine if these parameters can add value to standard radiographic assessments of tumor size. Further research in to functional imaging in RCC is sorely needed.

Combinations of targeted agents with each other or with cytokines are a recent area of investigation in metastatic RCC. Sorafenib and interferon have been combined in two separate single-arm phase II trials (19, 244). These trials demonstrated objective response rates of 18% and 35%, perhaps owing to differences in enrollment criteria between these two studies, as the first study was limited to cancers with a clear cell component. Toxicity observed was typical of that observed with each single agent with a notable reduction in hand foot syndrome compared to historical sorafenib monotherapy data. The benefit/toxicity ratio of this combination regimen awaits further investigation.

Cytokine Therapy. Cytokine therapy with IL-2 or IFN-α is of modest benefit in unselected populations. It would be unwise, however, to completely abandon this therapy given that metastatic RCC is still a fatal disease for the vast

majority of patients. Two strategies emerge for harnessing the benefit of cytokines in an era of active targeted therapy: patient selection and combination therapy.

An example of the potential value of using a molecular marker to select patients and also an example of combination therapy is a phase II trial of IFNA in combination with the cyclooxygenase-2 (COX-2) inhibitor celecoxib in patients with maximal COX-2 expression. A previous trial in unselected metastatic RCC patients demonstrated an enhanced response rate in the subgroup of patients with maximal COX-2 expression as assessed by immunohistochemical staining of primary RCC tumors (245). This trial generated a hypothesis that COX-2 inhibition in tumors with maximal COX-2 expression overcomes inherent immunosuppression and may enhance the clinical value of cytokines. A prospective trial of IFNA and celecoxib is thus ongoing in RCC patients with maximal COX-2 expression. In addition, two completed large phase III trials of interferon plus bevacizumab versus interferon alone are awaited and will define the activity of this combination regimen.

VHL and Clear Cell Renal Cell Carcinoma. Both VHL Disease-associated and sporadic ccRCC progresses from renal cysts and dysplasia to local and invasive disease. Mutation and LOH of *VHL* are evident in every stage of sporadic ccRCC, and VHL Disease kidneys display HIF target gene activation in morphologically single cells as well as cysts, dysplastic foci, and RCC(44), indicating that *VHL* loss is an early or initiating event in renal tumorigenesis(8). VHL patients develop many renal cysts with increasing age (44). The average

age of diagnosis of ccRCC in VHL disease patients, however, is in the 4th to 5th decade of life (41), suggesting that genetic events in addition to *VHL* LOH are required for progression to RCC. Evidence from mouse models suggests that signaling through the AKT and MEK/ERK pathways are required in the transition from *VHL*–initiated single cell to renal cyst(140), but the genetic and epigenetic events required for progression of *VHL*-initiated cysts to invasive RCC are poorly understood. Renal tumors often display PTEN down-regulation(137, 139), resulting in increased AKT pathway activity(138). Metastatic tumors can additionally harbor mutations in *RB* and *TP53* and display increased myc and EGFR expression. Unlike many smoking-associated tumors, however, *RAS* mutation is not a common feature of RCC(246).

The HIF axis is central to renal tumorigenesis: the gene products associated with renal tumor predisposition syndromes such as VHL Disease, Birt-Hogg-Dube Syndrome, Hereditary Papillary Renal Cancer, Hereditary Leiomyomatosis and Renal Cell Carcinoma, and Tuberous Sclerosis all impinge upon HIF-α translation or post-translational stability. The *VHL* tumor suppressor gene is mutated or lost in both inherited clear cell RCC as part of VHL Disease and in sporadic ccRCC. Though pVHL has a well-described role in the normoxic suppression of HIF-α, its contribution to primary cilium maintenance may also feature in renal tumorigenesis via the putative RCC precursor lesion, the renal cyst. Mouse models of human VHL Disease suggest that one or more genetic or epigenetic lesions are required for progression of a *VHL*-initiated cell to a renal cyst and an unknown number of additional lesions are required to progress a

VHL-initiated renal cyst to renal adenocarcinoma, if the renal cyst is a precursor lesion at all. In my dissertation work, I have taken advantage of the genotype-phenotype correlations observed in human VHL Disease to study mutant pVHL ubiquitin ligase structure and function using molecular biology techniques and to model the *in vitro* and *in vivo* functions of a representative Type 2B VHL Disease mutant using a gene replacement mouse model.

CHAPTER TWO

VHL Type 2B mutations retain VBC complex form and function

Modified from Hacker KE *et al.* 2008 (247).

Abstract

Von Hippel-Lindau disease is characterized by a spectrum of hypervascular tumors, including renal cell carcinoma, hemangioblastoma, and pheochromocytoma, which occur with *VHL* genotype-specific differences in penetrance. *VHL* loss causes a failure to regulate the hypoxia inducible factors (HIF-1α and HIF-2α), resulting in accumulation of both factors to high levels. Although HIF dysregulation is critical to VHL disease-associated renal tumorigenesis, increasing evidence points toward gradations of HIF dysregulation contributing to the degree of predisposition to renal cell carcinoma and other manifestations of the disease. This investigation examined the ability of disease-specific *VHL* missense mutations to support the assembly of the VBC complex and to promote the ubiquitylation of HIF. Our interaction analysis supported previous observations that VHL Type 2B mutations disrupt the interaction between pVHL and Elongin C but maintain partial regulation of HIF. We additionally demonstrated that Type 2B mutant pVHL forms a remnant VBC complex containing the active members ROC1 and Cullin-2 which retains the ability to ubiquitylate HIF-1α.

Our results suggest that subtypes of *VHL* mutations support an intermediate level of HIF regulation via a remnant VBC complex. These findings provide a mechanism for the graded HIF dysregulation and genetic predisposition for cancer development in VHL disease.

Introduction

von Hippel-Lindau (VHL) disease is an autosomal dominant familial cancer syndrome caused by germline mutation or loss of the *VHL* tumor suppressor gene that affects approximately 1 in 36,000 individuals (248). Individuals with VHL disease develop an array of tumors, including clear cell renal cell carcinomas (ccRCC), cerebellar and retinal hemangioblastomas, and pheochromocytomas (248). VHL disease is divided by genotype into subtypes which predict the spectrum of risk for development of *VHL*-associated lesions (48, 49, 249). Type 1 VHL disease predisposes to the development of ccRCC and hemangioblastoma. All patients with Type 2 VHL disease are at risk for pheochromocytoma. Type 2A VHL disease is further characterized by high risk for hemangioblastoma, and Type 2B VHL disease is associated with high risk for both hemangioblastoma and RCC. Type 2C VHL disease individuals exclusively develop pheochromocytoma (250). Patients homozygous for the Arg200Trp (R200W) *VHL* mutation, located in the extreme C-terminal domain of the 213 amino acid VHL protein (pVHL), develop Chuvash Polycythemia (52, 53). Biallelic inactivation of pVHL has also been reported in upwards of 90% of individuals with sporadic ccRCC (251). Thus, a thorough understanding of wild-

type and disease-associated mutant pVHL activities has potential to impact a broad spectrum of affected patients (248, 252, 253)

The VHL protein acts as the substrate recognition subunit of an E3 ubiquitin ligase complex analogous in structure to the SCF complex. The SCF and SCF-like complexes typically contain four subunits, including a RING finger protein (ROC1/Rbx1), a cullin protein (CUL/Cul), and two adaptor proteins linking the cullin to the substrate binding protein (254). In the pVHL E3 complex (VBC), pVHL acts as the substrate binding protein and is responsible for the specificity of the complex-target interaction (255). Human pVHL directly interacts with Elongin C, while Elongin B links pVHL-Elongin C to cullin 2 (CUL2)-ROC1 (55, 58, 60). The VBC complex serves as a platform through which the E2 ubiquitin-conjugating enzyme, bound by CUL2-ROC1, and the pVHL-bound substrate are brought into proper positioning for ubiquitin transfer (254). In the VBC complex, ROC1 functions to recruit the E2 enzyme and also promotes internal complex stability (60, 255).

The primary targets of the VBC complex are the hypoxia inducible factors, HIF-1α and HIF-2α. The HIF factors direct the transcriptional response to hypoxia by activating the expression of genes involved in angiogenesis, cell proliferation, erythropoiesis, energy metabolism, and apoptosis (51, 63-65, 256, 257).

Loss of the pVHL tumor suppressor, as occurs with Type 1 *VHL* mutations, is believed to promote renal tumorigenesis primarily through loss of

pVHL-mediated HIF regulation (258). Correspondingly, Type 2C *VHL* missense mutations display fully intact regulation of HIF factors, consistent with the lack of conveyed risk for RCC development (100). In the case of Type 2A and Type 2B *VHL* missense mutations, titrated degrees of HIF regulation appear to correlate with the subtype-specific risk of ccRCC (257, 259). While the differing capabilities of VHL disease-associated mutants to regulate HIF have been explored (51, 100, 107, 257, 259), the mechanism of retained HIF regulation and the link between differing levels of HIF regulation and the clinical spectrum observed in VHL disease is not yet fully understood. In this study, we re-examined the effect of *VHL* missense mutations to disrupt the formation of the VBC complex, and demonstrate that characteristic Type 2B *VHL* mutations form a low-abundance VBC complex which retains the ability to ubiquitylate HIF-1α.

Results

Type 2B mutant pVHL proteins promote incomplete normoxic HIF-2α stabilization. We have previously shown that human *VHL* mutations representative of Types 2A and 2B VHL disease impart an intermediate degree of HIF-2α regulation in a *Vhl*-null murine ES cell expression system (107). In order to evaluate this trend in human RCC cells, 786-0 RCC-derived cells, known to lack pVHL expression and over-express HIF-2α, were reconstituted with expression vectors encoding wild-type or VHL disease-specific mutant *VHL* cDNA. Individual clones expressing mutant pVHL comparable to wild-type levels were selected for subsequent experiments. Figure 2.1A depicts a representative immunoblot for the expression of wild-type as well as RCC-

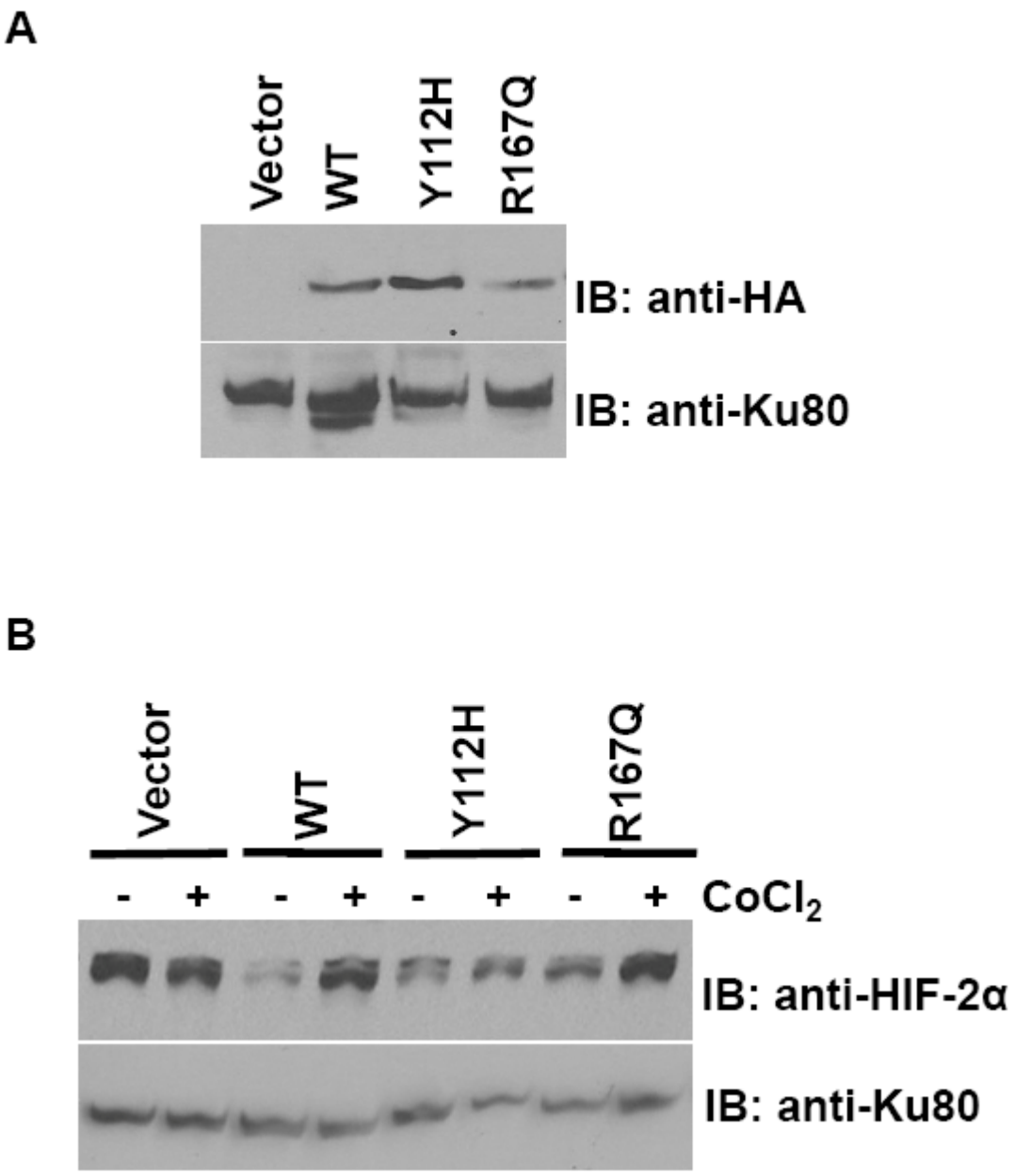

Figure 2.1. VHL disease-associated mutations demonstrate a graded amount of HIF Regulation. A. Anti-HA immunoblot for expression of HA-tagged human pVHL in transgenic 786-0 clones. Whole-cell protein extracts were prepared from 786-0 clones deficient for *VHL* expression (Vector) or modestly expressing wild-type (WT) or missense (Y112H, R167Q) mutant HA-tagged human pVHL. B. Anti-HIF-2α immunoblot for HIF stabilization in 786-0 clones. Whole-cell protein extracts were prepared from *VHL*-deficient 786-0 cells or WT or mutant HA-pVHL-rescued 786-0 cells incubated in the presence or absence of the hypoxia mimetic $CoCl_2$ for 24 hours. Ku80 immunoblot was used as a control for equal loading.

associated Type 2A (Y112H) and 2B (R167Q) mutant HA-tagged pVHL in 786-0 RCC clones.

To study the ability of RCC-associated mutant pVHL to regulate HIF in 786-0 cells, the hypoxia mimetic cobalt chloride ($CoCl_2$) was used to simulate hypoxic conditions. Cells were placed in either standard growth media or media supplemented with 100mM $CoCl_2$for 24 hours followed by analysis of HIF-2α protein levels by immunoblot (Figure 2.1B). *VHL*-null vector-only transfected cells (vector) failed to suppress HIF-2α under standard conditions and lacked further induction under simulated hypoxic conditions. Introduction of wild-type HA-pVHL restored normoxic suppression and $CoCl_2$ induction of HIF-2α. Type 2A *VHL* mutant Y112H cells failed to completely suppress HIF-2α levels, as expected due to the predicted disruption of the HIF interaction domain (55). Type 2B *VHL* mutant R167Q cells displayed partial suppression of HIF-2α while retaining HIF-2α stabilization in response to $CoCl_2$. These observations were confirmed in multiple independently-derived 786-0 clones (data not shown).

Type 2B mutant protein participates in a VBC complex containing Cullin2. To determine the correspondence between the observed partial retention of HIF-2α regulation and formation of a competent VBC complex, we analyzed the interaction of wild-type and disease-specific mutant HA-pVHL with known components of the VBC complex by co-IP and reverse co-IP studies in transgenic human 786-0 and murine ES cells. Based on prevailing models, Type 2B mutant pVHL proteins, including R167Q, are predicted to disrupt VBC complex formation by eliminating Elongin C binding to pVHL (57-59, 260, 261).

We have previously observed the inability of R167Q HA-pVHL to bind Elongin C in a transgenic murine ES cell system (107).

VBC complex formation was assessed by co-IP analysis of proteins interacting with HA-pVHL in *Vhl*-null murine ES cells expressing wild-type pVHL (WT), mutants Y112H, R167Q, L188V, and R200W, or no transgene (-/-). HA-pVHL pull-down was confirmed in each IP by anti-HA immunoblot (HA, Figure 2.2A). Each HA-pVHL-containing complex was then individually tested for interaction with known members of the VBC complex through protein-specific co-IP immunoblot (Figure 2.2A). As expected based on both previous reports and the localization of the respective mutations (51, 107), the R167Q HA-pVHL failed to substantially co-immunoprecipitate Elongin C, whereas wild-type HA-pVHL and mutant HA-pVHL representing Y112H, L188V, and R200W retained this interaction. Furthermore, wild-type HA-pVHL and mutant HA-pVHL representing Y112H, L188V, and R200W demonstrated interaction with complete VBC complex detecting the presence of murine Elongin B, Cul2, and Rbx1. Elongin B, Cul2, and Rbx1 also clearly associated with the R167Q HA-pVHL, suggesting that the VBC complex is at least partially intact in cells expressing this representative Type 2B *VHL* mutation.

In order to discern if the observed remnant VBC complex in R167Q HA-pVHL-expressing murine ES cells was an artifact of human-mouse interactions, we examined the same panel of *VHL* mutations for VBC complex formation in stably-transfected human 786-0 RCC cells. A second representative Type 2B *VHL* mutation D121G was included in this analysis to determine whether the

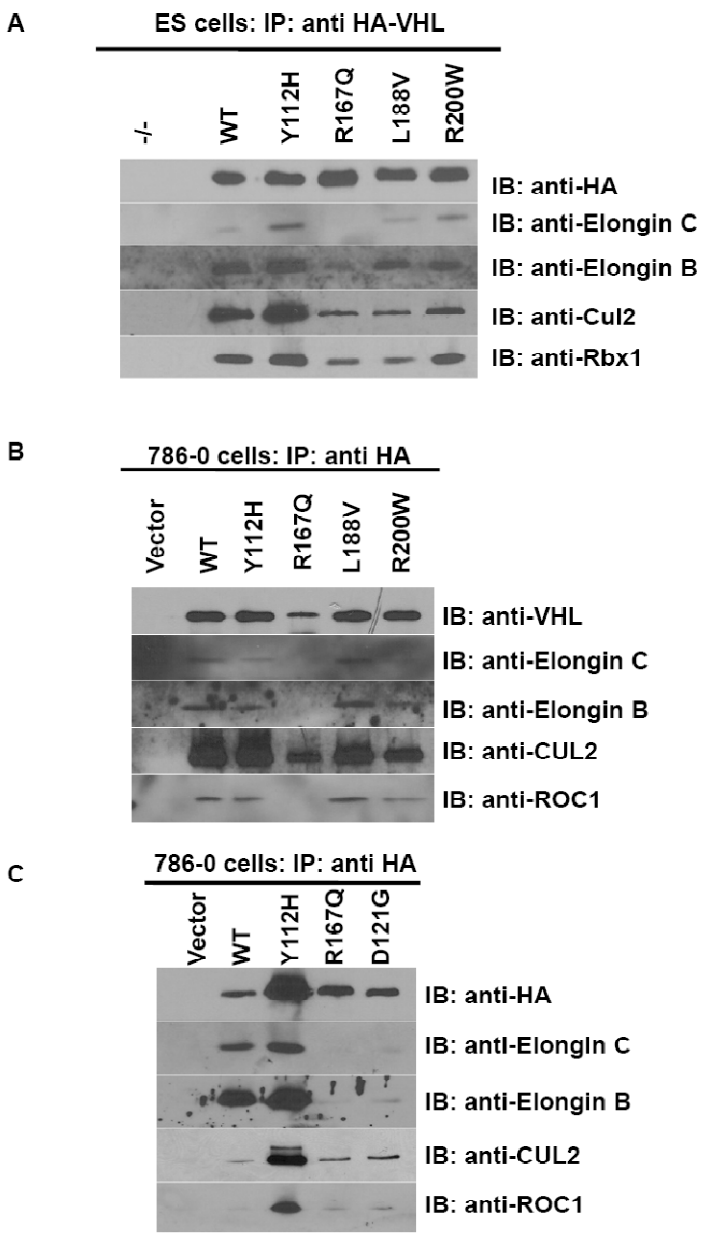

Figure 2.2. Co-immunoprecipitation of VBC complex proteins with type 2B mutant pVHL. A. Anti-HA immunoprecipitation of HA-pVHL and associated VBC complex members in transgenic ES cell clones. Anti-HA IP products were probed for successful pull-down of WT or mutant HA-pVHL and for co-IP of the indicated VBC complex members in stably-transfected *Vhl*$^{-/-}$ murine ES cells. B. and C. Anti-HA immunoprecipitation of HA-pVHL from transgenic 786-0 clones. Anti-HA IP products were probed for successful pull-down of WT or mutant HA-pVHL by anti-pVHL (B) or anti-HA (C) immunoblot and for co-IP of the indicated VBC complex members in stably-transfected 786-0 cells.

formation of a remnant complex is limited to the specific Type 2B mutant R167Q HA-pVHL or is more broadly relevant to Type 2B VHL disease. Again, pVHL-associated proteins were co-immunoprecipitated, and pull-down of HA-pVHL was confirmed for each IP by anti-VHL (Figure 2.2B) or anti-HA (Figure 2.2C) immunoblot, followed by detection of known VBC complex members by protein-specific co-IP immunoblot (Figures 2.2B and 2.2C). Both R167Q and D121G mutant HA-pVHL failed to demonstrate a strong interaction with Elongin C, although robust association was detected for wild-type and the other mutant HA-pVHL proteins. The remaining VBC complex members were again associated with wild-type and all of the HA-pVHL mutants tested, including the Type 2B mutants R167Q and D121G. This experiment suggests that both of the Type 2B mutant HA-pVHL proteins studied may retain at least partial interaction with Elongin C and recruit a complex containing the essential human VBC E3 ubiquitin ligase components CUL2 and ROC1.

To confirm the observed interaction between R167Q HA-pVHL and CUL2, a myc-tagged CUL2 protein was transiently expressed in stable 786-0 cell lines expressing wild-type or RCC-associated mutant HA-pVHL for reverse co-IP studies (Figure 2.3). Cell extracts were subjected to anti-myc-agarose IP, and pull-down of myc-CUL2 was confirmed by anti-CUL2 immunoblot. Anti-HA co-IP immunoblot verified the results depicted in Figure 2B-C, displaying myc-CUL2 interaction with wild-type, Y112H, and R167Q HA-pVHL.

Type 2B mutant pVHL retains HIF-1α-ubiquitylating activity. To determine if the remnant R167Q HA-pVHL – CUL2 complex retained E3 ubiquitin ligase

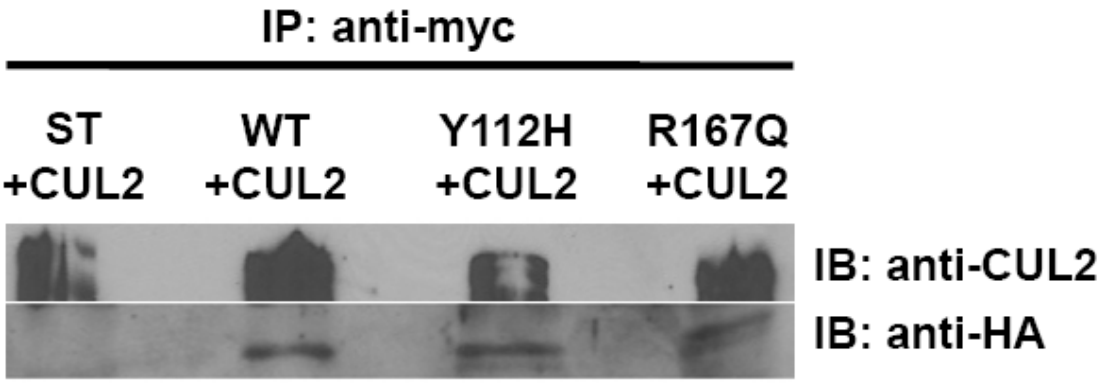

Figure 2.3. Reverse co-immunoprecipitation confirms CUL2-pVHL protein interaction in R167Q mutation. Anti-myc immunoprecipitation of myc-CUL2 and associated HA-pVHL in 786-0 clones. Stable 786-0 clones expressing vector-only (ST) or WT or mutant HA-pVHL were transiently transfected with wild-type myc-tagged CUL2 and subjected to myc-IP. Upper panel, IP of Myc-tagged Cul2 detected by anti-CUL2 immunoblot. Lower panel, co-IP of WT and mutant HA-pVHL detected by anti-HA immunoblot.

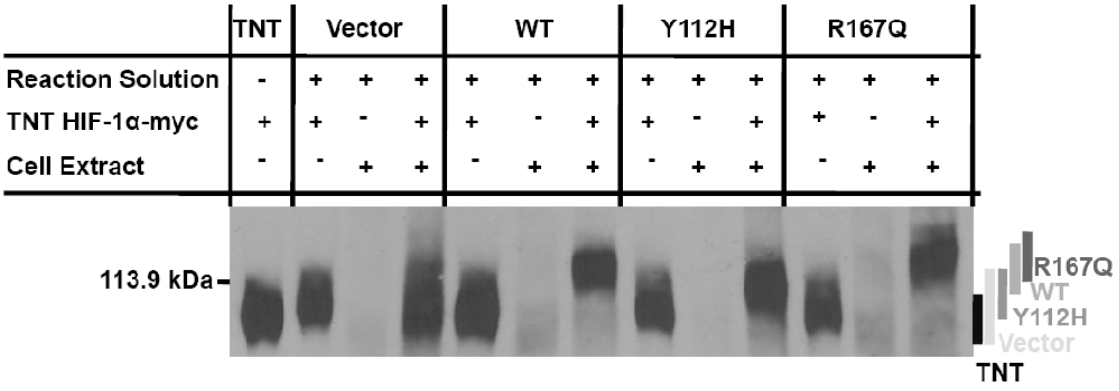

Figure 2.4. pVHL-dependent HIF-1α ubiquitylation in 786-0 cell lines. Anti-myc immunoblot to visualize migration shift of myc-tagged HIF-1α *in vitro*. Cell extracts from 786-0 clones expressing vector alone or WT or mutant HA-pVHL were incubated in the presence or absence of ubiquitylation reaction solution and TNT HIF-1α-myc and subjected to anti-myc immunoblot. A band representing unmodified TNT HIF-1α-myc, as depicted in the TNT lane, runs just below the ladder marker at 113.9 kDa. Upward shift of myc-HIF-1α, as seen in complete reaction lanes for WT and R167Q, indicates poly-ubiquitylation. The TNT HIF-1α-myc migration pattern for each complete reaction lane is graphically summarized to the right of the immunoblot.

activity, wild-type and mutant HA-pVHL were analyzed for competence to ubiquitinate HIF-1α using a modified version of the *in vitro* assay developed by Cockman *et al.* (63). Exogenous HIF-1α was used as the ubiquitylation target in this experiment as the 786-0 parental cell line lacks confounding endogenous HIF-1α expression. The R167Q and a second Type 2B mutation (Q195X) have been shown to retain interaction with HIF-1α (51). Retention of E3 ligase activity by the remnant R167Q mutant pVHL-CUL2 VBC complex, therefore, should correspond to preserved HIF-1α ubiquitylation *in vitro*.

In vitro-transcribed (TNT) myc-tagged full-length wild type human HIF-1α (HIF-1α-myc) was subjected to a modified *in vitro* ubiquitylation assay, using anti-myc immunoblot to visualize ubiquitylation of the HIF-1α-myc substrate (Figure 2.4, components of each analysis indicated above lane). The HIF-1α-myc protein migration for each cell line is summarized by a shaded line to the right of the immunoblot. TNT HIF-1α-myc substrate in the absence of reaction solution or cell extract served as a negative control for the unmodified electrophoretic mobility of the HIF-1α-myc protein. For each cell line in our assay, further controls were provided by excluding cell extract (first reaction) or TNT HIF-1α-myc substrate (second reaction). The third reaction for each cell line contained all three necessary components for the ubiquitylation reaction. An upward shift in HIF1α-myc mobility, as exemplified by the wild-type (WT) complete reaction, indicates HIF-1α-myc poly-ubiquitylation. The HIF-1α-myc protein was shifted only slightly upwards in the reaction utilizing extract from control vector-only 786-0 cells, demonstrating the basal pVHL-independent HIF-1α ubiquitylation present

in this system. Type 2A Y112H mutant HA-pVHL failed to promote HIF-1α-myc mobility shift beyond basal levels, confirming previous work by Cockman *et al*. (63). Notably, Type 2B R167Q mutant HA-pVHL promoted HIF-1α-myc mobility shift similar to WT HA-pVHL, demonstrating that the remnant R167Q HA-pVHL – Cullin-2 complex retains E3 ligase activity towards HIF-1α *in vitro*.

Discussion

In addition to the strong association of sporadic ccRCC with biallelic *VHL* inactivation and of VHL disease-associated ccRCC with subtype-specific germline *VHL* mutations, evidence from xenograft models of tumor growth strongly supports the requirement for pVHL-mediated HIF regulation in suppression of renal tumorigenesis. However, several lines of evidence suggest that dose-dependent effects on basal HIF levels influence *VHL*-associated tumor development and behavior. Our prior investigation in eupoloid primary ES cell lines, utilized as a strategy to avoid interference from transforming cancer cell events, demonstrated a bias toward HIF-2α dysregulation for VHL Type 2B mutation, and a graduated degree of HIF dysregulation across the disease subtypes (107). *In vitro* studies of RCC-predisposing Type 2A and Type 2B *VHL* missense mutations have revealed a correlation between the degree of mutant pVHL-mediated HIF-α dysregulation and risk of ccRCC (259). In a recent study performed in both 786-0 and a second RCC-derived cell line, RCC4, representative Type 2A and Type 2B *VHL* mutations demonstrated intermediate levels of HIF stabilization (257). Taken together, these results suggest that Type 2A and Type 2B mutant pVHL proteins retain an intermediate degree of HIF

regulation, rather than an “all-or-none” pattern of regulation, likely contributing to the distinct phenotypes observed in these VHL disease subtypes.

In this study, we observed intermediate HIF regulatory activity by Type 2A Y112H and Type 2B R167Q mutant HA-pVHL, which could underlie the distinct genotype-phenotype correlations and may provide insight into the biology of sporadic RCC as well. In previous reports of VBC complex formation, the ability of disease-specific mutant pVHL to bind Elongin C was used as a proxy for ability to recruit the remainder of the VBC complex. The absence of 2B mutant HA-pVHL interaction with Elongin C in co-IP studies led to conclusions that α-domain mutations in pVHL abolish VBC complex formation (57-59, 260, 261). We report here, however, that both R167Q and D121G Type 2B mutant HA-pVHL participate in a complex with CUL2, ROC1, and Elongin B, as well as potentially with Elongin C either transiently or with greatly reduced abundance.

The co-immunoprecipitation of VBC complex members with R167Q and D121G mutant HA-pVHL could be due to reduced or transient formation of a wild-type VBC complex and/or formation of an alternate pVHL-Cullin-2 complex with ubiquitin ligase activity. The low abundance of Elongins C and B in association with both representative Type 2B mutant pVHL proteins may represent a limited quantity of stable complete VBC complex. Existing crystal structures depict the pVHL α-domain interacting with the VBC complex only through Elongin C (55). However, the relatively abundant CUL2 and ROC1 in the mutant 2B VBC complex could point to a direct interaction between mutant HA-pVHL and CUL2 or the replacement of Elongins C and B with alternate adaptors

linking the mutant HA-pVHL to CUL2 – ROC1. Silver stain and proteomic analysis of our Type 2B mutant HA-pVHL immunoprecipitates failed to detect additional bands that could function as replacement adaptors in an alternate HA-pVHL – CUL2 complex (data not shown).

The Type 2B mutation R167Q has been shown to permit interaction between pVHL and HIF-α (51). Therefore, if able to recruit an active complete or alternate VBC complex, Type 2B pVHL should be able to direct HIF-α ubiquitylation. Indeed, we observed that R167Q mutant HA-pVHL existed in complex with CUL 2 and ROC1 and mediated wild-type levels of HIF-1α poly-ubiquitylation *in vitro*. Though the presence of ROC1 has been shown to stabilize the VBC complex (255), our results cannot discern whether endogenous levels of Type 2B mutant pVHL expression support formation of a stable or transient complex with CUL2. R167Q mutant pVHL has been shown to be relatively unstable *in vitro* (259), and subtype-specific clinical manifestations of VHL disease may derive from a combination of mutant pVHL stability and the stability and activity of the mutant VBC complex.

In summary, we have demonstrated that disease-associated mutant pVHL proteins retain endogenous HIF-2α regulation. Two representative Type 2B mutant pVHL proteins partially preserved interaction with VBC complex members despite reduced binding to Elongin C, and the Type 2B mutant R167Q pVHL retained wild-type levels of ubiquitin ligase activity towards its target HIF-1α *in vitro*. Taken together, our results show that at least a subset of Type 2B *VHL* missense mutations result in a partial or unstable but active VBC complex which

retains the ability to regulate HIF-α levels. Furthermore, our results support observations that *VHL* missense mutations generally confer lower levels of HIF-α stabilization than null or truncating Type 1 *VHL* mutations (107, 257) and provide mechanistic insight into this retained ubiquitin ligase activity.

Materials and methods

Cell Lines. *Vhl*-null embryonic stem (ES) cells or *VHL*-deficient 786-0 RCC cells were transfected with vectors specifying human wild-type *VHL* or representative *VHL* mutants Y112H (Type 2A), R167Q (Type 2B), L188V (Type 2C), or R200W (Chuvash polycythemia) using vectors and techniques as previously described (107). 786-0 cells expressing the *VHL* mutant D121G (Type 2B), generated as previously described (262), were generously provided by Dr. William Kim, Chapel Hill, NC. *Vhl*-null murine ES cells and transfected derivatives were maintained in culture media comprised of Dulbecco's Modified Eagle Medium (DMEM, various manufacturers), supplemented with 10% ES cell-certified fetal bovine serum (Invitrogen, Carlsbad, CA), non-essential amino acids, L-glutamine, 2-mercaptoethanol, and leukemia inhibitory factor, and were grown on gelatin-coated plates in the absence of feeder cells. Renal cell carcinoma 786-0 cells were acquired from the American Type Culture Collection (Manassas, VA). 786-0 cells and transfected derivatives were maintained in DMEM, supplemented with 10% FBS, non-essential amino acids, L-glutamine, and 2-mercaptoethanol. All cultures were maintained at 37ºC in 5% CO_2. For hypoxia mimetic experiments, cells in log-phase growth were placed in media

supplemented with 100mM cobalt chloride (Sigma, St. Louis, MO) or fresh unsupplemented media.

Immunoblot analysis. Cells were lysed in Mammalian Protein Extraction Reagent (M-PER; Pierce Biotechnology, Rockford, IL) supplemented with Complete Mini Protease Inhibitor Cocktail (Roche, Basel, Switzerland). The Bradford Quantification Method (Amresco, Solon, OH) was used to determine protein concentration. Cell lysates were resolved by SDS-PAGE and subsequently transferred to Hybond ECL nitrocellulose membrane (GE Healthcare, United Kingdom). Immediately following transfer, membranes were stained with Ponceau S to confirm even transfer, blocked in 5% nonfat dry milk diluted in phosphate-buffered saline containing 0.1% Tween-20 (PBS-T), and then probed with the following primary antibodies: rabbit polyclonal anti-HA tag (Abcam, Cambridge, MA: ab9110, 1:1000), mouse monoclonal anti-pVHL (Abcam, ab11189, 1:2000), rabbit polyclonal anti-cullin-2 (Abcam: ab1870, 1:1000), rabbit polyclonal anti-ROC1 (Abcam: ab2977, 1:500), goat polyclonal anti-Elongin C (Santa Cruz, Santa Cruz, CA: sc-1559, 1:200), rabbit polyclonal anti-Elongin B (Santa Cruz: sc-11447, 1:200), mouse monoclonal anti-Myc tag (Cell Signaling, Danvers, MA: 9B11, 1:1000), mouse monoclonal anti-HIF-2α (GeneTex, San Antonio, TX: GTX30123, 1:1000), and rabbit polyclonal anti-Ku80 (GeneTex: GTX70485, 1:2000). Secondary antibodies used were anti-mouse, anti-rabbit, and anti-goat IgG conjugated to horseradish peroxidase (various manufacturers) and detected with the ECL Plus Western Blotting System (GE Healthcare) using exposure to BlueLite autoradiography film (ISC BioExpress,

Kaysville, UT) and processing via a Kodak RP X-OMAT Processor (Rochester, NY).

Immunoprecipitation analysis. M-PER cell lysates were subjected to immunoprecipitation (IP) using either the Profound Mammalian HA Tag IP/Co IP Kit or the Profound Mammalian Myc Tag IP/Co IP Kit, as per manufacturer's specifications (Pierce Biotechnology). For the reverse co-IP analysis, stably-transfected 786-0 cell lines were transiently transfected with a plasmid encoding myc-tagged cullin-2, a generous gift from Dr. Y. Xiong, Chapel Hill, NC, using Solution V of the Amaxa Tranfection System (Amaxa, Gaithersberg, MD). Twenty hours post-transfection, transfected cells were incubated in media supplemented with 5 μM MG-132 (Calbiochem, Gibbstown, NJ) proteasome inhibitor or fresh unsupplemented media for four hours, followed by protein extraction with M-PER and IP analysis as above.

In vitro HIF-1α ubiquitylation assay. An *in vitro* ubiquitylation assay was adapted from the protocol developed by Cockman et al. (63). 786-0 cell lines incubated for four hours in 5μM MG-132 were washed and collected in PBS. The cells were then washed twice in Ub Extraction Buffer (20 mM Tris, pH 7.5, 5 mM Kcl, 1.5 mM $MgCl_2$, 1 mM DTT) and disrupted using a dounce homogenizer. The cell lysates were centrifuged at 10,000xg for 10 minutes at 4°C. Each reaction was set up in a total volume of 40 μL, containing 23 μL cell extract, 5 μL HIF1α-myc substrate, and 12 μL reaction solution. The "reaction solution" was composed of ATP Regenerating System (20mM Tris, pH 7.5, 10mM ATP (GE

Healthcare)), 10mM magnesium acetate (Promega Corporation, Madison, WI), 300 mM creatine phosphate, 0.5 mg/mL creatine phosphokinase (MP Biomedicals, LLC, Irvine, California), 20 μg ubiquitin, and 150 uM ubiquitin aldehyde (Biomol International, Plymouth Meeting, PA). When reactions excluded a specific component, nuclease-free dH_2O was substituted to maintain the total reaction volume. Reactions were incubated at 30°C for 270 minutes and then subjected to immunoblot analysis. HIF1α-myc substrate was produced through TNT® coupled Wheat Germ Extract Systems (Promega, Madison, WI) from a plasmid encoding full-length functional human HIF1α-myc protein, a generous gift from Dr. M. C. Simon, Philadelphia, PA.

Acknowledgements

The authors would like to acknowledge William Y. Kim, Yue Xiong, and Ian Davis for many helpful discussions.

CHAPTER THREE

VHL Type 2B gene models HIF-2α dysregulation *in vitro* and *in vivo*

Modified from Lee CM *et al*. 2009 (263).

Abstract

Von Hippel-Lindau (VHL) disease is caused by germline mutations in the *VHL* tumor suppressor gene, with Type 2B missense *VHL* mutations predisposing to renal cell carcinoma, hemangioblastoma, and pheochromocytoma. Type 2B mutant pVHL is predicted to be defective in hypoxia inducible factor (HIF)-α regulation. Murine embryonic stem (ES) cells in which the endogenous wild-type *Vhl* gene was replaced with the representative Type 2B *VHL* hotspot mutation R167Q ($Vhl^{2B/2B}$) displayed preserved physiologic regulation of both HIF factors with slightly more normoxic dysregulation of HIF-2α. Differentiated $Vhl^{2B/2B}$-derived teratomas over-expressed the joint HIF targets *Vegf* and *EglN3* but not the HIF-1α-specific target *Pfk1* and displayed a growth advantage over $Vhl^{-/-}$-derived teratomas, suggestive of a tight connection between perturbations in the degree and ratio of HIF-1α and HIF-2α stabilization and cell growth. $Vhl^{2B/2B}$ mice displayed mid-gestational embryonic lethality, while adult $Vhl^{2B/+}$ mice exhibited susceptibility to carcinogen-promoted renal neoplasia compared with wild-type littermates at twelve months. Our experiments support a model in which the representative Type 2B R167Q mutant

pVhl produces a unique profile of HIF dysregulation, thereby promoting tissue-specific effects on cell growth, development, and tumor predisposition.

Introduction

Von Hippel-Lindau (VHL) disease is an autosomal dominant inherited cancer susceptibility syndrome resulting from germline mutation of the *VHL* tumor suppressor gene which affects 1 in 36,000 live births in the US (27, 28). Specific classes of *VHL* mutations predispose to different spectrums of morbidity- and mortality-causing clinical phenotypes of VHL disease: retinal and central nervous system (CNS) hemangioblastoma, pheochromocytoma/paraganglioma, and renal cell carcinoma with clear cell histology (ccRCC) (48, 49). Type 1 *VHL* mutations predispose to ccRCC and hemangioblastoma (50). Type 2 missense *VHL* mutations predispose to pheochromocytoma, either alone (Type 2C) or in combination with hemangioblastoma and a high (Type 2B) or low (Type 2A) risk of ccRCC (51). Finally, individuals with homozygosity for the germline R200W *VHL* mutation develop Chuvash Polycythemia (CP), a rare benign congenital erythrocytosis with no associated cancer risk (52, 53).

The *VHL* gene encodes a 30 kDa protein, pVHL (21, 264). Wild-type pVHL has been reported to play roles in diverse biological processes including acting as the recognition domain for an E3 ubiquitin ligase complex (61, 62) composed of Elongins B and C (56, 57), cullin-2 (58), ROC1 (Rbx1) (60), and an E2 conjugating enzyme (61, 256). pVHL E3 ligase activity targets hypoxia inducible factor (HIF)-α subunits (63-66), a family of transcription factor subunits including HIF-1α and HIF-2α.

HIF-1α and HIF-2α coordinate cellular and whole-organism responses to hypoxia and are controlled at the level of stability and activity by oxygen-dependent hydroxylation. In normoxic conditions, a family of prolyl hydroxylases (74, 126, 127, 129) mediates the hydroxylation of HIF-α prolyl residues (71, 72, 128, 130), targeting HIF-α to pVHL for degradation (73, 75). In hypoxic conditions, the prolyl hydroxylases are inactive (127, 130, 265), resulting in stabilized, transcriptionally active HIF-α. Stabilized HIF-α heterodimerizes with ARNT/HIF-1β (76) to activate the transcription of target genes (77, 78). HIF-1α and HIF-2α target gene sets overlap in a highly context-dependent manner (79), but HIF-1α uniquely activates glycolytic enzymes (83).

Several lines of evidence implicate the *VHL/HIF* axis in the initiation of renal tumorigenesis. First, biallelic inactivation of *VHL* and over-expression of HIF targets is observed in both VHL disease-associated renal lesions and also 70-90% of sporadic ccRCC tumors (252, 266-268). Second, over-expression of HIF targets accounts for many histological and clinical features of ccRCC tumors, including their highly vascular natures and paraneoplastic erythrocytosis (269). Third, *Vhl* loss in primary cells directly results in upregulation of both HIF-1α and HIF-2α and recapitulates many features of RCC (106). Finally, emerging evidence points to the degree of HIF dysregulation impacting renal tumorigenesis. *In vitro* studies of cDNA expressed Type 2A and Type 2B mutant pVHL models revealed graded dysregulation of HIF-1α and HIF-2α (51, 63), correlating with the degree of risk for ccRCC (Type 1≥ Type 2B > Type 2A) (257, 259). Additionally, while Type 2B mutations are predicted to disrupt

pVHL:Elongin C interactions, preservation of HIF ubiquitylation activity has been observed, which would provide a permissive environment for HIF regulation (Hacker et al, 2008). The profile of HIF dysregulation may also have ramifications for tumor predisposition, as selective HIF-2α stabilization has been observed in murine embryonic stem (ES) cells transgenic for a Type 2B mutant *VHL* gene (107). These systems in addition to demonstrating mutation specificity are sensitive to pVHL levels.

Existing mouse models of VHL disease utilize null (110) or conditional null (111, 116) *Vhl* alleles, display homozygous embryonic lethality, and show a high penetrance of hepatic angiomas, uncommon in the human disease. A *Vhl* gene replacement model of Chuvash Polycythemia, however, was viable and conferred erythrocytosis in a milieu of very mild HIF-2α stabilization (112). To examine the activities of mutant pVHL relevant to human cancer, particularly with respect to missense mutation-specific effects on HIF regulation, we undertook a gene replacement approach to study Type 2B VHL disease in a mouse model. This model provides the first opportunity to examine the effect of a VHL disease-causing missense mutations in its pre-malignant context and under endogenous transcriptional, translational, and post-translational regulation. Murine ES cells homozygous for a representative mutant 2B *Vhl* allele displayed mild HIF-2α stabilization but functionally preserved HIF-1α suppression. *In vivo*, while homozygosity for the mutant 2B *Vhl* allele conferred mid-gestational embryonic lethality, heterozygous $Vhl^{2B/+}$ mice were viable and susceptible to carcinogen-promoted renal adenocarcinoma. Our genetic knock-in mouse model thus

provides a species-congruent cellular system and *in vivo* model in which to further examine the contributions of Type 2B *VHL* missense mutation to VHL disease-associated cancers.

Results

Generation and characterization of Type 2B Vhl ES cell lines. The Arginine 167 → Glutamine (R167Q) missense mutation is a hotspot in the human *VHL* gene with a tight genotype-phenotype correlation to Type 2B disease (27, 49). Localized to the pVHL α helical domain (Figure 3.1A), R167 is predicted to stabilize the α/β domain interface and interaction with Elongin C (55, 261). In the murine *Vhl* allele, this mutation corresponds to a guanine to alanine transition at position 518 (G518A).

To study the effect of 2B mutant pVhl on regulation of HIF-α and HIF targets, we targeted the endogenous murine *Vhl* locus with an R167Q mutant *Vhl* construct (Figure 3.1B) to generate $Vhl^{2B/+}$ and $Vhl^{2B/2B}$ ES cell lines. The targeting construct introduced a *HindIII* site, enabling verification of recombination by Southern analysis (Figure 3.1C), and the G518A mutation introduced a novel *HpyIV* restriction site for restriction-based PCR genotyping (Figure 3.1D). Quantitative RT-PCR analysis in $Vhl^{2B/2B}$ ES cells confirmed that 2B mutant *Vhl* was transcribed at wild-type levels (Figure 3.2A). $Vhl^{2B/+}$ cells expressed wild-type levels of pVhl, but $Vhl^{2B/2B}$ cells expressed greatly reduced levels of the 2B mutant pVhl (Figure 3.2B). A similar reduction in detectable 2B

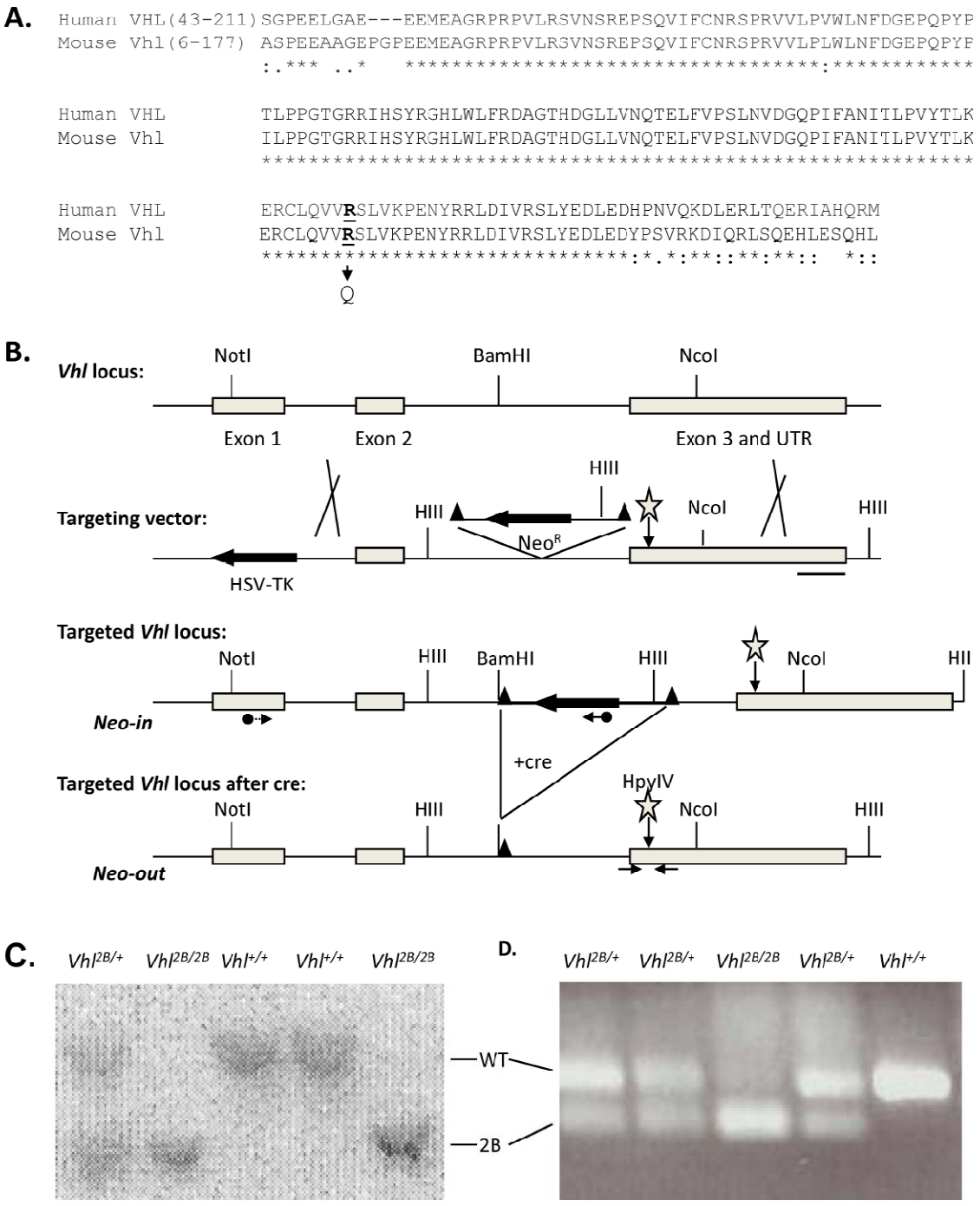

Figure 3.1. Type 2B *Vhl* mutation knock-in strategy and genotyping. A. Human:Mouse pVHL protein alignment. The R167Q pVHL substitution representing human Type 2B VHL disease is embedded in a highly homologous region. B. Type 2B mutant murine *Vhl* containing the G518A (R167Q) representative missense mutation (star) was prepared with site-directed mutagenesis and then cloned into the targeting vector as shown. Following electroporation of the targeting vector into J1 ES cells, neomycin and gancyclovir

mutant pVhl was also observed by immunoblot with an antibody raised against an alternate epitope suggesting that reduced detection of 2B mutant pVhl was not due to epitope-masking alone. Rescue with MG-132 treatment was not observed, consistent with the reduced protein expression and incomplete MG-132 rescue observed in the Chuvash Polycythemia *Vhl* gene replacement model (112).

Analysis of HIF and HIF target expression in Type 2B Vhl ES cells. The R167Q human pVHL mutation is predicted to destabilize the pVhl protein (259) and to disrupt pVhl recruitment of Elongin C (55), resulting in HIF factor dysregulation. ES cells in the presence or absence of the chemical hypoxia mimetic cobalt chloride ($CoCl_2$) were examined for HIF-1α (Figure 3.2C) and HIF-2α (Figure 3.2D) protein levels by immunoblot. Wild-type and $Vhl^{2B/+}$ ES cells displayed low basal levels of HIF-1α and HIF-2α and responded to $CoCl_2$ exposure with induction of both factors. $Vhl^{-/-}$ ES cells displayed maximal stabilization of both HIF-1α and HIF-2α without further induction. In contrast, $Vhl^{2B/2B}$ ES cells retained physiologic induction of both HIF-α factors with $CoCl_2$.

Figure 3.1. continued. resistance was used to select clones with homologous recombination at the endogenous murine locus (*Neo-in*). Cre recombinase exposure *in vitro* or *in vivo* resulted in excision of the floxed Neo^R cassette (*Neo-out*). C. Southern blot genotyping distinguished between wild-type and targeted *Vhl* alleles based on the introduction of new HindIII restriction sites. HindIII-digested murine *Vhl* was detected with a probe recognizing the *Vhl* 3' untranslated region (UTR, bar). D. Restriction PCR was used as an alternative genotyping strategy. Primers (arrows) flanking the targeted mutation generated a 300-bp PCR product. The novel restriction site introduced by the G518A mutation rendered the targeted *Vhl*-origin PCR product susceptible to HpyIV digestion.

While normoxic HIF-1α levels in *Vhl*$^{2B/2B}$ cells were similar to wild-type cells in independently-derived clones (Figure 3.2C), normoxic HIF-2α levels tended to be modestly elevated (Figure 3.2D). Qualitative comparisons were confirmed by densitometry analysis (Figure 3.3).

HIF-2α is transcriptionally inactive in ES cells (270). To determine whether *Vhl*$^{2B/2B}$ ES cells activate transcription of HIF target genes, we performed quantitative (q) RT-PCR for four known HIF target mRNAs (Figure 3.2E): the joint HIF-1α and HIF-2α targets *vascular endothelial growth factor* (*Vegf*), *glucose transporter 1* (*Glut1*), and *prolyl hydroxylase three* (*EglN3)* and the HIF-1α-specific glycolytic enzyme *phosphofructokinase (Pfk1*). *Vhl*$^{-/-}$ ES cells displayed transcription of all four HIF target mRNAs relative to wild-type J1 cells ($p<0.05$): *Vegf* (4.26-fold), *Glut1* (2.66-fold), *EglN3* (11.80-fold), and *Pfk1* (2.32-fold). Two independently-derived *Vhl*$^{2B/2B}$ clones, in contrast, failed to significantly over-transcribe any of the four HIF targets, consistent with the observation that *Vhl*$^{2B/2B}$ ES cells exhibit wild-type HIF-1α expression. Mirroring the qRT-PCR results, *Vhl*$^{-/-}$ ES cells secreted robust levels of Vegf protein (4.4-fold) compared to wild-type ($p<0.01$), while *Vhl*$^{2B/2B}$ ES cells did not secrete measurable Vegf (Figure 3.2F).

Type 2B Vhl promotes teratoma growth and vascularization. To observe the functional effects of Type 2B *Vhl* mutation, we differentiated our panel of ES cells in a teratoma assay. As expected from previous studies (107), *Vhl*$^{-/-}$-derived teratomas displayed a growth disadvantage. In contrast, the presence of one or two Type 2B *Vhl* alleles conferred a persistent growth advantage, such that

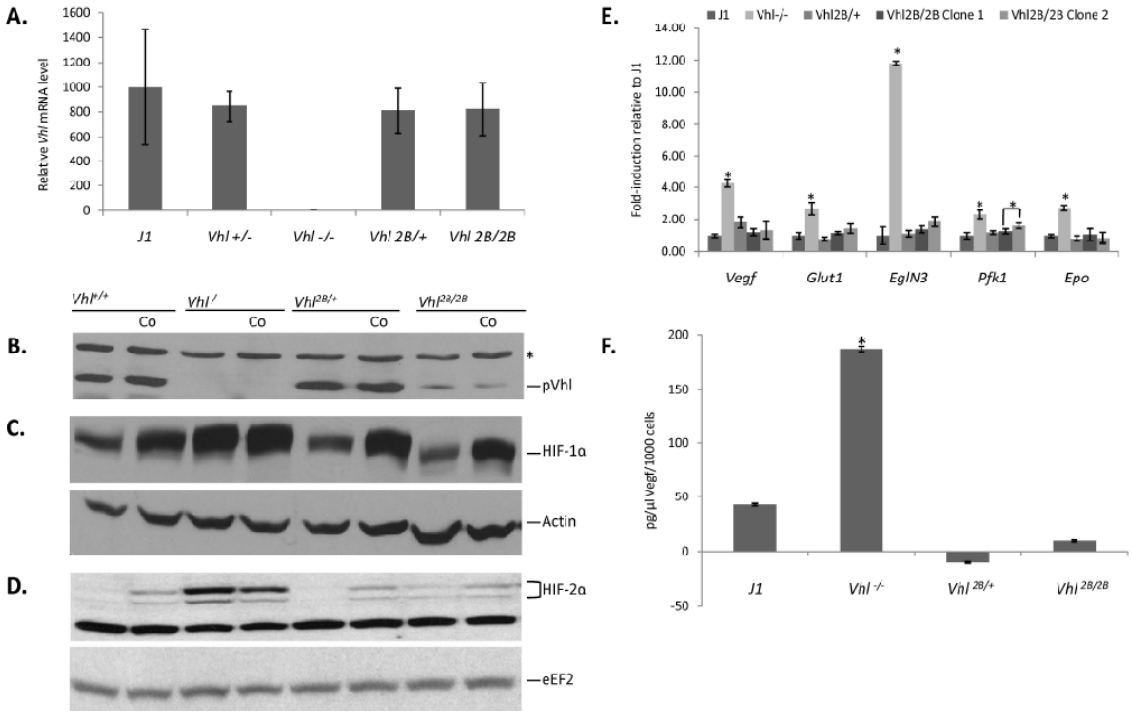

Figure 3.2. The Type 2B *Vhl* missense mutation results in a post-transcriptional reduction in mutant pVHL levels and slight normoxic HIF dysregulation but normal normoxic suppression of HIF target gene transcription in ES cells. A. Quantitative RT-PCR analysis for *Vhl* cDNA levels in ES cells relative to expression of the wild-type allele. Quantitation was normalized to an internal *18S* ribosomal RNA standard. Error bars indicate standard error of the mean (SEM). B.-D. Immunoblots for pVhl (B.), HIF-1α (C.), and HIF-2α (D.) expression in ES cells treated with or without the hypoxia mimetic $CoCl_2$ (Co) for four hours. E. Quantitative RT-PCR for normoxic transcriptional activation of HIF targets *Vegf*, *Glut1*, *EglN3*, and *Pfk1* in ES cells relative to J1. Cycle thresholds were corrected with *18S* ribosomal RNA. Error bars indicate SEM. *p<0.05 in paired comparison to J1. ELISA for secreted Vegf protein in ES cells relative to J1. *p<0.01 in paired comparison to J1.

Vhl$^{2B/2B}$-derived teratomas grew faster than *Vhl*$^{2B/+}$-derived teratomas, which in turn grew faster than wild-type teratomas (Figure 3.4A). At harvest, J1, *Vhl*$^{-/-}$, and *Vhl*$^{2B/+}$ teratomas were well-encapsulated, while *Vhl*$^{2B/2B}$ teratomas adhered to the overlying skin (not shown). *Vhl*$^{2B/2B}$ teratomas (Figure 3.4B, left) were also grossly hemorrhagic compared to *Vhl*$^{2B/+}$ (Figure 3. 4B, right) teratomas. Histologically, *Vhl*$^{-/-}$ teratomas were characterized by hemangioma (*) formation (Figure 3.4E), which was markedly enhanced in *Vhl*$^{2B/2B}$ teratomas (Figure 3.4F).

To determine whether Type 2B mutant pVhl preserves HIF regulation *in vivo*, teratomas were analyzed for HIF-1α and HIF-2α protein expression by immunoblot, confirming low levels of both HIF factors (Figure 3.5). To evaluate the effect on target gene expression, we performed quantitative RT-PCR for the panel of HIF target genes described above in three independent sets of teratomas. In one representative set (Figure 3.4G), the *Vhl*$^{-/-}$ teratoma displayed highly significant ($p<0.001$) over-expression of three of the four HIF targets relative to the J1 teratoma: *Vegf* (1.99-fold), *EglN3* (3.15-fold), and *Pfk1* (2.12-fold). In contrast to ES cells, the *Vhl*$^{2B/2B}$-derived teratoma exhibited significant over-expression of both *EglN3* (1.46-fold, $p<0.05$) and *Vegf* (1.87-fold, $p<0.001$) but failed to over-express the HIF-1α-specific target *Pfk1*. *Glut1* expression was not elevated for either *Vhl* mutant in this differentiated system.

Because *Vegf* expression alone was unlikely to account for the dramatic difference in vascularity between *Vhl*$^{-/-}$ and *Vhl*$^{2B/2B}$ teratomas, we performed a screen for candidate genes contributing to the vascular phenotype. The same

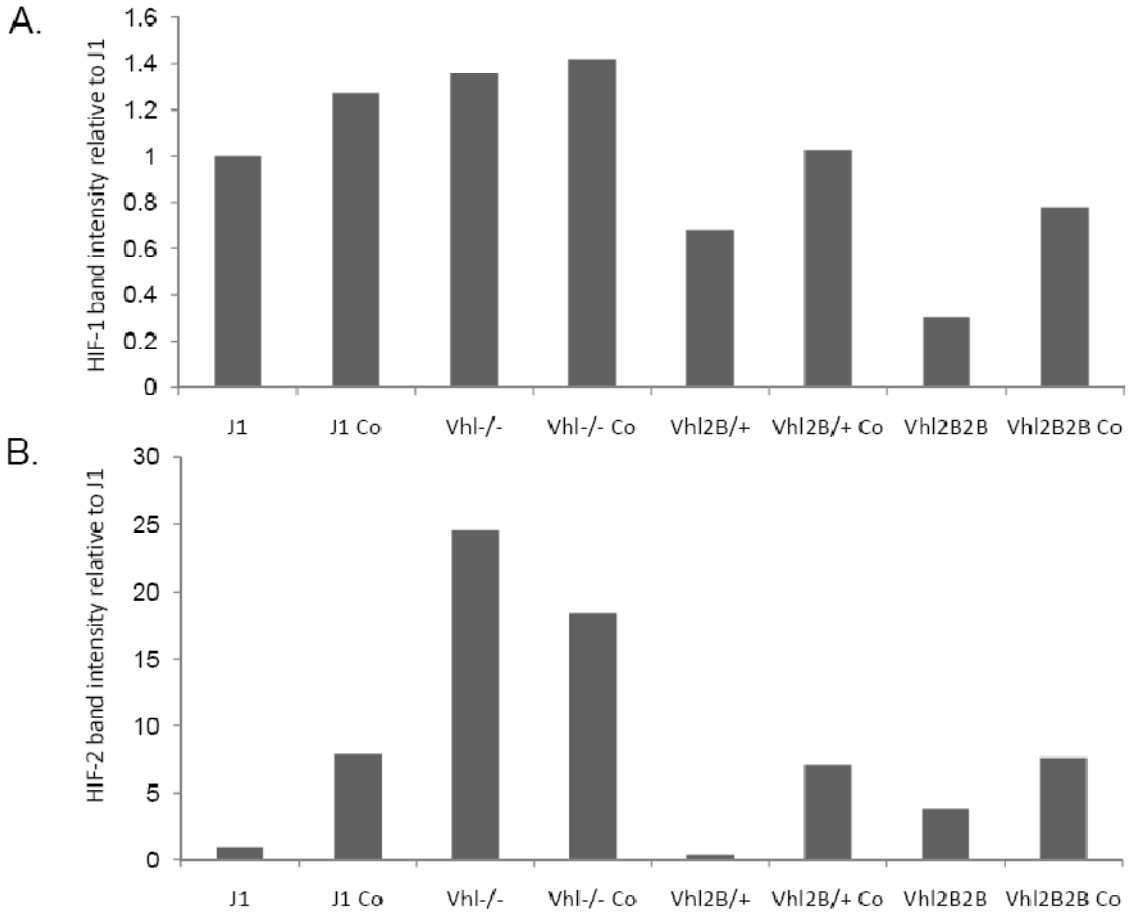

Figure 3.3. Densitometry analysis for ES cell HIF-1α and HIF-2α immunoblots. Experimental band intensity for each sample was determined relative to the corresponding loading control band using the ImageJ gel analysis tool. Co, treatment with Cobalt Chloride.

Figure 3.4 (next page). Homozygous Type 2B *Vhl* teratomas display growth advantage, enhanced hemangioma formation, and transcriptional dysregulation of HIF target genes. A. Growth curve for ES cell-derived teratomas (n=6 per genotype). Error bars indicate SEM. B. Gross appearance of representative $Vhl^{2B/2B}$ (left) and $Vhl^{2B/+}$ teratomas. C.-F. Histological analysis of representative J1 (C.), $Vhl^{-/-}$ (D.), $Vhl^{2B/+}$ (E.), and $Vhl^{2B/2B}$ (F.) teratoma morphology by H&E at 20X magnification. Note enhanced hemangioma (*) formation and hemorrhage in $Vhl^{2B/2B}$ relative to $Vhl^{-/-}$ teratoma. Scale bars indicate 100μm. G. Quantitative RT-PCR for transcriptional activation of HIF targets *Vegf*, *Glut1*, *EglN3*, and *Pfk1* in representative set of teratomas relative to J1. Cycle thresholds were corrected with *18S* ribosomal RNA. Error bars indicate standard deviation. *$p<0.05$. **$p<0.001$.

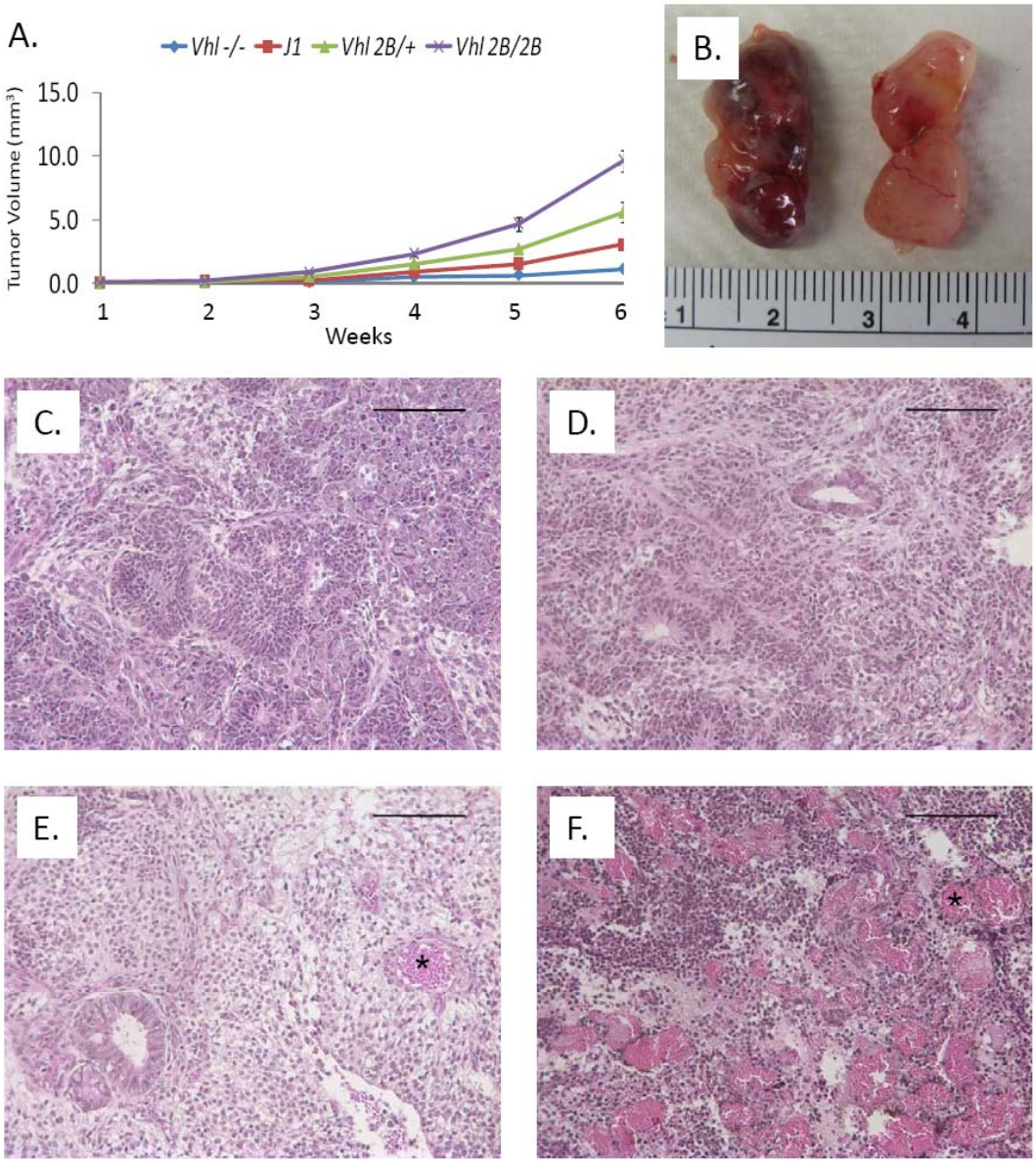
A.
Vhl -/-
J1
Vhl 2B/+
Vhl 2B/2B
Tumor Volume (mm³)
15.0
10.0
5.0
0.0
1
2
3
4
5
6
Weeks
B.
C.
D.
E.
F.
G.
J1
Vhl -/-
Vhl 2B/+
Vhl 2B/2B
Fold-induction relative to J1
4.0
3.0
2.0
1.0
0.0
Vegf
Glut1
EglN3
Pfk1

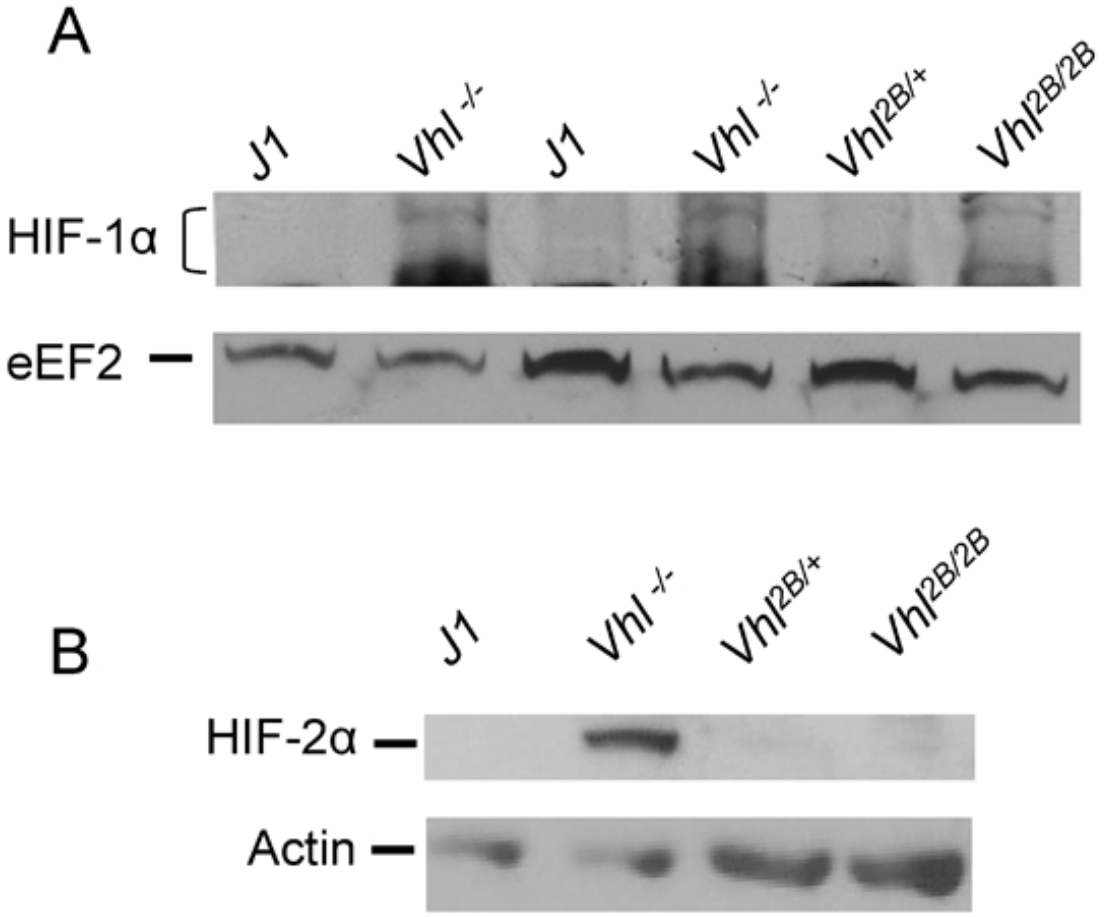

Figure 3.5. Homozygous Type 2B teratomas display sub-maximal HIF stabilization compared to null. Immunoblots for HIF-1α (A), and HIF-2α (B), and eEF2 and actin (loading controls, respectively) on extracts prepared from fresh teratoma tissue harvested at six weeks post-injection.

three independent sets of teratomas described above were assayed for expression of 84 angiogenesis-related genes using the commercial qRT-PCR RT^2 Profiler system. Genes selected for further assessment were significantly or near-significantly ($p<0.06$) over-expressed (>2.0-fold) or under-expressed (<0.3-fold) in one *Vhl*$^{-/-}$ and/or *Vhl*$^{2B/2B}$ teratoma relative to the average expression of three independent J1 teratomas.

Four novel angiogenesis-related candidate genes, in addition to *Vegfa,* were uncovered in the candidate screen and validated by qRT-PCR with independent primers : *vascular endothelial (VE)-cadherin* (*Cdh5*), the TgfβR endothelial co-receptor *endoglin* (*Eng*), *Vegf receptor 2* (*Kdr*), and the Vegfr2 co-receptor *neuropilin-1* (*Nrp1*). All four are considered direct HIF targets (271-274). While both the *Vhl*$^{-/-}$ and *Vhl*$^{2B/2B}$ teratomas significantly over-expressed *Cdh5*, *Eng*, and *Kdr* relative to the J1 teratoma, the *Vhl*$^{2B/2B}$ teratoma additionally significantly ($p<0.001$) over-expressed *Nrp1* relative to both J1 and *Vhl*$^{-/-}$ (Figure 3.6A).

To further explore the differences in vascular proclivity between *Vhl*$^{-/-}$ and *Vhl*$^{2B/2B}$ teratomas, we examined the ability of embryoid bodies derived from ES cells of each genotype to differentiate into primitive vascular structures *in vitro*. As visualized by PECAM immunofluorescence, J1-derived embryoid bodies developed a vascular plexus consisting of long, well-formed primitive vessels with branching at regular intervals (Figure 3.6B). *Vhl*$^{-/-}$-derived embryoid bodies

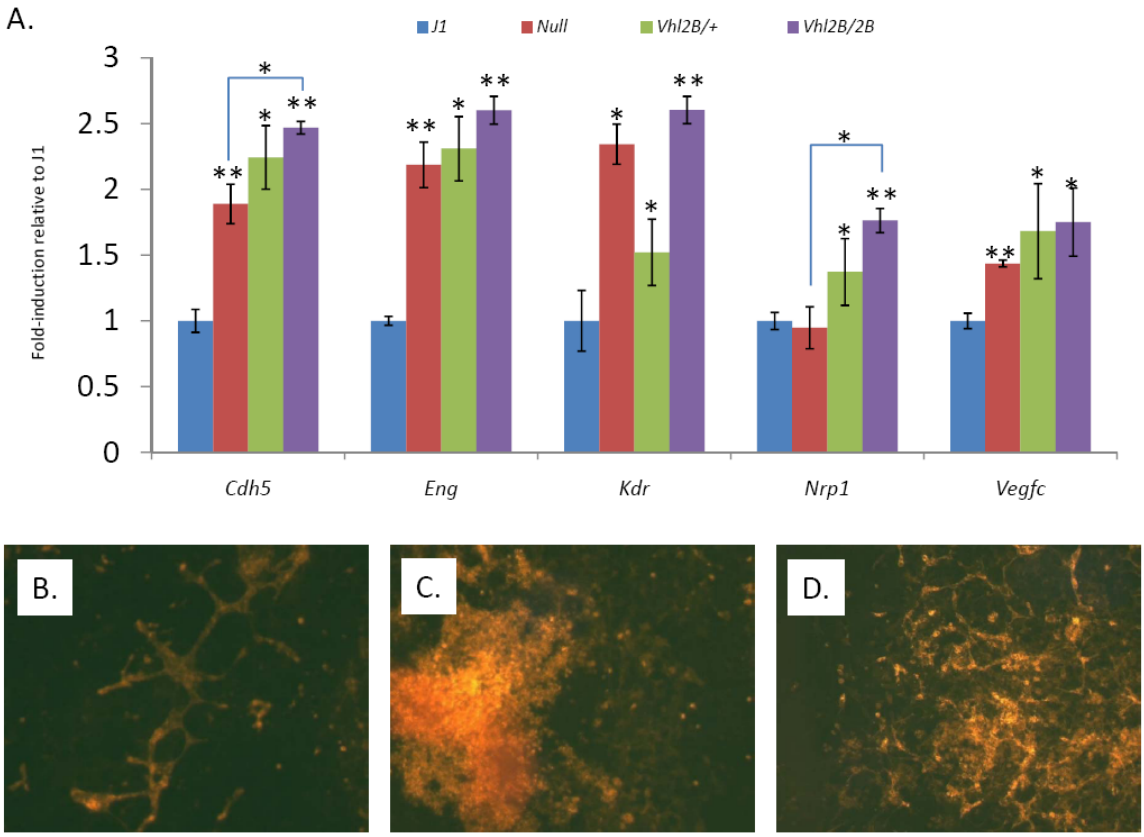

Figure 3.6. Exploration of hyper-angiogenic phenotype of homozygous Type 2B *Vhl* teratomas. A. Quantitative RT-PCR for transcriptional activation of angiogenesis-related genes *Cdh5*, *Eng*, *Kdr*, *Nrp1*, and *Vegfc* in a representative set of teratomas relative to J1. Cycle thresholds were corrected with *18S* ribosomal RNA. Error bars indicate standard deviation. *p<0.05. **p<0.001. B.-D. PECAM immunofluorescent visualization of vascular structures generated from *in vitro* differentiation of embryoid bodies derived from J1 (B.), $Vhl^{-/-}$ (C.), and $Vhl^{2B/2B}$ (D.) ES cells.

differentiated into large, diffuse clumps of PECAM-positive cells but failed to sprout primary vessels (Figure 3.6C). Finally, *Vhl*$^{2B/2B}$-derived embyroid bodies differentiated into a disorganized vascular plexus characterized by relatively short primitive vessels with haphazard, excessive sprouting and a background of unincorporated PECAM-positive cells (Figure 3.6D). Altogether, these results suggest that the *Vhl*$^{2B/2B}$ genotype engenders conditions more permissive for angiogenesis and cell growth than the *Vhl*$^{-/-}$ genotype.

*Homozygosity for Type 2B Vhl confers embryonic lethality***.** To examine 2B mutant pVhl function in murine development *in vivo*, we derived *Vhl*$^{2B/+}$ knock-in mice from our targeted murine ES cells. Inter-heterozygous matings resulted in a 2:1 ratio of *Vhl*$^{2B/+}$ to wild-type pups and a complete absence of *Vhl*$^{2B/2B}$ pups (Table 3.1). To pinpoint the window of *Vhl*$^{2B/2B}$ intrauterine demise, we genotyped embryos resulting from timed matings at embryonic day (E) 9.5 and E10.5. While *Vhl*$^{2B/2B}$ embryos were present at near-expected levels at E9.5, only one *Vhl*$^{2B/2B}$ embryo (3%) survived at E10.5. Because reliance switches from yolk sac to placenta around E9.5 (275), *Vhl*$^{2B/2B}$ embryonic lethality observed at E9.5-E10.5 implicates placental failure.

Table 3.1. *Vhl* genotype analysis of inter-heterozygous matings at birth and embryonic time points.

Vhl	**E9.5**	**E10.5**	**Birth**
+/+	14 (32%)	13 (45%)	60 (36%)
2B/+	20 (49%)	15 (52%)	107 (64%)
2B/2B	8 (19%)	1 (3%)	0 (0%)
Total	42	29	167

Vhl$^{-/-}$ embryos display embryonic lethality at E9.5-E12.5 due to an embryonic-origin defect in placental labyrinth vascularization. While the presumptive *Vhl*$^{-/-}$ labyrinth is normal in histological appearance at E9.5, *Vhl*$^{-/-}$ allantoic vessels fail to invade the chorionic plate, preventing induction of chorionic plate trophoblast cell differentiation into syncitiotrophoblast cells and later manifesting as an absence of fetal blood spaces in the labyrinth at E10.5 (110). To visualize whether the 2B mutant *Vhl* allele acts similarly to the null allele in the placenta, we compared wild-type (not shown), *Vhl*$^{2B/+}$, and *Vhl*$^{2B/2B}$ placentas by H&E for morphology and IHC for pVhl and the HIF target Vegfa. By H&E, representative E9.5 *Vhl*$^{2B/+}$ (Figure 3.7A) and *Vhl*$^{2B/2B}$ (Figure 3.7D) placentas displayed comparable chorionic villous fold formation and maternal red blood cell content in the spongiotrophoblast layer, but allantoic vessels, demarcated by the presence of nucleated fetal red blood cells (*), invaded the chorionic villi to a lesser extent in the *Vhl*$^{2B/2B}$ placenta. Despite the reduced Type 2B pVhl levels observed by immunoblot in *Vhl*$^{2B/2B}$ ES cells, spongiotrophoblast and giant cell pVhl expression was comparable between representative *Vhl*$^{2B/2B}$ (Figure 3.7E) and *Vhl*$^{2B/+}$ (Figure 3.7B) placentas by IHC. Finally, consistent with findings in *Vhl*$^{-/-}$ placentas at E10.5 (110), *Vhl*$^{2B/2B}$ placenta (Figure 3.7F) displayed absent or greatly reduced spongiotrophoblast and giant cell Vegf expression relative to *Vhl*$^{2B/+}$ (Figure 3.7C) by IHC. While perhaps counter-intuitive, evidence supports decreased Vegf expression as a marker of placental failure rather than an indicator of HIF dysregulation in the murine placenta (276).

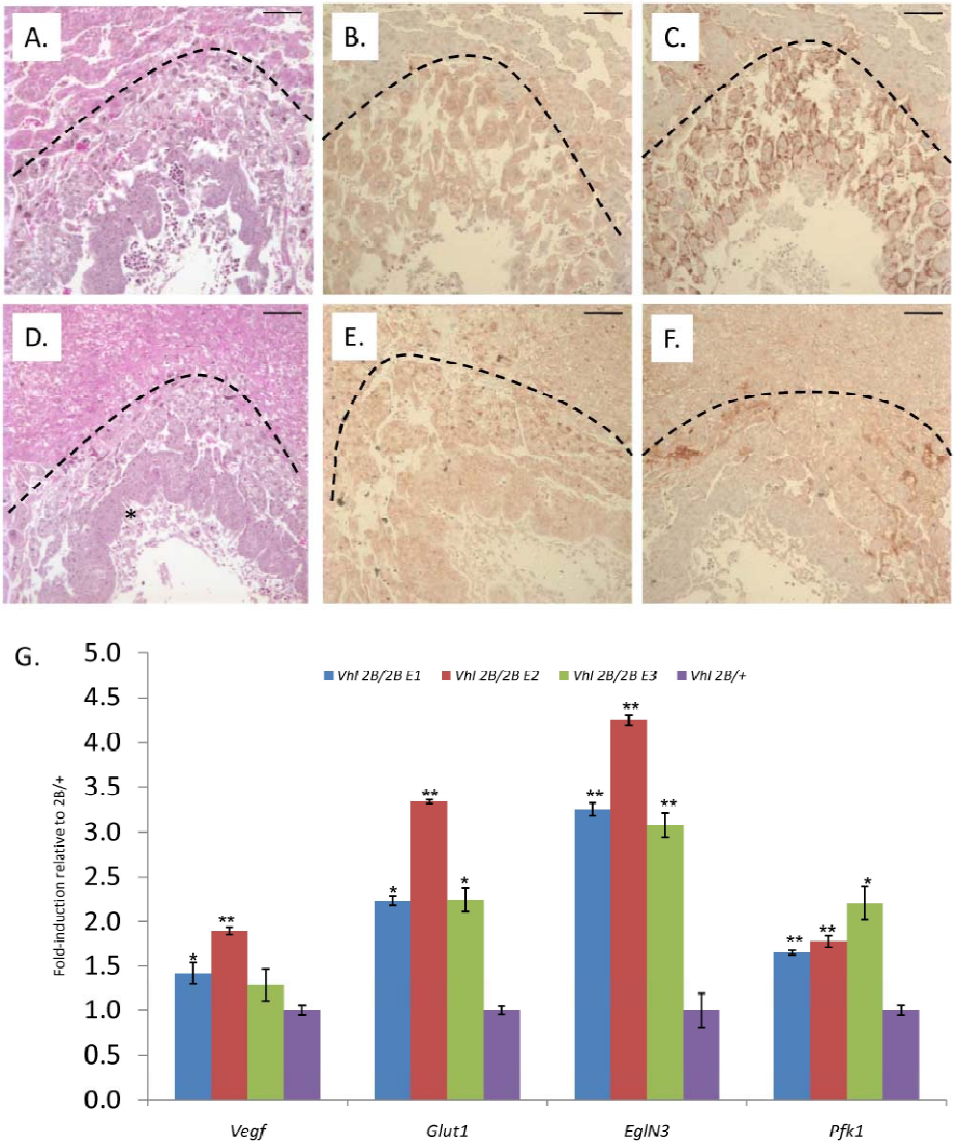

Figure 3.7. Homozygous Type 2B *Vhl* placentas display subtle vascular defects consistent with a *Vhl*-null phenotype, and corresponding embryos display HIF target dysregulation despite normal morphology. A.-F. Histological analysis of $Vhl^{2B/+}$ (A.-C.) and $Vhl^{2B/2B}$ (D.-F.) murine placentas, with H&E stain for morphology (A., C.) and immunohistochemistry for pVhl (B., E.) and for the HIF target Vegfa (C., F.) at 10X magnification. Arcs demarcate the maternal decidua (above) and placental (below) tissues. Note the lack of nucleated fetal RBCs (*) in the chorionic villi in $Vhl^{2B/2B}$ (D.) versus $Vhl^{2B/+}$ (A.) placentas. G. Quantitative RT-PCR for transcriptional activation of HIF targets *Vegf*, *Glut1*, *EglN3*, and *Pfk1* in E9.5 $Vhl^{2B/2B}$ embryos relative to representative $Vhl^{2B/+}$ littermate. Cycle thresholds were corrected with *18S* ribosomal RNA. Error bars indicate SEM. *p<0.05. **p<0.001.

Because E9.5 embryos were the only *Vhl*$^{2B/2B}$ animal tissues available for molecular study, we used these tissues to analyze the competence of Type 2B pVhl to regulate HIF target genes *in vivo*. Though *Vhl*$^{2B/2B}$ embryos are grossly and histologically normal at E9.5, we hypothesized that they might still demonstrate subtle HIF target gene dysregulation. Quantitative RT-PCR on three *Vhl*$^{2B/2B}$ E9.5 embryos showed significant ($p<0.05$) over-expression of the four HIF target genes studied relative to a *Vhl*$^{2B/+}$ E9.5 embryo, paralleling the effect of *Vhl* mutation on HIF-regulated signaling observed in the differentiated teratoma model system (Figure 5G): *Vegf* (average 1.54–fold), *Glut1* (average 2.60–fold), *EglN3* (average 3.53–fold), and *Pfk1* (average 1.88–fold). In notable contrast to ES cells and teratomas and in keeping with the reported highly tissue- and context-specific transcriptional effects of HIF stabilization, homozygosity for the 2B *Vhl* allele produced sufficient HIF-1α dysregulation to permit over-expression of the HIF-1α-specific target *Pfk1* in the E9.5 embryo, with potential contribution by physiologic embryonic hypoxia.

Heterozygous Type 2B Vhl mice develop renal cysts. As Type 2B VHL disease predisposes to pheochromocytoma, hemangioblastoma, and ccRCC in humans, *Vhl*$^{2B/+}$ mice (n=105) were aged to three, six, nine, twelve, and eighteen months and observed for tumor susceptibility. Representative H&E images of *Vhl*$^{2B/+}$ tissues at twelve months are presented in Figure 3.8 (A-C). Similar to prior models, *Vhl*$^{2B/+}$ mice displayed frequent enlarged vessels (angiectasis) in the kidney and adrenal gland (Figure 3.8B, *) (110, 111, 116) and renal cortical microcysts (3%, Figure 3.8A, Cy) (111). Renal cortical cysts were not observed

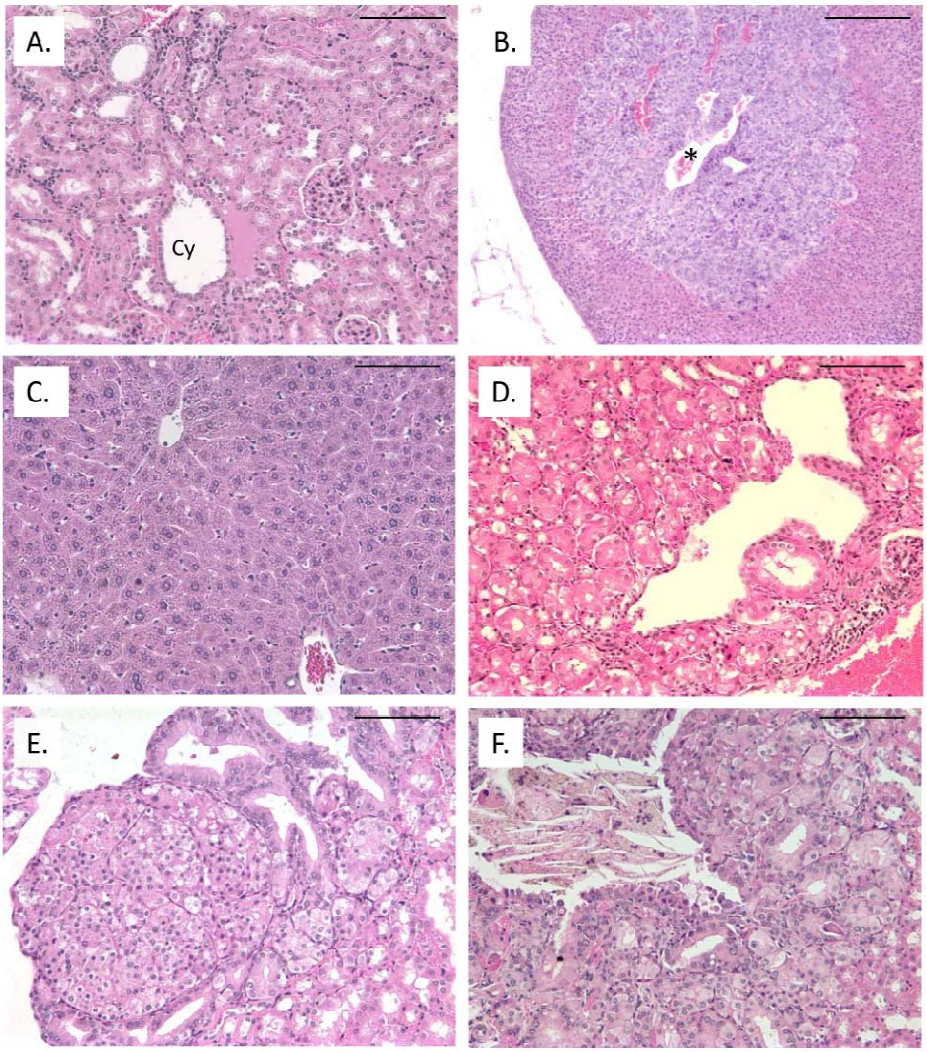

Figure 3.8. Adult Type 2B *Vhl* heterozygous mice develop mild vascular lesions and rare renal cortical microcysts, while transplacental ENU mutagenesis reveals renal tumor predisposition. A. – D. Histological analysis of representative adult Type $Vhl^{2B/+}$ mouse tissues, including kidney (A.), adrenal gland (B.), and liver (C.) by H&E stain at 20X magnification. $Vhl^{2B/+}$ mice frequently developed renal (not shown) and adrenal (B., *) angiectasis and occasionally developed simple renal cortical microcysts (A., Cy). E. – F. Histological analysis of ENU-mutagenized $Vhl^{2B/+}$ mice by H&E stain at 20X magnification. While ENU mutagenesis promoted benign simple and papillary microcysts formation in both $Vhl^{2B/+}$ (not shown) and wild-type littermates (D.), borderline adenoma/adenocarcinoma (E.) and adenocarcinoma (F.) were selectively observed in mutagenized $Vhl^{2B/+}$ mice at twelve months. Scale bars indicate 100μm.

in wild-type littermates. In contrast to prior studies, *Vhl*$^{2B/+}$ liver histology was uniformly normal (Figure 3.8C).

*Transplacental mutagenesis promotes renal tumorigenesis in Type 2B Vhl mice***.** We hypothesized that accelerating somatic mutations via mutagenesis might reveal predisposition to cancer development in *Vhl*$^{2B/+}$ mice. ENU mutagenesis has traditionally been used as a tool to screen for dominant and recessive mutations in the mouse germline but has also been used in mouse adults and embryos. ENU is a DNA alkylating agent which primarily generates A-T→T-A transversions and A-T→G-C transitions, most often resulting in missense mutations and splicing errors(277). ENU is an ideal chemical for transplacental (*in utero*) renal mutagenesis: ENU does not require metabolic activation, the DNA repair enzymes responsible for repairing ENU lesions display low activity in the fetal kidney, and the fetal kidney is susceptible to mutagenesis in a wide range of embryonic days and ENU dosages (278). Transplacental ENU mutagenesis has been utilized successfully in mouse models of another HIF-related autosomal dominant tumor predisposition syndrome called Tuberous Sclerosis. In mice heterozygous for a null allele of *Tsc2* or *Tsc1*, transplacental ENU mutagenesis accelerates onset of renal cysts and hepatic angiomas (192, 193). Wild-type and *Vhl*$^{2B/+}$ embryos from timed inter-heterozygous matings were treated with ENU at E14.5 and allowed to age to four (n=12) and twelve months (n=24) in a pilot study. At sacrifice, grossly abnormal organs and organs of interest were harvested. Renal lesions observed in mutagenized mice are summarized in Table 3.2 below.

Table 3.2. Summary of renal lesions observed in ENU-mutagenized *Vhl*$^{2B/+}$ and wild-type littermates.

	4 months		*12 months*	
	Vhl $^{+/+}$ (n=4)	*Vhl* $^{2B/+}$ (n=8)	*Vhl* $^{+/+}$ (n=14)	*Vhl* $^{2B/+}$ (n=10)
Renal Microcyst(s)	3	6	11	7
-Papillary	3	1	2	1
Pre-neoplasia	0	1	0	0
Neoplasia	0	0	0	2

At four months, both wild-type (2/4) and *Vhl*$^{2B/+}$ (6/8) mutagenized mice displayed macroscopic subpleural lung nodules, indicating successful ENU mutagenesis (279). Both wild-type and *Vhl*$^{2B/+}$ mutagenized mice displayed simple and papillary cortical renal microcysts on H&E-stained sections, suggesting that ENU mutagenesis effectively promotes benign renal cyst formation in this C57BL/6 genetic background. While all three papillary renal cysts observed in mutagenized wild-type mice displayed benign histology, the papillary cyst in observed in a mutagenized *Vhl*$^{2B/+}$ mouse displayed pre-neoplastic changes (not shown).

At twelve months, histological findings in wild-type mutagenized mice were limited to benign papillary cysts (Figure 3.8D). However, *Vhl*$^{2B/+}$ mutagenized mice (2/10) developed pathological findings typical of VHL disease. One *Vhl*$^{2B/+}$ mouse developed a borderline clear-cell adenoma/adenocarcinoma (Figure 3.8E) featuring a large nest of cells (alveolus) with clear-cell histology, vascular stroma, and absent tubular architecture as well as several clear-cell alveoli invading into the underlying renal cortex. A second affected *Vhl*$^{2B/+}$ mouse developed

adenocarcinoma (Figure 3.8F) featuring nests of clear cells, central necrosis, absent tubular architecture, vascular stroma, and a poorly defined border. Statistical analysis suggested that *Vhl* mutation correlated with or trended toward development of neoplasia at 12 months (Pearson's χ^2 p=0.037, Fisher's exact test p=0.101).

Discussion

Germline Type 2B missense mutations in *VHL* predispose to ccRCC, CNS and retinal hemangioblastoma, and pheochromocytoma and paraganglioma. In our murine gene replacement system, which models one VHL type 2B disease mutation, R167Q, generated a unique pattern of HIF-1α and HIF-2α dysregulation, differing from *Vhl*-null both in degree and ratio of HIF stabilization as well as in functional outcome in *in vitro* and *in vivo* studies.

Our gene replacement system takes advantage of the euploid genetic background of murine ES cells and avoids the potential mouse-human interactions and over- and mis-expression artifacts inherent to transgenic models. We observed reduced levels of 2B mutant pVhl protein in homozygous ES cells, supporting the hypothesis that ccRCC-predisposing *VHL* missense mutations produce less stable proteins, as posited on the basis of structure analysis (55, 259). In contrast to $Vhl^{-/-}$ ES cells, $Vhl^{2B/2B}$ knock-in ES cells expressed low basal levels of HIF-1α and HIF-2α and induced both subunits physiologically in response to the hypoxia mimetic $CoCl_2$. Consistent with this finding, $Vhl^{2B/2B}$ ES cells displayed wild-type levels of four HIF target genes studied, suggesting that HIF-1α levels in $Vhl^{2B/2B}$ cells failed to surpass a

threshold required for transcriptional activation at target promoters in this cell type.

The differentiated teratoma system allowed observation of 2B mutant pVhl function in a setting permissive for both HIF-1α and HIF-2α transcriptional activity. Previous work in *Vhl*$^{-/-}$ teratomas has demonstrated that maximal activation of both HIF-1α and HIF-2α promotes angiogenesis but retards three-dimensional tumor growth (106). Genetic knock-out of HIF-1α (280) or replacement of HIF-1α with HIF-2α (281) in teratomas enhances tumor growth and implicates HIF-1α as the growth-suppressive factor in this assay. In our studies, *Vhl*$^{-/-}$ teratomas likewise displayed a growth disadvantage relative to wild-type and additionally featured over-expression of the joint HIF targets *Vegfa* and *EglN3* and the HIF-1α-specific target *Pfk1*, all indicating HIF-1α and HIF-2α stabilization. *Vhl*$^{2B/2B}$ teratomas, in contrast, displayed a marked growth advantage relative to wild-type, and over-expression of *Vegfa* and *EglN3,* but not *Pfk1*, suggestive of sub-threshold HIF-1α but sufficient HIF-2α stabilization to promote transcriptional activity.

The placental failure and lethality observed in *Vhl*$^{2B/2B}$ embryos at E9.5-E10.5 was consistent with severely hypomorphic mutant pVhl function in the embryonic allantoic endothelium. Reduced pVhl stability alone is unlikely to be the cause of *Vhl*$^{2B/2B}$ embryonic lethality. First, 2B mutant pVhl levels in the E9.5 *Vhl*$^{2B/2B}$ placenta were similar to pVhl levels observed in the E9.5 *Vhl*$^{2B/+}$ placenta by IHC. Second, *Vhl*$^{CP/CP}$ mice are viable despite the measurable instability of R200W (CP) pVhl both *in vitro* and in murine tissues (112). Finally, there is

evidence of more severe HIF dysregulation in this *in vivo* system, with evidence of induction of the HIF-1α-specific target *Pfk1*, indicating both HIF-1α and HIF-2α stabilization. Thus, while it remains possible that the degree of pVhl reduction has a threshold effect on early developmental events, the reduced levels in these models serves to unmask added levels of regulation of the HIF transcriptional network.

Vhl$^{2B/+}$ mice developed renal cysts with frequency similar to that observed in *Vhl*$^{+/-}$ mice (~3%) and likewise failed to develop dysplasia or renal adenocarcinoma, indicating that *Vhl* mutation alone is insufficient for invasive renal tumor formation in the murine kidney. To accelerate the accumulation of somatic mutations in this mouse model and reveal tumor predisposition, we mutagenized *Vhl*-initiated and wild-type littermate mice with transplacental ENU. At twelve months post-ENU, renal adenocarcinoma was observed in mutagenized *Vhl*$^{2B/+}$ mice, representing the first demonstration of this tumor in a genetically-predisposed mouse model and validating *Vhl* mutation as a tumor-initiating event in the development of RCC.

Our gene replacement model of the representative Type 2B R167Q *Vhl* mutation bolsters emerging evidence that relative HIF-1α and HIF-2α protein abundance modulates the VHL Disease clinical phenotype and provides motivation for identifying the relevant genetic events involved in progressing *Vhl*-initiated tumors to invasive disease. More broadly, our *Vhl* gene replacement model provides a comprehensive species-congruent system for future

investigations of mutant pVhl HIF and non-HIF functions underpinning human VHL Disease both *in vitro* and *in vivo*.

Materials and methods

Generation of Vhl Type 2B ES cell lines and heterozygous mice. *Vhl* exons 2 and 3 (E2 and E3) were cloned into targeting and mutagenesis vectors, respectively, from a BAC clone as previously described (112, 281). PCR-based site-directed mutagenesis of G→A at position 518 was performed using forward primer 5'-AGAGCCTGGTCAAGCCTGAGAACTA-3' and reverse primer 5'-GCACAACCTGAAGGCACCGCTCTTT-3'. The G518A mutant E3 fragment was then cloned into pLNT-E2 adjacent to the neo^R cassette (pLNT-E2-E3) and reconfirmed with bidirectional sequencing.

The pLNT-E2-E3 targeting construct (Figure 3.1B) was electroporated into *Vhl* wild-type J1 strain Sv/129 ES cells for gene replacement at the endogenous murine *Vhl* locus. Homologous recombinants heterozygous for the $Vhl^{2B\ neo\text{-}in}$ allele were selected by gancyclovir and neomycin resistance, and positive clones confirmed by Southern blot analysis. Conversion of the second *Vhl* allele was achieved by selection with increasing amounts of neomycin to yield ES cells homozygous for the $Vhl^{2B\ neo\text{-}in}$ allele. $Vhl^{2B\ neo\text{-}in/+}$ and $Vhl^{2B\ neo\text{-}in/2B\ neo\text{-}in}$ ES cells were transiently transfected with a cre-expressing vector to remove the floxed neo^R cassette. The ES cells were screened at each stage by Southern blot for *in vitro* and *in vivo* studies of Type 2B mutant pVhl function.

Animal Models Core (University of Pennsylvania) staff injected karyotyped *Vhl*$^{2B\ neo\text{-}in/+}$ ES cells into C57BL/6 blastocysts. The chimeric blastocysts were then implanted in pseudopregnant C57BL/6 females. Highly chimeric mice (F0) were selected by Agouti coat color for crossing to C57BL/6 females. Germline transmission of the targeted allele to Agouti offspring (F1) was confirmed by Southern blot. A *Vhl*$^{2B\ neo\text{-}in/+}$ line was crossed to a cre deleter mouse strain (EIIa-cre) (282) for multiple generations, with excision of the floxed *neo*^{R} cassette verified by Southern blot, and then backcrossed to C57BL/6 to make a *Vhl*$^{2B/+}$ founder line. All subsequent generations were genotyped by restriction PCR utilizing PCR primers flanking a novel HpyIV restriction site introduced by the G518A *Vhl* mutation (Figure 3.1D).

All mouse procedures were approved by the University of Pennsylvania and University of North Carolina Institutional Animal Care and Use Committees.

Cell Culture Studies. Cell culture studies were performed at 37ºC, 5% CO_2. ES cell lines were maintained in ES media consisting of high glucose Dulbecco's Modified Eagle Medium (Gibco, Carlsbad, CA, USA) supplemented with 5% fetal bovine serum, L-glutamine, β-mercaptoethanol, non-essential amino acids, and leukemia inhibitory factor (LIF), and grown on gelatin-coated tissue culture-grade plates (Corning, Corning, NY, USA). For chemical hypoxia mimetic experiments, cells were grown in the presence or absence of $CoCl_2$ (100 μM) for four hours. For proteasome inhibition experiments, cells were treated with vehicle (DMSO) or MG-132 (5 μM, Calbiochem, San Diego, CA, USA) for four hours.

In vitro differentiation studies were performed as previously described (283). Briefly, overgrown undifferentiated ES cells were re-plated in differentiation media (ES media without LIF) on non-tissue culture-treated plates and allowed to differentiate in suspended culture into embryoid bodies over a three-day period. Embryoid bodies were then transferred at low density to tissue culture-grade plates, permitting attachment, and allowed to differentiate for an additional eight days. Both suspended and attached cultures were fed with differentiation media every two days. Fully-differentiated attached cultures were briefly fixed in ice-cold methanol/acetone (1:1) and subjected to staining with primary rat anti-mouse PECAM (MEC 13.3, BD Pharmingen, San Diego, CA, USA) and secondary TRITC-conjugated donkey anti-rat IgG (Jackson Immunoresearch, West Grove, PA, USA) for immunofluorescent visualization of endothelial cells and primitive vascular morphology.

For *in vivo* teratoma studies, undifferentiated ES cells of each genotype (5 x 10^6) were injected subcutaneously into the flanks of *nu/nu* mice (Taconic Labs, Hudson, NY, USA) and allowed to grow for six weeks with weekly caliper measurements of tumor size. Harvested tumors were bisected and either flash-frozen in liquid nitrogen for molecular analysis or formalin-fixed and paraffin-embedded for histological analysis.

Molecular analysis of Vhl, HIF, and HIF targets. Whole-cell protein extracts or fresh extracts from teratomas harvested six weeks post-injection were prepared for immunoblot in NET lysis buffer (20mM Tris, 100mM NaCl, 1mM EDTA, 1% NP-40) and quantitated by Bradford assay. Immunoblot primary

antibodies used were: pVhl (M20 and FL181, Santa Cruz Biotechnology, Santa Cruz, CA, USA), HIF-1α (10006421, Cayman Chemical, Ann Arbor, MI, USA and (284)), HIF-2α (NB100-122, Novus Biologicals, Littleton, CO, USA), and eEF2 (Cell Signaling Technology, Danvers, MA, USA). Murine Vegf ELISA was performed on conditioned medium from cultured ES cells (R & D Systems, Minneapolis, MN, USA).

RNA isolation from ES cells, teratomas, and E9.5 embryos was performed using the RNeasy Mini system according to manufacturer's instructions (Qiagen, Germantown, MD, USA) and quantified by UV spectroscopy. cDNA was prepared from 0.5μg of RNA using Superscript reverse transcription reagents (Stratagene, Cedar Creek, TX, USA). Quantitative RT-PCR was performed in triplicate using stock commercial primer-probe sets for *Vhl*, *Vegfa*, *Glut1*, *EglN3*, *Pfk1*, and *18S* ribosomal subunit according to manufacturer's instructions (Applied Biosystems, Foster City, CA, USA). A candidate screen for teratoma hemangioma-associated genes was performed in triplicate on the RT^2 Profiler Mouse Angiogenesis Array using cycle parameters according to manufacturer's instructions (SABiosciences, Frederick, MD, USA). Genes identified for further validation were analyzed by quantitative RT-PCR in triplicate using stock commercial primer-probe sets for *Cdh5*, *Eng*, *Kdr*, *Nrp1*, *Vegfc*, and *18S* ribosomal subunit and cycle parameters according to manufacturer's instructions (Applied Biosystems). All quantitative RT-PCR output raw cycle thresholds were normalized to the internal *18S* ribosomal RNA standard.

Densitometric analysis of HIF immunoblots. HIF-1α and HIF-2α experimental immunoblots, along with corresponding actin and eEF2 loading control immunoblots, were obtained on whole-cell protein extracts from untreated or cobalt chloride-treated ES cells as described in primary Materials and Methods section. Densitometry was performed on scanned immunoblot images using the ImageJ gel analysis tool (285). The gel analysis tool was used to obtain the absolute intensity (AI) for each experimental HIF band and corresponding control band. Relative intensity (RI) for each experimental band was calculated by normalizing the experimental AI to the corresponding control AI.

Embryonic lethality and transplacental ethyl nitrosourea (ENU) mutagenesis studies. *Vhl*$^{2B/+}$ mice were set up for timed inter-heterozygous mating. Embyronic day (E) 0.5 was defined as noon on the day the vaginal plug was observed, and embryos and placentas were harvested at E9.5 and E10.5. For placental studies, embryos were examined for gross defects and genotyped by restriction PCR, and placentas were processed for histological examination. For embryonic studies, E9.5 embryos were used for both RNA extraction and genotyping by restriction PCR.

For transplacental mutagenesis studies, intraperitoneal (i.p.) injection of 50 mg/kg ENU (Sigma, St. Louis, MO, USA) dissolved in ethanol was administered to the pregnant dam at E14.5 (192). Mutagenized *Vhl*$^{2B/+}$ and wild-type littermates were aged in four- and twelve-month cohorts and sacrificed for gross and histological examination.

Histological analysis of murine tissues. Harvested tissues were fixed in 10% buffered formalin. Paraffin-embedded tissues were sectioned and stained with hematoxylin and eosin (H&E) or for pVhl (FL181) or Vegfa (VG-1, Santa Cruz).

Statistical analysis. A two-tailed Student's *t* test was used to make paired comparisons for quantitative RT-PCR and Vegf ELISA data. A value of $p \leq 0.05$ was used as the threshold for statistical significance. Pearson's χ^2 test and Fisher's exact test were used to compare development of neoplasia in wild-type versus *Vhl*-mutant mutagenized mice.

Acknowledgements

We thank Dr. T. Van Dyke and members of her laboratory, Dr. I. Davis, and Dr. W. Y. Kim for many helpful discussions. This work was supported by the V Foundation, the American Cancer Society, the VHL Family Alliance, and the NCI K08098410 and R01121781 (WKR); by the Howard Hughes Medical Institute (MCS, MMH); and by the NIEHS F30015248 (CML).

Chapter Four

Summary, Discussion, Future Directions, and Conclusion

Summary

R167Q HA-VHL assembles into a ubiquitin ligase complex with activity towards HIF-α. Biallelic loss of the von Hippel-Lindau (VHL) tumor suppressor gene is a nearly universal feature of sporadic clear cell renal cell carcinoma (ccRCC). Germline mutations in VHL likewise predispose to development of tumors including retinal and CNS hemangioblastoma, pheochromocytoma, and ccRCC in a genotype-specific manner. I have chosen to focus my dissertation work on the representative hotspot Type 2B *VHL* mutation R167Q which confers risk for all three VHL Disease-associated tumors.

We have previously shown that over-expression of HA-tagged human R167Q VHL protein (pVHL) rescues HIF-1α but not HIF-2α normoxic suppression in *Vhl*$^{-/-}$ murine embryonic stem (ES) cells(107), despite structural predictions that the R167Q mutation disrupts pVHL recruitment of Elongin C and thereby recruitment of the remaining VBC ubiquitin ligase complex members Elongin B, CUL2, and ROC1 (Rbx1)(56-59). In an effort to elucidate the mechanism behind the observed partial retention of HIF-α regulation, we studied the structure and function of the VBC complex in *Vhl*$^{-/-}$ J1 murine ES cells and *VHL*$^{-/-}$ 786-0 human RCC cells complemented with wild-type human HA-tagged

VHL or mutant HA-tagged *VHL* representing each subtype of human VHL Disease(247).

We first examined wild-type and mutant VBC structure by co-immunoprecipitation immunoblot analysis of HA-VHL with known complex members. We were unable to detect co-immunoprecipitation (IP) of Elongin C with R167Q HA-VHL in transgenic murine ES cells as predicted and previously shown(107) but, surprisingly, found that R167Q HA-VHL retained binding with Cul2 and Rbx1. In order to rule out potential artifacts of mouse-human interaction, we confirmed our results in the equivalent complemented 786-0 cell line. We showed that 786-0 + R167Q HA-VHL cells retained partial normoxic suppression of HIF-2α. We also again found that R167Q HA-VHL failed to interact with Elongin C but retained interaction with CUL2 and ROC1. We were able to replicate this result by co-IP of CUL2 with a second representative Type 2B mutant HA-VHL, D121G, and by reverse co-IP of R167Q HA-VHL with myc-tagged CUL2. We next assessed the function of R167Q VBC with an *in vitro* ubiquitylation assay (modified from (63)). 786-0 cell extracts (vector only or wild-type or mutant HA-VHL) were incubated with *in vitro*-transcribed HIF-1α and a defined reaction solution and then subjected to HIF-1α immunoblot in order to detect an upward shift in HIF-1α molecular weight indicative of ubiquitination. We found that R167Q HA-VHL permitted wild-type ubiquitylation of HIF-1α *in vitro*.

In summary, we have shown that R167Q HA-pVHL assembles into a VBC ubiquitin ligase complex with activity towards HIF-α. We postulate that R167Q

HA-VHL retains a transient association with Elongin C and/or maintains contact with CUL2 via a novel interaction with an alternate Cullin/adaptor pair.

A mouse-specific gene replacement model of Type 2B VHL Disease. Having shown that Type 2B mutant R167Q pVHL is capable of directing HIF-α ubiquitylation when over-expressed in a VHL-deficient RCC-derived cell line, we endeavored to address the function of R167Q pVHL expressed under endogenous control using a comprehensive gene replacement (knock-in) mouse model of Type 2B VHL Disease(263). The R167Q missense mutation (G518A) was targeted to the endogenous wild-type *Vhl* locus in J1 murine ES cells, generating $Vhl^{2B/+}$ and $Vhl^{2B/2B}$ ES cells for comparison to $Vhl^{-/-}$ and parental $Vhl^{+/+}$ J1 ES cells. The panel of ES cells was used directly for studies of pVhl, HIF, and HIF target gene expression and in an *in vivo* teratoma assay for tumor growth. $Vhl^{2B/+}$ ES cells were used to generate knock-in mice for timed mating studies of murine development and aging studies of tumor predisposition.

We first analyzed the pVhl/HIF axis in the panel of 2B ES cells. While the *2B Vhl* allele was expressed at wild-type levels by quantitative RT-PCR, the 2B mutant pVhl was present at greatly reduced levels relative to wild-type pVhl. Despite hypomorphic expression of 2B pVhl, $Vhl^{2B/2B}$ ES cells retained near-normal normoxic suppression of HIF-α (HIF-1α > HIF-2α) and normal hypoxia mimetic-induced HIF-α stabilization. $Vhl^{2B/2B}$ ES cells, furthermore, appropriately suppressed a panel of HIF target genes including the joint HIF targets *Vegfa*, *EglN3*, and *Glut1* and the HIF-1α-specific target *Pfk1* under normoxic conditions by quantitative RT-PCR. $Vhl^{-/-}$ ES cells, in contrast, over-expressed all four HIF

target genes. Because HIF-2α is expressed but not transcriptionally active in J1 ES cells, the lack of normoxic HIF target gene expression in *Vhl*$^{2B/2B}$ ES cells indicates insufficient HIF-1α levels.

We next examined 2B mutant pVhl function in an *in vivo* teratoma assay. Teratomas were generated from ES cells of each genotype injected into the flanks of nude mice and followed over the course of six weeks. *Vhl*$^{-/-}$ ES cell-derived teratomas displayed a growth disadvantage relative to J1-derived teratomas, confirming earlier work in the lab(107). Surprisingly, however, *Vhl*$^{2B/2B}$ teratomas displayed a growth advantage relative to J1. By gross examination, *Vhl*$^{2B/2B}$ teratomas were markedly hemorrhagic and by histological examination displayed enhanced hemangioma formation relative to *Vhl*$^{-/-}$. As both HIF-1α and HIF-2α are expressed and transcriptionally active in teratomas, we next examined HIF target gene expression by quantitative RT-PCR. *Vhl*$^{-/-}$ teratomas over-expressed *Vegfa*, *EglN3*, and *Pfk1* relative to J1. *Vhl*$^{2B/2B}$ teratomas over-expressed *Vegfa* and *EglN3* but not *Pfk1*, suggestive of sufficient HIF-2α but insufficient HIF-1α stabilization to direct target gene expression. As HIF-1α has been shown to be growth-suppressive and HIF-2α has been shown to be growth-promoting, we postulate that enhanced *Vhl*$^{2B/2B}$ teratoma growth results from 2B mutant pVhl-associated maximal HIF-2α and sub-maximal HIF-1α stabilization.

Because differences in *Vegfa* expression alone could not account for the dramatically enhanced hemangioma formation observed in *Vhl*$^{2B/2B}$ teratomas relative to *Vhl*$^{-/-}$, we used an RT2 Profiler quantitative RT-PCR array to query 84 angiogenesis-related genes for association with the hemangioma phenotype in

teratomas. Six angiogenesis-related genes, including *Vegfa*, screened positive as significantly over-expressed in *Vhl*$^{-/-}$ and/or *Vhl*$^{2B/2B}$ relative to J1 teratomas. The five novel genes were validated using independent primers. Briefly, *Vhl*$^{-/-}$ and *Vhl*$^{2B/2B}$ teratomas were confirmed to over-express *Cdh5* (VE-cadherin), *Kdr* (VegfR2), and *Eng* (endoglin). In addition, *Vhl*$^{2B/2B}$ teratomas uniquely over-expressed *Nrp1* (neuropilin-1).

We next compared *Vhl*$^{-/-}$ and *Vhl*$^{2B/2B}$ to J1 ES cells in an *in vitro* vascular differentiation assay. Briefly, ES cells were allowed to differentiate into spherical tri-laminar embryoid bodies in suspended culture for three days. Embryoid bodies were then grown in attached culture conditions to encourage vascular differentiation, as visualized by PECAM immunofluorescent stain. J1-derived embryoid bodies sprouted a network of well-formed primitive vessels with branching at regular intervals, while *Vhl*$^{-/-}$ embryoid bodies differentiated into PECAM+ cells but failed to sprout primary vessels. *Vhl*$^{2B/2B}$ embryoid bodies displayed an intermediate phenotype, differentiating into a disorganized network defined by haphazard sprouting. These results suggest that the enhanced hemangioma formation observed in *Vhl*$^{2B/2B}$ teratomas relative to *Vhl*$^{-/-}$ may derive from an imbalance in Vegfa signaling in association with an exuberant, if aberrant, vascular potential.

Finally, we examined Type 2B mutant pVhl function in murine development and tumor predisposition using *Vhl*$^{2B/+}$ knock-in mice derived from *Vhl*$^{2B/+}$ murine ES cells. Timed inter-heterozygous matings revealed the 2B *Vhl* allele to be homozygous lethal at E9.5-10.5. Coupled with the grossly normal

embryo at E9.5 and the fact that *Vhl*$^{-/-}$ embryos die at approximately E10.5 from defective placental labyrinthine vascularization, we examined the histology of *Vhl*$^{2B/2B}$ placentas. While wild-type and *Vhl*$^{2B/+}$ placentas at E9.5 showed allantoic vascular invasion of the chorionic plate in the presumptive labyrinth, allantoic vessels failed to invade the chorionic plate in *Vhl*$^{2B/2B}$ placentas, pointing to a severely hypomorphic role for the 2B *Vhl* allele in murine development. Quantitative RT-PCR for our panel of HIF target genes failed to reveal any differences between *Vhl*$^{2B/+}$ and *Vhl*$^{2B/2B}$ E9.5 placentas due to the relatively large contribution of maternal decidua to the placenta at that time-point. We did find, however, that *Vhl*$^{2B/2B}$ E9.5 embryos over-expressed all four HIF target genes compared to *Vhl*$^{2B/+}$ littermates. The stabilization of HIF-1α +/- HIF-2α in *Vhl*$^{2B/2B}$ E9.5 embryos could be due to mutant 2B pVhl activity and/or pathophysiological hypoxia due to the failing placenta.

We next used *Vhl*$^{2B/+}$ mice for aging studies of tumor predisposition. Similar to mice heterozygous for a *Vhl*-null allele, *Vhl*$^{2B/+}$ mice developed rare renal microcysts (3%), no renal adenocarcinoma, and frequent adrenal and renal angiectasis. In dramatic contrast to *Vhl*-null models, however, *Vhl*$^{2B/+}$ mice did not develop hepatic angiomas, pointing to a missense mutation-specific alteration in the spectrum of susceptible tissues.

In order to determine whether *Vhl* initiation could predispose mice to development of renal tumors, I modeled the accumulation of somatic mutations using *in utero* mutagenesis with ENU (50 mg/kg IP to pregnant dam at E14.5). In

a small pilot study, mutagenized *Vhl*$^{2B/+}$ and mutagenized wild-type littermates were aged to four and twelve months and assessed for tumor predisposition.

Both *Vhl*$^{2B/+}$ and wild-type mutagenized mice had developed simple and papillary renal cysts at four and twelve months. At twelve months, however, 2/10 mutagenized *Vhl*$^{2B/+}$ mice developed renal adenocarcinoma, representing the first demonstration of this tumor in a genetically predisposed mouse model. Step serial sections of kidneys from wild-type mutagenized mice failed to reveal any neoplastic changes. In summary, we have shown that the representative R167Q 2B mutant pVhl generates a unique profile of HIF-1α and HIF-2α stabilization with dramatic effects on three dimensional tumor growth and tissue susceptibility to tumorigenesis.

Discussion

HIF-α accumulation is a central feature of renal tumorigenesis. Inactivating mutations in the tumor suppressors *BHD*, *TSC1*, or *TSC2* and activating mutations in the proto-oncogene *MET* contribute to HIF-α accumulation by enhancing translation through the mTOR pathway, while inactivating mutations in *VHL*, *FH*, and *SDHB* promote HIF-α stabilization by permitting HIF-α to evade oxygen-dependent regulation. Renal tumors arising in patients with germline mutations in these genes display accumulation of both HIF-1α and HIF-2α, though HIF-2α predominates in VHL-, BHD-, and MET/HPRC-associated RCC and HIF-1α predominates in FH/HLRCC-associated RCC. The penetrance, histology, and clinical course associated with RCC predisposition in each of these inherited syndromes likely derives from the dosage or relative ratio of HIF-

1α and HIF-2α accumulation as well as HIF-independent factors specific to each genetic lesion.

HIF-α stabilization is not an all-or-nothing phenomenon. The representative Type 2B VHL mutant R167Q produces a unique profile of HIF-α stabilization in comparison to both wild-type, null, and other VHL Disease-associated mutant VHL proteins. Wild-type J1 murine ES cells suppress while *Vhl*-null murine ES cells maximally stabilize both HIF-1α and HIF-2α under normoxic conditions. *Vhl*-null ES cells complemented with the representative Type 2A VHL mutant Y112H display wild-type normoxic suppression of HIF-1α but dose-dependent suppression of HIF-2α. Finally, *Vhl*-null ES cells complemented with the representative Type 2B VHL mutant R167Q display wild-type normoxic suppression of HIF-1α but impaired normoxic suppression of HIF-2α (Ref Rathmell 2004). ES cells homozygous for a gene replacement allele for R167Q likewise displayed normal normoxic suppression of HIF-1α but stabilization, though sub-maximal, of HIF-2α.

We have elucidated one potential mechanism for the intermediate HIF-α stabilization profile associated with Type 2B VHL mutants: the assembly of a remnant VBC complex. Despite an absent or drastically reduced capability to bind Elongin C, both R167Q and a second representative Type 2B VHL mutant D121G retain interaction with VBC complex members CUL2 and ROC1 in complemented *VHL*-null 786-0 RCC cells. Furthermore, cell extract from R167Q HA-VHL-expressing cells retains the ability to direct ubiquitylation of HIF-α in an *in vitro* assay. These results suggest that R167Q pVHL assembles into a

remnant VBC complex, either containing Elongin C in reduced amounts or bypassing the requirement for Elongins C and B entirely by directly interacting with CUL2 or interacting with CUL2 via a second cullin-adaptor pair.

In a structural homology threading model of the VBC complex based on the solved crystal structure of the related yeast SCF complex, we have shown that VHL is indeed likely to bind directly with CUL2, though the small interface between the two is unlikely to be a stabilizing factor in the absence of Elongins C and B (data not shown, Brian Kuhlman, UNC). In addressing the latter possibility, we have thus far been unable to detect an interaction between R167Q mutant pVHL and CUL1-SCF1 or CUL4-DDB1, though interaction with CUL3 and any number of BTB-domain adaptors remains a possibility.

The stability of the mutant pVHL likely influences both its ubiquitin ligase-dependent and –independent functions. In the HA-VHL-complemented ES cell and 786-0 cell systems used in the above studies, clones expressing near wild-type levels of R167Q HA-VHL were used in experiments of VBC structure and function. In murine ES cells, however, the Type 2B mutant R167Q pVhl is expressed at greatly reduced levels compared to wild-type pVhl.

Imbalances in HIF-α family members contribute to differences in disease biology. Sporadic ccRCC tumors expressing both HIF-1α and HIF-2α (H1H2) differ significantly from those expressing HIF-2α alone (H2)(286). In a recent study, 57 independent sporadic ccRCC tumors were classified as VHL WT (neither HIF-1α nor HIF-2α detected, 12%), H1H2 (61%), or H2 (27%) by HIF

immunostaining. *VHL* inactivation by mutation, deletion, or promoter methylation was confirmed in 49/50 H1H2 and H2 ccRCC tumors. Consistent with earlier studies suggesting that HIF-2α enhances and HIF-1α tends to oppose c-Myc activity, H2 tumors displayed enhanced c-Myc activation and proliferation (55% increase in Ki67 positivity) and reduced genomic copy number changes (40% decrease) in comparison to VHL WT and H1H2 tumors. In contrast, VHL WT and H1H2 tumors uniquely displayed activation of the AKT/mTORC1 (phospho-S6) and MAPK/ERK (phospho-ERK) pathways. Intriguingly, both *in vivo* studies on ccRCC tumors and *in vitro* studies utilizing HIF-1α and HIF-2α knock-down in RCC cell lines suggested that H2 tumors stimulate DNA repair by enhancing expression of homologous recombination effectors, thereby limiting G1/S checkpoint activation. Overall, these studies suggest that ccRCC tumors characterized by HIF-2α stabilization correlates with c-Myc activation and efficient transit through S phase, while ccRCC tumors characterized by stabilization of both HIF-1α and HIF-2α correlate with growth factor signaling through AKT/mTORC1 and MAPK/ERK.

Studies of the VHL/HIF pathway in teratoma models suggest that the profile of HIF-α stabilization directly influences tumor growth and angiogenesis. Teratomas generated from HIF-1$\alpha^{-/-}$ murine ES cells display poor vascularization, reduced hemangioma formation, and similar early growth (through week three) but enhanced delayed growth (weeks four through seven) in comparison to transgenic HIF-1α-rescued ES cells(280). The growth phenotype transition at three weeks, together with the observation of three-fold more hypoxic zones in

comparison to HIF-1α-rescued, suggests that physiological hypoxic stabilization of HIF-2α played a role. Teratomas derived from ES cells in which a HIF-2α allele replaces endogenous HIF-1α (*HIF-2α*$^{KI/KI}$, also functionally *HIF-1α*$^{-/-}$) display more rapid growth, greater hemorrhage and mass, increased vessel density, and increased hemangioma formation relative to wild-type teratomas(281). Altogether, these studies suggest that HIF-2α stabilization is tumor growth-promoting and that HIF-1α is growth-suppressive. As evidenced by the HIF-2α$^{KI/KI}$ model, teratoma hemangioma formation appears to depend not upon HIF-1α expression specifically but more generally on HIF-1α locus-specific control, perhaps directing a specific temporal and/or spatial context for HIF-α expression.

Teratomas derived from *Vhl*$^{-/-}$ ES cells, predicted to maximally stabilize both HIF-1α and HIF-2α, display reduced growth but enhanced hemangioma formation relative to wild-type teratomas(106, 107). Teratoma growth and hemangioma suppression were completely rescued by wild-type HA-VHL, while the representative Type 2B VHL mutant R167Q HA-VHL rescued teratoma growth but not hemangioma suppression(107). Surprisingly, *Vhl*$^{2B/2B}$ teratomas grow more rapidly than both *Vhl*$^{-/-}$ and J1 and display enhanced hemangioma formation relative to *Vhl*$^{-/-}$. We suspect the differences in tumor growth and hemangiogenesis in teratomas derived from *Vhl*$^{-/-}$ + R167Q HA-VHL and those derived from *Vhl*$^{2B/2B}$ ES cells arise from hypomorphic expression of 2B mutant pVhl from the endogenous locus and a resulting shift in the HIF-α profile. In addition to a growth profile consistent with enhanced HIF-2α stabilization, *Vhl*$^{2B/2B}$

teratomas fail to stabilize sufficient HIF-1α to activate transcription of the HIF-1α-specific target *Pfk1*. The severity of the 2B *Vhl* allele in this three-dimensional tumor model suggests that a HIF balance shifted towards HIF-2α may promote better tumor growth than maximal stabilization of both HIF-1α and HIF-2α.

R167Q pVhl is associated with a unique pattern of angiogenesis-related gene expression. $Vhl^{2B/2B}$ teratomas display greatly enhanced hemangioma formation relative to $Vhl^{-/-}$ teratomas despite over-expressing an equivalent amount of *Vegfa*. In an effort to generate hypotheses about the genes involved in the hemangioma phenotype, we compared the expression of 84 angiogenesis-related genes in $Vhl^{2B/2B}$ and $Vhl^{-/-}$ relative to J1 wild-type teratomas. We found that both $Vhl^{2B/2B}$ and $Vhl^{-/-}$ teratomas over-expressed *Vegfa*, *Kdr*, *Cdh5*, and *Eng*, but $Vhl^{2B/2B}$ teratomas uniquely over-expressed *Nrp1* as well. *Kdr* and *Nrp1* are both involved in Vegfa signaling, encoding, respectively, the Vegfa receptor VegfR2 and its co-receptor neuropilin-1. Neuropilin-1 has been shown to enhance isoform-specific Vegfa signaling through VegfR2(287).

In an independent approach, we tested the *in vitro* vascular differentiation potential of $Vhl^{2B/2B}$ and $Vhl^{-/-}$ relative to J1 wild-type ES cells in an embryoid body assay. We found that J1-derived embryoid bodies sprouted a well-formed vascular plexus of PECAM+ cells, $Vhl^{-/-}$-derived embryoid bodies appeared to proliferate but did not sprout vessels, and $Vhl^{2B/2B}$-derived embryoid bodies developed an intermediate phenotype of a robust but disorganized vascular network. Studies of the Vegfa signaling pathway in this *in vitro* embryoid body vascular differentiation system indicate that the balance of endothelial

proliferation versus generation of vessels is exquisitely sensitive to the absolute and relative dosages of critical individual pathway components such as VegfR2, VegfR1, and Vegfa(288-290). The importance of dosage in Vegfa signaling is underscored *in vivo* by the haplo-insufficient embryonic lethality observed in *Vegfa*$^{+/-}$ mice(291, 292). The results of the *in vitro* vascular differentiation assay and the hemangioma-related gene signature of *Vhl*$^{2B/2B}$ versus *Vhl*$^{+/-}$ teratomas suggest that the 2B mutant pVhl does indeed promote tumor hemangioma formation, perhaps via HIF-dependent or mutant pVhl-dependent effects on Vegfa signaling.

The discovery of a mutant 2B pVhl-specific hemangioma-associated gene profile warrants further study for its implications in renal tumor biology and in human VHL Disease. In order to address the former, we are currently developing a primary renal tubule epithelial cell culture system designed to permit dissection of HIF- and mutant pVhl-dependent effects on tumorigenic potential, three-dimensional tumor growth and vascularity, and gene expression. This system is described in detail below. In order to address the latter, we are collaborating with a rare-disease tissue bank in order to obtain ccRCC and adjacent normal tissue from VHL Disease patients with Type 1, Type 2A, and Type 2B *VHL* mutations. These tissues will be used to define missense mutation-specific gene expression profiles for correlation with clinical history and histopathological features.

A gene replacement model of Type 2B VHL phenocopies the null allele in embryonic development but changes target tissue spectrum. Vhl$^{2B/2B}$ embryos

die at E9.5-10.5 with a placental phenotype consistent with the phenotype reported for *Vhl*-null. At E10.5, $Vhl^{-/-}$ placental labyrinths display reduced fetal vessel content and, as a consequence, separation of the maternal and fetal circulations (110). At E9.5, the latest time-point we could examine histologically, $Vhl^{2B/2B}$ placentas display reduced fetal vessel invasion into the chorionic plate, a defect which would presumably manifest as reduced fetal vascularization of the labyrinth 1-2 days later if the embryos had survived. The $Vhl^{-/-}$ labyrinthine defect has been localized to *Vhl* deficiency in the embryonic endothelial compartment(132). Though we observed over-expression of both joint HIF targets and the HIF-1α specific target *Pfk1* in whole $Vhl^{2B/2B}$ embryos relative to $Vhl^{2B/+}$ embryos at E9.5, this HIF target gene expression most likely reflects physiological hypoxia near associated with embryonic death and is unlikely to capture the absolute dosage and relative stabilization of HIF-α factors due to genetic loss of *Vhl* in the relevant endothelial compartment.

Though *Vhl* heterozygous-null mice develop hepatic angiomas with moderate to dramatic, age- and genetic background-dependent penetrance, $Vhl^{2B/+}$ mice never developed hepatic angiomas. Though genetic background may have conferred a degree of resistance to hepatic angioma formation in our mouse model – the penetrance of hepatic angioma in $Vhl^{+/-}$ mice on the C57BL/6 is a modest 18% at 12 months – we suspect that the lack of hepatic angiomas derives from a 2B missense mutation-specific effect on HIF-α stabilization. Addressing the former, our lab has independently shown that $Vhl^{f/f}$ injected with Adenoviral-cre recombinase develop hepatic angiomas with high penetrance,

while Adeno-cre-injected *Vhl*$^{2B/f}$ mice do not develop hepatic angiomas (Shufen Chen). Addressing the latter, hepatocytic HIF-2α stabilization has been shown to be both necessary in the context of *Vhl* loss (134) and independently sufficient (135) to generate hepatic angiomas. Thus, the lack of hepatic angioma formation observed in *Vhl*$^{2B/+}$ mice is likely to result primarily from insufficient HIF-2α stabilization in hepatocytes.

Our mouse model of Type 2B VHL Disease emphasizes the tissue- and/or context-dependent effect of R167Q mutant pVhl on HIF-α stabilization. First, the 2B *Vhl* allele confers greater HIF-2α than HIF-1α stabilization in association with enhanced tumor growth and hemangioma formation in a three-dimensional tumor growth model. Second, the 2B *Vhl* allele appears to phenocopy the *Vhl* null allele in contribution of the embryonic endothelium to the placental labyrinth in development. Finally, the 2B *Vhl* allele confers a reduction in hepatic angioma formation in the adult mouse likely attributable to sub-threshold HIF-2α stabilization.

Vhl mutation predisposes to renal tumorigenesis subsequent to mutagenesis. Though rats develop both spontaneous and inherited renal adenocarcinomas, thus far genetic targeting of loci associated with human renal tumor predisposition syndromes has failed to recapitulate RCC in the mouse. *PEPCK*-cre;*Vhl*$^{f/f}$ mice develop renal cysts with modest penetrance and long latency(136). Addition of a second genetic event, *Pten* loss, results in a highly penetrant renal cyst phenotype with short latency in *Ksp1.3-cre;Vhl*$^{f/f}$ mice, but the associated progressive renal failure prevented assessment of tumor

predisposition after 3-6 months(140). These mouse models suggest that the generation of renal cysts in *Vhl*-initiated mice requires at least one additional genetic event but do not indicate whether *Vhl* initiation of renal cysts is a requisite step in the progression to renal adenocarcinoma or whether *Vhl* initiation of renal adenocarcinoma occurs via an independent or bifurcated path.

In an effort to determine whether *Vhl*-initated mice could be pushed to develop renal adenocarcinoma, we modeled the accumulation of somatic mutations in $Vhl^{2B/+}$ mice using transplacental ENU mutagenesis. ENU was equally renal cystogenic in $Vhl^{2B/+}$ and wild-type littermate controls at four and twelve months. At twelve months, however, 2/10 mutagenized $Vhl^{2B/+}$ mice and 0/14 mutagenized wild-type mice developed renal adenocarcinoma with clear cells and vascular stroma reminiscent of human ccRCC. We believe this is the first demonstration of renal adenocarcinoma in a genetically predisposed mouse.

Future Directions

Type 2B *VHL* mutations predispose to the full spectrum of VHL disease-associated tumors and are additionally postulated to foster more aggressive renal tumors than Type 1 and Type 2A *VHL* mutations. Our lab has undertaken both *in vitro* and *in vivo* approaches to examine the tumor-promoting activities of a representative hotspot Type 2B *VHL* mutation, R167Q. We have demonstrated that xenografts expressing human Type 2B *VHL* cDNA (107) and teratomas homozygous for the equivalent murine Type 2B *Vhl* mutation (263) grow more rapidly than the corresponding Type 1 tumors. Our gene replacement mouse model of Type 2B VHL disease, furthermore, is the first *Vhl* model to

demonstrate a predisposition for renal adenocarcinoma (263). Together with our *in vitro* findings that Type 2B VHL retains intermediate ubiquitin ligase activity towards hypoxia inducible factor (HIF)-α (247), our *in vivo* studies suggest that the maximal HIF stabilization conferred by Type 1 *VHL* mutations is detrimental to tumor growth.

We propose to study the interplay of *Vhl* Type 2B mutation or loss and HIF-α stabilization by generating renal epithelial and dermal fibroblast primary cell cultures from our existing Type 2B *Vhl* mouse strain, a conditional *Vhl* deletion strain, and conditional transgenic strains encoding stable HIF-1α and HIF-2α. We hypothesize that Type 2B *VHL* mutation generates a profile of relative and absolute HIF-1α and HIF-2α levels that activates a unique subset of the total HIF target gene repertoire. Our proposed primary cell culture-based system models *Vhl* mutation, *Vhl* loss, and HIF stabilization in a euploid epithelial setting similar to the native kidney in early renal tumorigenesis and is highly tractable for functional and molecular studies of VHL Disease-associated phenotypes.

First, cell culture and allograft growth of *Vhl* $^{2B/flox}$ cells will be compared with *Vhl* $^{flox/flox}$ cells and cells with *Vhl*-independent HIF stabilization. A panel of primary cell cultures will be developed from newborn kidneys and skin from Type 2B, conditional *Vhl*-null, and conditionally stabilized HIF mice and exposed to viral cre in culture. Tumorigenic potential *in vitro* will be assessed by cellular doubling time, duration of continuous culture, growth in soft agar, and formation of primary cilia. Tumorigenic potential *in vivo* will be assessed by implanting cells

subcutaneously or orthotopically in nude mice to study tumor growth, histology, and invasiveness.

Secondly, the above primary cell cultures and derivative allografts will be probed for pVhl and HIF pathway function in order to define the HIF target gene repertoire associated with Type 2B *Vhl* expression compared with wild-type or null *Vhl* alleles. Primary cell cultures will be used to compare basal and hypoxia-stimulated levels of HIF-1α and HIF-2α and examine basal and hypoxia-stimulated HIF transcriptional effects on both conventional and putative Type 2B *Vhl*-associated HIF targets genes. We will then attempt to define a Type 2B *Vhl* gene expression profile using comparative gene expression profile analysis on both primary cell cultures and derivative allografts.

Our investigations of the representative *VHL* hotspot mutation R167Q suggest that missense Type 2B *VHL* mutations can confer a more severe phenotype than *VHL* loss. Coupled with the use of conditional alleles, our primary cell culture system will allow us to directly compare the tumor-promoting characteristics of the Type 2B *Vhl* mutation to *Vhl* loss and *Vhl*-independent HIF stabilization at the molecular level.

Conclusion

Altogether, this dissertation work suggests that maximal stabilization of both HIF-1α and HIF-2α may create an environment detrimental to some aspects of tumor growth. Instead, a molecular scenario in which HIF-2α is intermediately stabilized or stabilized to a greater degree than HIF-1α may be most conducive

to tumorigenesis. *VHL* mutations that generate such a profile of HIF-α stabilization, we propose, may cause a more severe clinical course in sporadic ccRCC. Understanding how the levels of HIF-α direct RCC tumor biology will be important for determining an individual's prognosis or likelihood to respond to targeted therapy as well as for generating new rational targeting strategies. Though targeted therapies against HIF-α are currently under development, our work indicates that such therapies may be ineffective or even counter-productive if they fail to completely inhibit HIF-α stabilization or activity or if they have greater efficacy towards one HIF-α subunit or the other. Finally and most importantly, this dissertation work both encourages ongoing attempts to develop genetically engineered mouse models of renal adenocarcinoma and urges further study of VHL Disease-associated mutations for insight into the molecular biology of both the sporadic and inherited renal cell carcinoma.

References

1. Cancer Facts and Figures 2008. Atlanta, GA: American Cancer Society, Inc.; 2008.

2. Horner MJ RL, Krapcho M, Neyman N, Aminou R, Howlader N, Altekruse SF, Feuer EJ, Huang L, Mariotto A, Miller BA, Lewis DR, Eisner MP, Stinchcomb DG, Edwards BK (eds). . SEER Cancer Statistics Review, 1975-2006. Bethedsa, MD: National Cancer Institute; 2009.

3. Harth V, Bruning T, Bolt HM. Renal carcinogenicity of trichloroethylene: update, mode of action, and fundamentals for occupational standard setting. Rev Environ Health 2005;20(2):103-18.

4. Lipworth L, Tarone RE, McLaughlin JK. The epidemiology of renal cell carcinoma. J Urol 2006;176(6 Pt 1):2353-8.

5. Cohen HT, McGovern FJ. Renal-cell carcinoma. N Engl J Med 2005;353(23):2477-90.

6. Kovacs G, Akhtar M, Beckwith BJ*, et al.* The Heidelberg classification of renal cell tumours. J Pathol 1997;183(2):131-3.

7. Linehan WM, Walther MM, Zbar B. The genetic basis of cancer of the kidney. J Urol 2003;170(6 Pt 1):2163-72.

8. Brauch H, Weirich G, Brieger J*, et al.* VHL alterations in human clear cell renal cell carcinoma: association with advanced tumor stage and a novel hot spot mutation. Cancer Res 2000;60(7):1942-8.

9. Kovacs G. Molecular differential pathology of renal cell tumours. Histopathology 1993;22(1):1-8.

10. Schmidt L, Duh FM, Chen F*, et al.* Germline and somatic mutations in the tyrosine kinase domain of the MET proto-oncogene in papillary renal carcinomas. Nature genetics 1997;16(1):68-73.

11. Jeffers M, Schmidt L, Nakaigawa N*, et al.* Activating mutations for the met tyrosine kinase receptor in human cancer. Proceedings of the National Academy of Sciences of the United States of America 1997;94(21):11445-50.

12. Fischer J, Palmedo G, von Knobloch R*, et al.* Duplication and overexpression of the mutant allele of the MET proto-oncogene in multiple hereditary papillary renal cell tumours. Oncogene 1998;17(6):733-9.

13. Kovacs G, Soudah B, Hoene E. Binucleated cells in a human renal cell carcinoma with 34 chromosomes. Cancer Genet Cytogenet 1988;31(2):211-5.

14. Iqbal MA, Akhtar M, Ali MA. Cytogenetic findings in renal cell carcinoma. Hum Pathol 1996;27(9):949-54.

15. Speicher MR, Schoell B, du Manoir S*, et al.* Specific loss of chromosomes 1, 2, 6, 10, 13, 17, and 21 in chromophobe renal cell carcinomas revealed by comparative genomic hybridization. Am J Pathol 1994;145(2):356-64.

16. Kuczyk MA, Anastasiadis AG, Zimmermann R, Merseburger AS, Corvin S, Stenzl A. Current aspects of the surgical management of organ-confined, metastatic, and recurrent renal cell cancer. BJU Int 2005;96(5):721-7; quiz i-ii.

17. Hudes G, Carducci M, Tomczak P*, et al.* A phase 3, randomized, 3-arm study of temsirolimus (TEMSR) or interferon-alpha (IFN) or the combination of TEMSR + IFN in the treatment of first-line, poor-risk patients with advanced renal cell carcinoma (adv RCC). Journal of Clinical Oncology, 2006 ASCO Annual Meeting Proceedings Part I 2006;24(18S):LBA4.

18. Motzer RJ, Escudier B, Oudard S*, et al.* Efficacy of everolimus in advanced renal cell carcinoma: a double-blind, randomised, placebo-controlled phase III trial. Lancet 2008;372(9637):449-56.

19. Ryan CW, Goldman BH, Lara PN, Beer TM, Drabkin HA, Crawford E. Sorafenib plus interferon-α2b (IFN) as first-line therapy for advanced renal cell carcinoma (RCC): SWOG 0412.

Journal of Clinical Oncology, 2006 ASCO Annual Meeting Proceedings Part I 2006;24(18S):4525.

20. Motzer RJ, Hutson TE, Tomczak P*, et al.* Phase III randomized trial of sunitinib malate (SU11248) versus interferon-alfa (IFN-α) as first-line systemic therapy for patients with metastatic renal cell carcinoma (mRCC). Journal of Clinical Oncology, 2006 ASCO Annual Meeting Proceedings Part I Vol 24, No 18S (June 20 Supplement), 2006: LBA3 2006;24(18S):LBA3.

21. Latif F, Tory K, Gnarra J*, et al.* Identification of the von Hippel-Lindau disease tumor suppressor gene. Science (New York, NY 1993;260(5112):1317-20.

22. Iliopoulos O, Ohh M, Kaelin WG, Jr. pVHL19 is a biologically active product of the von Hippel-Lindau gene arising from internal translation initiation. Proceedings of the National Academy of Sciences of the United States of America 1998;95(20):11661-6.

23. Schoenfeld A, Davidowitz EJ, Burk RD. A second major native von Hippel-Lindau gene product, initiated from an internal translation start site, functions as a tumor suppressor. Proceedings of the National Academy of Sciences of the United States of America 1998;95(15):8817-22.

24. Corless CL, Kibel AS, Iliopoulos O, Kaelin WG, Jr. Immunostaining of the von Hippel-Lindau gene product in normal and neoplastic human tissues. Hum Pathol 1997;28(4):459-64.

25. Los M, Jansen GH, Kaelin WG, Lips CJ, Blijham GH, Voest EE. Expression pattern of the von Hippel-Lindau protein in human tissues. Lab Invest 1996;75(2):231-8.

26. Richards FM, Schofield PN, Fleming S, Maher ER. Expression of the von Hippel-Lindau disease tumour suppressor gene during human embryogenesis. Human molecular genetics 1996;5(5):639-44.

27. Maher ER, Iselius L, Yates JR*, et al.* Von Hippel-Lindau disease: a genetic study. Journal of medical genetics 1991;28(7):443-7.

28. Neumann HP, Wiestler OD. Clustering of features of von Hippel-Lindau syndrome: evidence for a complex genetic locus. Lancet 1991;337(8749):1052-4.

29. Sgambati MT, Stolle C, Choyke PL*, et al.* Mosaicism in von Hippel-Lindau disease: lessons from kindreds with germline mutations identified in offspring with mosaic parents. Am J Hum Genet 2000;66(1):84-91.

30. Lonser RR, Glenn GM, Walther M*, et al.* von Hippel-Lindau disease. Lancet 2003;361(9374):2059-67.

31. Filling-Katz MR, Choyke PL, Oldfield E*, et al.* Central nervous system involvement in Von Hippel-Lindau disease. Neurology 1991;41(1):41-6.

32. Wanebo JE, Lonser RR, Glenn GM, Oldfield EH. The natural history of hemangioblastomas of the central nervous system in patients with von Hippel-Lindau disease. J Neurosurg 2003;98(1):82-94.

33. Webster AR, Maher ER, Moore AT. Clinical characteristics of ocular angiomatosis in von Hippel-Lindau disease and correlation with germline mutation. Arch Ophthalmol 1999;117(3):371-8.

34. Ammerman JM, Lonser RR, Dambrosia J, Butman JA, Oldfield EH. Long-term natural history of hemangioblastomas in patients with von Hippel-Lindau disease: implications for treatment. J Neurosurg 2006;105(2):248-55.

35. Vortmeyer AO, Gnarra JR, Emmert-Buck MR*, et al.* von Hippel-Lindau gene deletion detected in the stromal cell component of a cerebellar hemangioblastoma associated with von Hippel-Lindau disease. Hum Pathol 1997;28(5):540-3.

36. Butman JA, Linehan WM, Lonser RR. Neurologic manifestations of von Hippel-Lindau disease. JAMA 2008;300(11):1334-42.

37. Walther MM, Keiser HR, Choyke PL, Rayford W, Lyne JC, Linehan WM. Management of hereditary pheochromocytoma in von Hippel-Lindau kindreds with partial adrenalectomy. J Urol 1999;161(2):395-8.

38. Pavlovich CP, Linehan WM, Walther MM. Partial adrenalectomy in patients with multiple adrenal tumors. Curr Urol Rep 2001;2(1):19-23.

39. Baghai M, Thompson GB, Young WF, Jr., Grant CS, Michels VV, van Heerden JA. Pheochromocytomas and paragangliomas in von Hippel-Lindau disease: a role for laparoscopic and cortical-sparing surgery. Arch Surg 2002;137(6):682-8; discussion 8-9.

40. Brauch H, Hoeppner W, Jahnig H*, et al.* Sporadic pheochromocytomas are rarely associated with germline mutations in the vhl tumor suppressor gene or the ret protooncogene. J Clin Endocrinol Metab 1997;82(12):4101-4.

41. Maher ER, Yates JR, Ferguson-Smith MA. Statistical analysis of the two stage mutation model in von Hippel-Lindau disease, and in sporadic cerebellar haemangioblastoma and renal cell carcinoma. Journal of medical genetics 1990;27(5):311-4.

42. Choyke PL, Glenn GM, Walther MM, Patronas NJ, Linehan WM, Zbar B. von Hippel-Lindau disease: genetic, clinical, and imaging features. Radiology 1995;194(3):629-42.

43. Poston CD, Jaffe GS, Lubensky IA*, et al.* Characterization of the renal pathology of a familial form of renal cell carcinoma associated with von Hippel-Lindau disease: clinical and molecular genetic implications. J Urol 1995;153(1):22-6.

44. Mandriota SJ, Turner KJ, Davies DR*, et al.* HIF activation identifies early lesions in VHL kidneys: evidence for site-specific tumor suppressor function in the nephron. Cancer Cell 2002;1(5):459-68.

45. Choyke PL, Glenn GM, Walther MM*, et al.* The natural history of renal lesions in von Hippel-Lindau disease: a serial CT study in 28 patients. AJR Am J Roentgenol 1992;159(6):1229-34.

46. Walther MM, Choyke PL, Glenn G*, et al.* Renal cancer in families with hereditary renal cancer: prospective analysis of a tumor size threshold for renal parenchymal sparing surgery. J Urol 1999;161(5):1475-9.

47. Manski TJ, Heffner DK, Glenn GM*, et al.* Endolymphatic sac tumors. A source of morbid hearing loss in von Hippel-Lindau disease. JAMA 1997;277(18):1461-6.

48. Crossey PA, Richards FM, Foster K*, et al.* Identification of intragenic mutations in the von Hippel-Lindau disease tumour suppressor gene and

correlation with disease phenotype. Human molecular genetics 1994;3(8):1303-8.

49. Zbar B, Kishida T, Chen F*, et al.* Germline mutations in the Von Hippel-Lindau disease (VHL) gene in families from North America, Europe, and Japan. Hum Mutat 1996;8(4):348-57.

50. Gallou C, Chauveau D, Richard S*, et al.* Genotype-phenotype correlation in von Hippel-Lindau families with renal lesions. Human mutation 2004;24(3):215-24.

51. Clifford SC, Cockman ME, Smallwood AC*, et al.* Contrasting effects on HIF-1alpha regulation by disease-causing pVHL mutations correlate with patterns of tumourigenesis in von Hippel-Lindau disease. Hum Mol Genet 2001;10(10):1029-38.

52. Ang SO, Chen H, Hirota K*, et al.* Disruption of oxygen homeostasis underlies congenital Chuvash polycythemia. Nature genetics 2002;32(4):614-21.

53. Pastore YD, Jelinek J, Ang S*, et al.* Mutations in the VHL gene in sporadic apparently congenital polycythemia. Blood 2003;101(4):1591-5.

54. Gordeuk VR, Sergueeva AI, Miasnikova GY*, et al.* Congenital disorder of oxygen sensing: association of the homozygous Chuvash polycythemia VHL mutation with thrombosis and vascular abnormalities but not tumors. Blood 2004;103(10):3924-32.

55. Stebbins CE, Kaelin WG, Jr., Pavletich NP. Structure of the VHL-ElonginC-ElonginB complex: implications for VHL tumor suppressor function. Science 1999;284(5413):455-61.

56. Duan DR, Pause A, Burgess WH*, et al.* Inhibition of transcription elongation by the VHL tumor suppressor protein. Science (New York, NY 1995;269(5229):1402-6.

57. Kibel A, Iliopoulos O, DeCaprio JA, Kaelin WG, Jr. Binding of the von Hippel-Lindau tumor suppressor protein to Elongin B and C. Science 1995;269(5229):1444-6.

58. Pause A, Lee S, Worrell RA*, et al.* The von Hippel-Lindau tumor-suppressor gene product forms a stable complex with human CUL-2, a member of the Cdc53 family of proteins. Proceedings of the National Academy of Sciences of the United States of America 1997;94(6):2156-61.

59. Lonergan KM, Iliopoulos O, Ohh M*, et al.* Regulation of hypoxia-inducible mRNAs by the von Hippel-Lindau tumor suppressor protein requires binding to complexes containing elongins B/C and Cul2. Mol Cell Biol 1998;18(2):732-41.

60. Kamura T, Koepp DM, Conrad MN*, et al.* Rbx1, a component of the VHL tumor suppressor complex and SCF ubiquitin ligase. Science 1999;284(5414):657-61.

61. Iwai K, Yamanaka K, Kamura T*, et al.* Identification of the von Hippel-lindau tumor-suppressor protein as part of an active E3 ubiquitin ligase complex. Proceedings of the National Academy of Sciences of the United States of America 1999;96(22):12436-41.

62. Lisztwan J, Imbert G, Wirbelauer C, Gstaiger M, Krek W. The von Hippel-Lindau tumor suppressor protein is a component of an E3 ubiquitin-protein ligase activity. Genes & development 1999;13(14):1822-33.

63. Cockman ME, Masson N, Mole DR*, et al.* Hypoxia inducible factor-alpha binding and ubiquitylation by the von Hippel-Lindau tumor suppressor protein. The Journal of biological chemistry 2000;275(33):25733-41.

64. Iliopoulos O, Levy AP, Jiang C, Kaelin WG, Jr., Goldberg MA. Negative regulation of hypoxia-inducible genes by the von Hippel-Lindau protein. Proceedings of the National Academy of Sciences of the United States of America 1996;93(20):10595-9.

65. Maxwell PH, Wiesener MS, Chang GW*, et al.* The tumour suppressor protein VHL targets hypoxia-inducible factors for oxygen-dependent proteolysis. Nature 1999;399(6733):271-5.

66. Ohh M, Park CW, Ivan M*, et al.* Ubiquitination of hypoxia-inducible factor requires direct binding to the beta-domain of the von Hippel-Lindau protein. Nature cell biology 2000;2(7):423-7.

67. Okuda H, Saitoh K, Hirai S*, et al.* The von Hippel-Lindau tumor suppressor protein mediates ubiquitination of activated atypical protein kinase C. The Journal of biological chemistry 2001;276(47):43611-7.

68. Li Z, Wang D, Na X, Schoen SR, Messing EM, Wu G. Identification of a deubiquitinating enzyme subfamily as substrates of the von Hippel-Lindau tumor suppressor. Biochemical and biophysical research communications 2002;294(3):700-9.

69. Na X, Duan HO, Messing EM*, et al.* Identification of the RNA polymerase II subunit hsRPB7 as a novel target of the von Hippel-Lindau protein. EMBO J 2003;22(16):4249-59.

70. Kuznetsova AV, Meller J, Schnell PO*, et al.* von Hippel-Lindau protein binds hyperphosphorylated large subunit of RNA polymerase II through a proline hydroxylation motif and targets it for ubiquitination. Proceedings of the National Academy of Sciences of the United States of America 2003;100(5):2706-11.

71. Huang J, Zhao Q, Mooney SM, Lee FS. Sequence determinants in hypoxia-inducible factor-1alpha for hydroxylation by the prolyl hydroxylases PHD1, PHD2, and PHD3. J Biol Chem 2002;277(42):39792-800.

72. Jaakkola P, Mole DR, Tian YM*, et al.* Targeting of HIF-alpha to the von Hippel-Lindau ubiquitylation complex by O2-regulated prolyl hydroxylation. Science 2001;292(5516):468-72.

73. Min JH, Yang H, Ivan M, Gertler F, Kaelin WG, Jr., Pavletich NP. Structure of an HIF-1alpha -pVHL complex: hydroxyproline recognition in signaling. Science (New York, NY 2002;296(5574):1886-9.

74. Ivan M, Kondo K, Yang H*, et al.* HIFalpha targeted for VHL-mediated destruction by proline hydroxylation: implications for O2 sensing. Science (New York, NY 2001;292(5516):464-8.

75. Hon WC, Wilson MI, Harlos K*, et al.* Structural basis for the recognition of hydroxyproline in HIF-1 alpha by pVHL. Nature 2002;417(6892):975-8.

76. Jiang BH, Rue E, Wang GL, Roe R, Semenza GL. Dimerization, DNA binding, and transactivation properties of hypoxia-inducible factor 1. The Journal of biological chemistry 1996;271(30):17771-8.

77. Semenza GL, Jiang BH, Leung SW*, et al.* Hypoxia response elements in the aldolase A, enolase 1, and lactate dehydrogenase A gene promoters contain essential binding sites for hypoxia-inducible factor 1. The Journal of biological chemistry 1996;271(51):32529-37.

78. Tian H, McKnight SL, Russell DW. Endothelial PAS domain protein 1 (EPAS1), a transcription factor selectively expressed in endothelial cells. Genes & development 1997;11(1):72-82.

79. Semenza GL. Targeting HIF-1 for cancer therapy. Nature reviews 2003;3(10):721-32.

80. Wiesener MS, Turley H, Allen WE*, et al.* Induction of endothelial PAS domain protein-1 by hypoxia: characterization and comparison with hypoxia-inducible factor-1alpha. Blood 1998;92(7):2260-8.

81. Compernolle V, Brusselmans K, Acker T*, et al.* Loss of HIF-2alpha and inhibition of VEGF impair fetal lung maturation, whereas treatment with VEGF prevents fatal respiratory distress in premature mice. Nat Med 2002;8(7):702-10.

82. Jurgensen JS, Rosenberger C, Wiesener MS*, et al.* Persistent induction of HIF-1alpha and -2alpha in cardiomyocytes and stromal cells of ischemic myocardium. FASEB J 2004;18(12):1415-7.

83. Hu CJ, Wang LY, Chodosh LA, Keith B, Simon MC. Differential roles of hypoxia-inducible factor 1alpha (HIF-1alpha) and HIF-2alpha in hypoxic gene regulation. Molecular and cellular biology 2003;23(24):9361-74.

84. Kim JW, Tchernyshyov I, Semenza GL, Dang CV. HIF-1-mediated expression of pyruvate dehydrogenase kinase: a metabolic switch required for cellular adaptation to hypoxia. Cell metabolism 2006;3(3):177-85.

85. Sowter HM, Ratcliffe PJ, Watson P, Greenberg AH, Harris AL. HIF-1-dependent regulation of hypoxic induction of the cell death factors BNIP3 and NIX in human tumors. Cancer Res 2001;61(18):6669-73.

86. Covello KL, Kehler J, Yu H*, et al.* HIF-2alpha regulates Oct-4: effects of hypoxia on stem cell function, embryonic development, and tumor growth. Genes & development 2006;20(5):557-70.

87. Baba M, Hirai S, Yamada-Okabe H*, et al.* Loss of von Hippel-Lindau protein causes cell density dependent deregulation of CyclinD1 expression through hypoxia-inducible factor. Oncogene 2003;22(18):2728-38.

88. Gort EH, van Haaften G, Verlaan I*, et al.* The TWIST1 oncogene is a direct target of hypoxia-inducible factor-2alpha. Oncogene 2008;27(11):1501-10.

89. Gunaratnam L, Morley M, Franovic A*, et al.* Hypoxia inducible factor activates the transforming growth factor-alpha/epidermal growth factor receptor growth stimulatory pathway in VHL(-/-) renal cell carcinoma cells. The Journal of biological chemistry 2003;278(45):44966-74.

90. Gruber M, Hu CJ, Johnson RS, Brown EJ, Keith B, Simon MC. Acute postnatal ablation of Hif-2alpha results in anemia. Proceedings of the National Academy of Sciences of the United States of America 2007;104(7):2301-6.

91. Young AP, Schlisio S, Minamishima YA*, et al.* VHL loss actuates a HIF-independent senescence programme mediated by Rb and p400. Nature cell biology 2008;10(3):361-9.

92. Kamada M, Suzuki K, Kato Y, Okuda H, Shuin T. von Hippel-Lindau protein promotes the assembly of actin and vinculin and inhibits cell motility. Cancer research 2001;61(10):4184-9.

93. Hergovich A, Lisztwan J, Barry R, Ballschmieter P, Krek W. Regulation of microtubule stability by the von Hippel-Lindau tumour suppressor protein pVHL. Nature cell biology 2003;5(1):64-70.

94. Esteban-Barragan MA, Avila P, Alvarez-Tejado M*, et al.* Role of the von Hippel-Lindau tumor suppressor gene in the formation of beta1-integrin fibrillar adhesions. Cancer Res 2002;62(10):2929-36.

95. Ohh M, Yauch RL, Lonergan KM*, et al.* The von Hippel-Lindau tumor suppressor protein is required for proper assembly of an extracellular fibronectin matrix. Molecular cell 1998;1(7):959-68.

96. Chan HM, Narita M, Lowe SW, Livingston DM. The p400 E1A-associated protein is a novel component of the p53 --> p21 senescence pathway. Genes & development 2005;19(2):196-201.

97. Grosfeld A, Stolze IP, Cockman ME*, et al.* Interaction of hydroxylated collagen IV with the von hippel-lindau tumor suppressor. The Journal of biological chemistry 2007;282(18):13264-9.

98. Kurban G, Duplan E, Ramlal N*, et al.* Collagen matrix assembly is driven by the interaction of von Hippel-Lindau tumor suppressor protein with hydroxylated collagen IV alpha 2. Oncogene 2008;27(7):1004-12.

99. Russell RC, Ohh M. NEDD8 acts as a 'molecular switch' defining the functional selectivity of VHL. EMBO Rep 2008;9(5):486-91.

100. Hoffman MA, Ohh M, Yang H, Klco JM, Ivan M, Kaelin WG, Jr. von Hippel-Lindau protein mutants linked to type 2C VHL disease preserve the ability to downregulate HIF. Human molecular genetics 2001;10(10):1019-27.

101. Schermer B, Ghenoiu C, Bartram M*, et al.* The von Hippel-Lindau tumor suppressor protein controls ciliogenesis by orienting microtubule growth. J Cell Biol 2006;175(4):547-54.

102. Kuehn EW, Walz G, Benzing T. Von hippel-lindau: a tumor suppressor links microtubules to ciliogenesis and cancer development. Cancer Res 2007;67(10):4537-40.

103. Yoder BK. Role of primary cilia in the pathogenesis of polycystic kidney disease. J Am Soc Nephrol 2007;18(5):1381-8.

104. Thoma CR, Frew IJ, Hoerner CR, Montani M, Moch H, Krek W. pVHL and GSK3beta are components of a primary cilium-maintenance signalling network. Nature cell biology 2007;9(5):588-95.

105. Hergovich A, Lisztwan J, Thoma CR, Wirbelauer C, Barry RE, Krek W. Priming-dependent phosphorylation and regulation of the tumor suppressor pVHL by glycogen synthase kinase 3. Molecular and cellular biology 2006;26(15):5784-96.

106. Mack FA, Rathmell WK, Arsham AM, Gnarra J, Keith B, Simon MC. Loss of pVHL is sufficient to cause HIF dysregulation in primary cells but does not promote tumor growth. Cancer Cell 2003;3(1):75-88.

107. Rathmell WK, Hickey MM, Bezman NA, Chmielecki CA, Carraway NC, Simon MC. In vitro and in vivo models analyzing von Hippel-Lindau disease-specific mutations. Cancer research 2004;64(23):8595-603.

108. Acker T, Diez-Juan A, Aragones J*, et al.* Genetic evidence for a tumor suppressor role of HIF-2alpha. Cancer Cell 2005;8(2):131-41.

109. Lee S, Nakamura E, Yang H*, et al.* Neuronal apoptosis linked to EglN3 prolyl hydroxylase and familial pheochromocytoma genes: developmental culling and cancer. Cancer Cell 2005;8(2):155-67.

110. Gnarra JR, Ward JM, Porter FD*, et al.* Defective placental vasculogenesis causes embryonic lethality in VHL-deficient mice. Proceedings of the National Academy of Sciences of the United States of America 1997;94(17):9102-7.

111. Haase VH, Glickman JN, Socolovsky M, Jaenisch R. Vascular tumors in livers with targeted inactivation of the von Hippel-Lindau tumor suppressor. Proceedings of the National Academy of Sciences of the United States of America 2001;98(4):1583-8.

112. Hickey MM, Lam JC, Bezman NA, Rathmell WK, Simon MC. von Hippel-Lindau mutation in mice recapitulates Chuvash polycythemia via hypoxia-inducible factor-2alpha signaling and splenic erythropoiesis. J Clin Invest 2007;117(12):3879-89.

113. Rossant J, Cross JC. Placental development: lessons from mouse mutants. Nat Rev Genet 2001;2(7):538-48.

114. Watson ED, Cross JC. Development of structures and transport functions in the mouse placenta. Physiology (Bethesda) 2005;20:180-93.

115. Kleymenova E, Everitt JI, Pluta L, Portis M, Gnarra JR, Walker CL. Susceptibility to vascular neoplasms but no increased susceptibility to renal carcinogenesis in Vhl knockout mice. Carcinogenesis 2004;25(3):309-15.

116. Ma W, Tessarollo L, Hong SB*, et al.* Hepatic vascular tumors, angiectasis in multiple organs, and impaired spermatogenesis in mice with conditional inactivation of the VHL gene. Cancer Res 2003;63(17):5320-8.

117. Hong SB, Furihata M, Baba M, Zbar B, Schmidt LS. Vascular defects and liver damage by the acute inactivation of the VHL gene during mouse embryogenesis. Lab Invest 2006;86(7):664-75.

118. Iyer NV, Kotch LE, Agani F*, et al.* Cellular and developmental control of O2 homeostasis by hypoxia-inducible factor 1 alpha. Genes & development 1998;12(2):149-62.

119. Peng J, Zhang L, Drysdale L, Fong GH. The transcription factor EPAS-1/hypoxia-inducible factor 2alpha plays an important role in vascular remodeling. Proceedings of the National Academy of Sciences of the United States of America 2000;97(15):8386-91.

120. Tian H, Hammer RE, Matsumoto AM, Russell DW, McKnight SL. The hypoxia-responsive transcription factor EPAS1 is essential for catecholamine homeostasis and protection against heart failure during embryonic development. Genes & development 1998;12(21):3320-4.

121. Adelman DM, Gertsenstein M, Nagy A, Simon MC, Maltepe E. Placental cell fates are regulated in vivo by HIF-mediated hypoxia responses. Genes & development 2000;14(24):3191-203.

122. Cowden Dahl KD, Fryer BH, Mack FA*, et al.* Hypoxia-inducible factors 1alpha and 2alpha regulate trophoblast differentiation. Molecular and cellular biology 2005;25(23):10479-91.

123. Kozak KR, Abbott B, Hankinson O. ARNT-deficient mice and placental differentiation. Dev Biol 1997;191(2):297-305.

124. Maltepe E, Schmidt JV, Baunoch D, Bradfield CA, Simon MC. Abnormal angiogenesis and responses to glucose and oxygen deprivation in mice lacking the protein ARNT. Nature 1997;386(6623):403-7.

125. Takeda K, Ho VC, Takeda H, Duan LJ, Nagy A, Fong GH. Placental but not heart defects are associated with elevated hypoxia-inducible factor alpha levels in mice lacking prolyl hydroxylase domain protein 2. Molecular and cellular biology 2006;26(22):8336-46.

126. Bruick RK, McKnight SL. A conserved family of prolyl-4-hydroxylases that modify HIF. Science (New York, NY 2001;294(5545):1337-40.

127. Epstein AC, Gleadle JM, McNeill LA*, et al.* C. elegans EGL-9 and mammalian homologs define a family of dioxygenases that regulate HIF by prolyl hydroxylation. Cell 2001;107(1):43-54.

128. Huang LE, Gu J, Schau M, Bunn HF. Regulation of hypoxia-inducible factor 1alpha is mediated by an O2-dependent degradation domain via the ubiquitin-proteasome pathway. Proceedings of the National Academy of Sciences of the United States of America 1998;95(14):7987-92.

129. Ivan M, Haberberger T, Gervasi DC*, et al.* Biochemical purification and pharmacological inhibition of a mammalian prolyl hydroxylase acting on hypoxia-inducible factor. Proceedings of the National Academy of Sciences of the United States of America 2002;99(21):13459-64.

130. Pugh CW, O'Rourke JF, Nagao M, Gleadle JM, Ratcliffe PJ. Activation of hypoxia-inducible factor-1; definition of regulatory domains within the alpha subunit. The Journal of biological chemistry 1997;272(17):11205-14.

131. Hirsila M, Koivunen P, Gunzler V, Kivirikko KI, Myllyharju J. Characterization of the human prolyl 4-hydroxylases that modify the hypoxia-inducible factor. The Journal of biological chemistry 2003;278(33):30772-80.

132. Tang N, Mack F, Haase VH, Simon MC, Johnson RS. pVHL function is essential for endothelial extracellular matrix deposition. Molecular and cellular biology 2006;26(7):2519-30.

133. Rankin EB, Higgins DF, Walisser JA, Johnson RS, Bradfield CA, Haase VH. Inactivation of the arylhydrocarbon receptor nuclear translocator (Arnt) suppresses von Hippel-Lindau disease-associated vascular tumors in mice. Molecular and cellular biology 2005;25(8):3163-72.

134. Rankin EB, Rha J, Unger TL*, et al.* Hypoxia-inducible factor-2 regulates vascular tumorigenesis in mice. Oncogene 2008;27(40):5354-8.

135. Kim WY, Safran M, Buckley MR*, et al.* Failure to prolyl hydroxylate hypoxia-inducible factor alpha phenocopies VHL inactivation in vivo. Embo J 2006;25(19):4650-62.

136. Rankin EB, Tomaszewski JE, Haase VH. Renal cyst development in mice with conditional inactivation of the von Hippel-Lindau tumor suppressor. Cancer Res 2006;66(5):2576-83.

137. Brenner W, Farber G, Herget T, Lehr HA, Hengstler JG, Thuroff JW. Loss of tumor suppressor protein PTEN during renal carcinogenesis. Int J Cancer 2002;99(1):53-7.

138. Hara S, Oya M, Mizuno R, Horiguchi A, Marumo K, Murai M. Akt activation in renal cell carcinoma: contribution of a decreased PTEN expression and the induction of apoptosis by an Akt inhibitor. Ann Oncol 2005;16(6):928-33.

139. Shin Lee J, Seok Kim H, Bok Kim Y, Cheol Lee M, Soo Park C. Expression of PTEN in renal cell carcinoma and its relation to tumor behavior and growth. J Surg Oncol 2003;84(3):166-72.

140. Frew IJ, Thoma CR, Georgiev S*, et al.* pVHL and PTEN tumour suppressor proteins cooperatively suppress kidney cyst formation. EMBO J 2008;27(12):1747-57.

141. Pazour GJ. Intraflagellar transport and cilia-dependent renal disease: the ciliary hypothesis of polycystic kidney disease. J Am Soc Nephrol 2004;15(10):2528-36.

142. Yoder BK, Hou X, Guay-Woodford LM. The polycystic kidney disease proteins, polycystin-1, polycystin-2, polaris, and cystin, are co-localized in renal cilia. J Am Soc Nephrol 2002;13(10):2508-16.

143. Fischer E, Legue E, Doyen A*, et al.* Defective planar cell polarity in polycystic kidney disease. Nature genetics 2006;38(1):21-3.

144. Ansley SJ, Badano JL, Blacque OE*, et al.* Basal body dysfunction is a likely cause of pleiotropic Bardet-Biedl syndrome. Nature 2003;425(6958):628-33.

145. Badano JL, Mitsuma N, Beales PL, Katsanis N. The ciliopathies: an emerging class of human genetic disorders. Annu Rev Genomics Hum Genet 2006;7:125-48.

146. Stoetzel C, Muller J, Laurier V*, et al.* Identification of a novel BBS gene (BBS12) highlights the major role of a vertebrate-specific branch of chaperonin-related proteins in Bardet-Biedl syndrome. Am J Hum Genet 2007;80(1):1-11.

147. Esteban MA, Harten SK, Tran MG, Maxwell PH. Formation of primary cilia in the renal epithelium is regulated by the von Hippel-Lindau tumor suppressor protein. J Am Soc Nephrol 2006;17(7):1801-6.

148. Schraml P, Frew IJ, Thoma CR*, et al.* Sporadic clear cell renal cell carcinoma but not the papillary type is characterized by severely reduced frequency of primary cilia. Mod Pathol 2009;22(1):31-6.

149. Cross DA, Alessi DR, Cohen P, Andjelkovich M, Hemmings BA. Inhibition of glycogen synthase kinase-3 by insulin mediated by protein kinase B. Nature 1995;378(6559):785-9.

150. Inoki K, Corradetti MN, Guan KL. Dysregulation of the TSC-mTOR pathway in human disease. Nature genetics 2005;37(1):19-24.

151. Rosner M, Hanneder M, Siegel N, Valli A, Fuchs C, Hengstschlager M. The mTOR pathway and its role in human genetic diseases. Mutat Res 2008;659(3):284-92.

152. Hara K, Maruki Y, Long X*, et al.* Raptor, a binding partner of target of rapamycin (TOR), mediates TOR action. Cell 2002;110(2):177-89.

153. Gingras AC, Raught B, Sonenberg N. Control of translation by the target of rapamycin proteins. Prog Mol Subcell Biol 2001;27:143-74.

154. Avruch J, Belham C, Weng Q, Hara K, Yonezawa K. The p70 S6 kinase integrates nutrient and growth signals to control translational capacity. Prog Mol Subcell Biol 2001;26:115-54.

155. Meyuhas O. Synthesis of the translational apparatus is regulated at the translational level. Eur J Biochem 2000;267(21):6321-30.

156. Gingras AC, Gygi SP, Raught B*, et al.* Regulation of 4E-BP1 phosphorylation: a novel two-step mechanism. Genes & development 1999;13(11):1422-37.

157. Hudson CC, Liu M, Chiang GG*, et al.* Regulation of hypoxia-inducible factor 1alpha expression and function by the mammalian target of rapamycin. Molecular and cellular biology 2002;22(20):7004-14.

158. Bai X, Ma D, Liu A*, et al.* Rheb activates mTOR by antagonizing its endogenous inhibitor, FKBP38. Science (New York, NY 2007;318(5852):977-80.

159. Garami A, Zwartkruis FJ, Nobukuni T*, et al.* Insulin activation of Rheb, a mediator of mTOR/S6K/4E-BP signaling, is inhibited by TSC1 and 2. Molecular cell 2003;11(6):1457-66.

160. Inoki K, Zhu T, Guan KL. TSC2 mediates cellular energy response to control cell growth and survival. Cell 2003;115(5):577-90.

161. Zhang Y, Gao X, Saucedo LJ, Ru B, Edgar BA, Pan D. Rheb is a direct target of the tuberous sclerosis tumour suppressor proteins. Nature cell biology 2003;5(6):578-81.

162. Carling D. The AMP-activated protein kinase cascade--a unifying system for energy control. Trends Biochem Sci 2004;29(1):18-24.

163. Cantley LC. The phosphoinositide 3-kinase pathway. Science (New York, NY 2002;296(5573):1655-7.

164. Inoki K, Li Y, Zhu T, Wu J, Guan KL. TSC2 is phosphorylated and inhibited by Akt and suppresses mTOR signalling. Nature cell biology 2002;4(9):648-57.

165. Manning BD, Tee AR, Logsdon MN, Blenis J, Cantley LC. Identification of the tuberous sclerosis complex-2 tumor suppressor gene product tuberin as a target of the phosphoinositide 3-kinase/akt pathway. Molecular cell 2002;10(1):151-62.

166. Yang CS, Song CH, Lee JS*, et al.* Intracellular network of phosphatidylinositol 3-kinase, mammalian target of the rapamycin/70 kDa ribosomal S6 kinase 1, and mitogen-activated protein kinases pathways for regulating mycobacteria-induced IL-23 expression in human macrophages. Cell Microbiol 2006;8(7):1158-71.

167. King A, Selak MA, Gottlieb E. Succinate dehydrogenase and fumarate hydratase: linking mitochondrial dysfunction and cancer. Oncogene 2006;25(34):4675-82.

168. Ehrismann D, Flashman E, Genn DN*, et al.* Studies on the activity of the hypoxia-inducible-factor hydroxylases using an oxygen consumption assay. Biochem J 2007;401(1):227-34.

169. Koivunen P, Hirsila M, Kivirikko KI, Myllyharju J. The length of peptide substrates has a marked effect on hydroxylation by the hypoxia-inducible factor prolyl 4-hydroxylases. The Journal of biological chemistry 2006;281(39):28712-20.

170. Berra E, Benizri E, Ginouves A, Volmat V, Roux D, Pouyssegur J. HIF prolyl-hydroxylase 2 is the key oxygen sensor setting low steady-state levels of HIF-1alpha in normoxia. EMBO J 2003;22(16):4082-90.

171. Minamishima YA, Moslehi J, Bardeesy N, Cullen D, Bronson RT, Kaelin WG, Jr. Somatic inactivation of the PHD2 prolyl hydroxylase causes polycythemia and congestive heart failure. Blood 2008;111(6):3236-44.

172. Takeda K, Aguila HL, Parikh NS*, et al.* Regulation of adult erythropoiesis by prolyl hydroxylase domain proteins. Blood 2008;111(6):3229-35.

173. Isaacs JS, Jung YJ, Mimnaugh EG, Martinez A, Cuttitta F, Neckers LM. Hsp90 regulates a von Hippel Lindau-independent hypoxia-inducible factor-1 alpha-degradative pathway. The Journal of biological chemistry 2002;277(33):29936-44.

174. Kong X, Lin Z, Liang D, Fath D, Sang N, Caro J. Histone deacetylase inhibitors induce VHL and ubiquitin-independent proteasomal degradation of hypoxia-inducible factor 1alpha. Molecular and cellular biology 2006;26(6):2019-28.

175. Hewitson KS, McNeill LA, Riordan MV*, et al.* Hypoxia-inducible factor (HIF) asparagine hydroxylase is identical to factor inhibiting HIF (FIH) and is related to the cupin structural family. The Journal of biological chemistry 2002;277(29):26351-5.

176. Lando D, Peet DJ, Whelan DA, Gorman JJ, Whitelaw ML. Asparagine hydroxylation of the HIF transactivation domain a hypoxic switch. Science (New York, NY 2002;295(5556):858-61.

177. Mahon PC, Hirota K, Semenza GL. FIH-1: a novel protein that interacts with HIF-1alpha and VHL to mediate repression of HIF-1 transcriptional activity. Genes & development 2001;15(20):2675-86.

178. Koivunen P, Hirsila M, Remes AM, Hassinen IE, Kivirikko KI, Myllyharju J. Inhibition of hypoxia-inducible factor (HIF) hydroxylases by citric acid cycle intermediates: possible links between cell metabolism and stabilization of HIF. The Journal of biological chemistry 2007;282(7):4524-32.

179. Carrero P, Okamoto K, Coumailleau P, O'Brien S, Tanaka H, Poellinger L. Redox-regulated recruitment of the transcriptional coactivators CREB-binding protein and SRC-1 to hypoxia-inducible factor 1alpha. Molecular and cellular biology 2000;20(1):402-15.

180. Huang LE, Arany Z, Livingston DM, Bunn HF. Activation of hypoxia-inducible transcription factor depends primarily upon redox-sensitive stabilization of its alpha subunit. The Journal of biological chemistry 1996;271(50):32253-9.

181. Kim CM, Vocke C, Torres-Cabala C*, et al.* Expression of hypoxia inducible factor-1alpha and 2alpha in genetically distinct early renal cortical tumors. J Urol 2006;175(5):1908-14.

182. Curatolo P, Bombardieri R, Jozwiak S. Tuberous sclerosis. Lancet 2008;372(9639):657-68.

183. Dabora SL, Jozwiak S, Franz DN*, et al.* Mutational analysis in a cohort of 224 tuberous sclerosis patients indicates increased severity of TSC2, compared with TSC1, disease in multiple organs. Am J Hum Genet 2001;68(1):64-80.

184. Hung CC, Su YN, Chien SC*, et al.* Molecular and clinical analyses of 84 patients with tuberous sclerosis complex. BMC Med Genet 2006;7:72.

185. Jones AC, Shyamsundar MM, Thomas MW*, et al.* Comprehensive mutation analysis of TSC1 and TSC2-and phenotypic correlations in 150 families with tuberous sclerosis. Am J Hum Genet 1999;64(5):1305-15.

186. Langkau N, Martin N, Brandt R*, et al.* TSC1 and TSC2 mutations in tuberous sclerosis, the associated phenotypes and a model to explain observed TSC1/ TSC2 frequency ratios. Eur J Pediatr 2002;161(7):393-402.

187. O'Callaghan FJ, Noakes MJ, Martyn CN, Osborne JP. An epidemiological study of renal pathology in tuberous sclerosis complex. BJU Int 2004;94(6):853-7.

188. Bjornsson J, Short MP, Kwiatkowski DJ, Henske EP. Tuberous sclerosis-associated renal cell carcinoma. Clinical, pathological, and genetic features. Am J Pathol 1996;149(4):1201-8.

189. Robertson FM, Cendron M, Klauber GT, Harris BH. Renal cell carcinoma in association with tuberous sclerosis in children. J Pediatr Surg 1996;31(5):729-30.

190. Hino O, Kobayashi T, Tsuchiya H*, et al.* The predisposing gene of the Eker rat inherited cancer syndrome is tightly linked to the tuberous sclerosis (TSC2) gene. Biochemical and biophysical research communications 1994;203(2):1302-8.

191. Yeung RS, Xiao GH, Jin F, Lee WC, Testa JR, Knudson AG. Predisposition to renal carcinoma in the Eker rat is determined by germ-line mutation of the tuberous sclerosis 2 (TSC2) gene. Proceedings of the National Academy of Sciences of the United States of America 1994;91(24):11413-6.

192. Kobayashi T, Minowa O, Kuno J, Mitani H, Hino O, Noda T. Renal carcinogenesis, hepatic hemangiomatosis, and embryonic lethality caused by a germ-line Tsc2 mutation in mice. Cancer Res 1999;59(6):1206-11.

193. Kobayashi T, Minowa O, Sugitani Y*, et al.* A germ-line Tsc1 mutation causes tumor development and embryonic lethality that are similar, but not identical to, those caused by Tsc2 mutation in mice. Proceedings of the National Academy of Sciences of the United States of America 2001;98(15):8762-7.

194. Wilson C, Idziaszczyk S, Parry L*, et al.* A mouse model of tuberous sclerosis 1 showing background specific early post-natal mortality and metastatic renal cell carcinoma. Human molecular genetics 2005;14(13):1839-50.

195. Liu MY, Poellinger L, Walker CL. Up-regulation of hypoxia-inducible factor 2alpha in renal cell carcinoma associated with loss of Tsc-2 tumor suppressor gene. Cancer Res 2003;63(10):2675-80.

196. Nickerson ML, Warren MB, Toro JR*, et al.* Mutations in a novel gene lead to kidney tumors, lung wall defects, and benign tumors of the hair follicle in patients with the Birt-Hogg-Dube syndrome. Cancer Cell 2002;2(2):157-64.

197. Toro JR, Wei MH, Glenn GM*, et al.* BHD mutations, clinical and molecular genetic investigations of Birt-Hogg-Dube syndrome: a new series of 50 families and a review of published reports. Journal of medical genetics 2008;45(6):321-31.

198. Pavlovich CP, Walther MM, Eyler RA*, et al.* Renal tumors in the Birt-Hogg-Dube syndrome. Am J Surg Pathol 2002;26(12):1542-52.

199. Okimoto K, Sakurai J, Kobayashi T*, et al.* A germ-line insertion in the Birt-Hogg-Dube (BHD) gene gives rise to the Nihon rat model of inherited renal cancer. Proceedings of the National Academy of Sciences of the United States of America 2004;101(7):2023-7.

200. Hartman TR, Nicolas E, Klein-Szanto A*, et al.* The role of the Birt-Hogg-Dube protein in mTOR activation and renal tumorigenesis. Oncogene 2009;28(13):1594-604.

201. Baba M, Furihata M, Hong SB*, et al.* Kidney-targeted Birt-Hogg-Dube gene inactivation in a mouse model: Erk1/2 and Akt-mTOR activation, cell hyperproliferation, and polycystic kidneys. J Natl Cancer Inst 2008;100(2):140-54.

202. Chen J, Futami K, Petillo D*, et al.* Deficiency of FLCN in mouse kidney led to development of polycystic kidneys and renal neoplasia. PLoS ONE 2008;3(10):e3581.

203. Robb VA, Karbowniczek M, Klein-Szanto AJ, Henske EP. Activation of the mTOR signaling pathway in renal clear cell carcinoma. J Urol 2007;177(1):346-52.

204. Baba M, Hong SB, Sharma N*, et al.* Folliculin encoded by the BHD gene interacts with a binding protein, FNIP1, and AMPK, and is involved in AMPK and mTOR signaling. Proceedings of the National Academy of Sciences of the United States of America 2006;103(42):15552-7.

205. Hasumi H, Baba M, Hong SB*, et al.* Identification and characterization of a novel folliculin-interacting protein FNIP2. Gene 2008;415(1-2):60-7.

206. Takagi Y, Kobayashi T, Shiono M*, et al.* Interaction of folliculin (Birt-Hogg-Dube gene product) with a novel Fnip1-like (FnipL/Fnip2) protein. Oncogene 2008;27(40):5339-47.

207. Schmidt L, Junker K, Nakaigawa N*, et al.* Novel mutations of the MET proto-oncogene in papillary renal carcinomas. Oncogene 1999;18(14):2343-50.

208. Schmidt L, Junker K, Weirich G*, et al.* Two North American families with hereditary papillary renal carcinoma and identical novel mutations in the MET proto-oncogene. Cancer Res 1998;58(8):1719-22.

209. Bottaro DP, Rubin JS, Faletto DL*, et al.* Identification of the hepatocyte growth factor receptor as the c-met proto-oncogene product. Science (New York, NY 1991;251(4995):802-4.

210. Bardelli A, Pugliese L, Comoglio PM. "Invasive-growth" signaling by the Met/HGF receptor: the hereditary renal carcinoma connection. Biochim Biophys Acta 1997;1333(3):M41-51.

211. Zbar B, Tory K, Merino M*, et al.* Hereditary papillary renal cell carcinoma. J Urol 1994;151(3):561-6.

212. Zhuang Z, Park WS, Pack S*, et al.* Trisomy 7-harbouring non-random duplication of the mutant MET allele in hereditary papillary renal carcinomas. Nature genetics 1998;20(1):66-9.

213. Graveel C, Su Y, Koeman J*, et al.* Activating Met mutations produce unique tumor profiles in mice with selective duplication of the mutant allele. Proceedings of the National Academy of Sciences of the United States of America 2004;101(49):17198-203.

214. Nakaigawa N, Yao M, Baba M*, et al.* Inactivation of von Hippel-Lindau gene induces constitutive phosphorylation of MET protein in clear cell renal carcinoma. Cancer Res 2006;66(7):3699-705.

215. Tomlinson IP, Alam NA, Rowan AJ*, et al.* Germline mutations in FH predispose to dominantly inherited uterine fibroids, skin leiomyomata and papillary renal cell cancer. Nature genetics 2002;30(4):406-10.

216. Toro JR, Nickerson ML, Wei MH*, et al.* Mutations in the fumarate hydratase gene cause hereditary leiomyomatosis and renal cell cancer in families in North America. Am J Hum Genet 2003;73(1):95-106.

217. Pollard PJ, Briere JJ, Alam NA*, et al.* Accumulation of Krebs cycle intermediates and over-expression of HIF1alpha in tumours which result from germline FH and SDH mutations. Human molecular genetics 2005;14(15):2231-9.

218. Merino MJ, Torres-Cabala C, Pinto P, Linehan WM. The morphologic spectrum of kidney tumors in hereditary leiomyomatosis and renal cell carcinoma (HLRCC) syndrome. Am J Surg Pathol 2007;31(10):1578-85.

219. Isaacs JS, Jung YJ, Mole DR*, et al.* HIF overexpression correlates with biallelic loss of fumarate hydratase in renal cancer: novel role of fumarate in regulation of HIF stability. Cancer Cell 2005;8(2):143-53.

220. Pollard PJ, Spencer-Dene B, Shukla D*, et al.* Targeted inactivation of fh1 causes proliferative renal cyst development and activation of the hypoxia pathway. Cancer Cell 2007;11(4):311-9.

221. Astuti D, Latif F, Dallol A*, et al.* Gene mutations in the succinate dehydrogenase subunit SDHB cause susceptibility to familial pheochromocytoma and to familial paraganglioma. Am J Hum Genet 2001;69(1):49-54.

222. Baysal BE, Ferrell RE, Willett-Brozick JE*, et al.* Mutations in SDHD, a mitochondrial complex II gene, in hereditary paraganglioma. Science (New York, NY 2000;287(5454):848-51.

223. Niemann S, Muller U. Mutations in SDHC cause autosomal dominant paraganglioma, type 3. Nature genetics 2000;26(3):268-70.

224. Maher ER, Eng C. The pressure rises: update on the genetics of phaeochromocytoma. Human molecular genetics 2002;11(20):2347-54.

225. Srirangalingam U, Walker L, Khoo B*, et al.* Clinical manifestations of familial paraganglioma and phaeochromocytomas in succinate dehydrogenase B (SDH-B) gene mutation carriers. Clin Endocrinol (Oxf) 2008;69(4):587-96.

226. Vanharanta S, Buchta M, McWhinney SR*, et al.* Early-onset renal cell carcinoma as a novel extraparaganglial component of SDHB-associated heritable paraganglioma. Am J Hum Genet 2004;74(1):153-9.

227. Ricketts C, Woodward ER, Killick P*, et al.* Germline SDHB mutations and familial renal cell carcinoma. J Natl Cancer Inst 2008;100(17):1260-2.

228. Cervera AM, Apostolova N, Crespo FL, Mata M, McCreath KJ. Cells silenced for SDHB expression display characteristic features of the tumor phenotype. Cancer Res 2008;68(11):4058-67.

229. Selak MA, Armour SM, MacKenzie ED*, et al.* Succinate links TCA cycle dysfunction to oncogenesis by inhibiting HIF-alpha prolyl hydroxylase. Cancer Cell 2005;7(1):77-85.

230. MacKenzie ED, Selak MA, Tennant DA*, et al.* Cell-permeating alpha-ketoglutarate derivatives alleviate pseudohypoxia in succinate dehydrogenase-deficient cells. Molecular and cellular biology 2007;27(9):3282-9.

231. Rathmell WK, Martz CA, Rini BI. Renal cell carcinoma. Current opinion in oncology 2007;19(3):234-40.

232. Yang XJ, Sugimura J, Schafernak KT*, et al.* Classification of renal neoplasms based on molecular signatures. J Urol 2006;175(6):2302-6.

233. Jones TD, Eble JN, Wang M, Maclennan GT, Jain S, Cheng L. Clonal divergence and genetic heterogeneity in clear cell renal cell carcinomas with sarcomatoid transformation. Cancer 2005;104(6):1195-203.

234. Skubitz KM, Zimmermann W, Kammerer R, Pambuccian S, Skubitz AP. Differential gene expression identifies subgroups of renal cell carcinoma. J Lab Clin Med 2006;147(5):250-67.

235. Zhao H, Ljungberg B, Grankvist K, Rasmuson T, Tibshirani R, Brooks JD. Gene expression profiling predicts survival in conventional renal cell carcinoma. PLoS Med 2006;3(1):e13.

236. Bukowski RM, Kabbinavar F, Figlin RA*, et al.* Bevacizumab with or without erlotinib in metastatic renal cell carcinoma (RCC). Journal of Clinical Oncology, 2006 ASCO Annual Meeting Proceedings Part I 2006;24(18S):4523.

237. Motzer RJ, Rini BI, Bukowski RM*, et al.* Sunitinib in patients with metastatic renal cell carcinoma. Jama 2006;295(21):2516-24.

238. Motzer RJ, Michaelson MD, Redman BG*, et al.* Activity of SU11248, a multitargeted inhibitor of vascular endothelial growth factor receptor and platelet-derived growth factor receptor, in patients with metastatic renal cell carcinoma. J Clin Oncol 2006;24(1):16-24.

239. Plas DR, Thompson CB. Akt-dependent transformation: there is more to growth than just surviving. Oncogene 2005;24(50):7435-42.

240. Motzer RJ, Bacik J, Murphy BA, Russo P, Mazumdar M. Interferon-alfa as a comparative treatment for clinical trials of new therapies against advanced renal cell carcinoma. J Clin Oncol 2002;20(1):289-96.

241. Smith JW, Ko Y-J, Dutcher J*, et al.* Update of a phase 1 study of intravenous CCI-779 given in combination with interferon-α to patients with advanced renal cell carcinoma. Journal of Clinical Oncology, 2004 ASCO Annual Meeting Proceedings (Post-Meeting Edition) 2004;22(14S):4513.

242. Mekhail TM, Abou-Jawde RM, Boumerhi G*, et al.* Validation and extension of the Memorial Sloan-Kettering prognostic factors model for survival in patients with previously untreated metastatic renal cell carcinoma. J Clin Oncol 2005;23(4):832-41.

243. Wang JH, Min PQ, Wang PJ*, et al.* Dynamic CT Evaluation of Tumor Vascularity in Renal Cell Carcinoma. AJR Am J Roentgenol 2006;186(5):1423-30.

244. Gollob J, Richmond T, Jones J*, et al.* Phase II trial of sorafenib plus interferon-alpha 2b (IFN-α2b) as first- or second-line therapy in patients (pts) with metastatic renal cell cancer (RCC). Journal of Clinical Oncology, 2006 ASCO Annual Meeting Proceedings Part I Vol 24, No 18S (June 20 Supplement), 2006: 4538 2006;24(18S):4538.

245. Rini BI, Weinberg V, Dunlap S*, et al.* Maximal COX-2 immunostaining and clinical response to celecoxib and interferon alpha therapy in metastatic renal cell carcinoma. Cancer 2006;106(3):566-75.

246. Vignoli GC, Martorana G. Molecular genetics of renal cell carcinoma. Arch Ital Urol Androl 1997;69(4):265-9.

247. Hacker KE, Lee CM, Rathmell WK. VHL type 2B mutations retain VBC complex form and function. PLoS ONE 2008;3(11):e3801.

248. Rathmell WK, Simon MC. VHL: oxygen sensing and vasculogenesis. J Thromb Haemost 2005;3(12):2627-32.

249. Chen F, Kishida T, Yao M*, et al.* Germline mutations in the von Hippel-Lindau disease tumor suppressor gene: correlations with phenotype. Human Mutation 1995;5(1):66-75.

250. Ritter MM, Frilling A, Crossey PA*, et al.* Isolated familial pheochromocytoma as a variant of von Hippel-Lindau disease. Journal of clinical endocrinology and metabolism 1996;81(3):1035-7.

251. Nickerson ML, Jaeger E, Shi Y*, et al.* Improved identification of von Hippel-Lindau gene alterations in clear cell renal tumors. Clin Cancer Res 2008;14(15):4726-34.

252. Banks RE, Tirukonda P, Taylor C*, et al.* Genetic and epigenetic analysis of von Hippel-Lindau (VHL) gene alterations and relationship with clinical variables in sporadic renal cancer. Cancer Res 2006;66(4):2000-11.

253. Rathmell WK, Chen S. VHL inactivation in renal cell carcinoma: implications for diagnosis, prognosis, and treatment. Expert Rev Anticancer Ther 2008;8(1):63-73.

254. Passmore LA, Barford D. Getting into position: the catalytic mechanisms and protein ubiquitylation. Biochemical Society 2004;379:513-25.

255. Megumi Y, Miyauchi Y, Sakurai H*, et al.* Multiple roles of Rbx1 in the VBC-Cul2 ubiquitin ligase complex. Genes to Cells 2005;10:679-91.

256. Kamura T, Sato S, Iwai K, Czyzyk-Krzeska M, Conaway RC, Conaway JW. Activation of HIF1alpha ubiquitination by a reconstituted von Hippel-Lindau (VHL) tumor suppressor complex. Proc Natl Acad Sci U S A 2000;97(19):10430-5.

257. Li L, Zhang L, Zhang X*, et al.* Hypoxia-inducible factor linked to differential kidney cancer risk seen with type 2A and type 2B VHL mutations. Mol Cell Biol 2007;27(15):5381-92.

258. Kondo K, Klco J, Nakamura E, Lechpammer M, Kaelin WG, Jr. Inhibition of HIF is necessary for tumor suppression by the von Hippel-Lindau protein. Cancer Cell 2002;1(3):237-46.

259. Knauth K, Bex C, Jemth P, Buchberger A. Renal cell carcinoma risk in type 2 von Hippel-Lindau disease correlates with defects in pVHL stability and HIF-1alpha interactions. Oncogene 2006;25(3):370-7.

260. Duan DR, Pause A, Burgess WH*, et al.* Inhibition of transcription elongation by the VHL tumor suppressor protein. Science 1995;269:1402-6.

261. Ohh M, Takagi Y, Aso T*, et al.* Synthetic peptides define critical contacts between elongin C, elongin B, and the von Hippel-Lindau protein. J Clin Invest 1999;104(11):1583-91.

262. Hansen WJ, Ohh M, Moslehi J, Kondo K, Kaelin WG, Welch WJ. Diverse effects of mutations in exon II of the von Hippel-Lindau (VHL) tumor suppressor

gene on the interaction of pVHL with the cytosolic chaperonin and pVHL-dependent ubiquitin ligase activity. Mol Cell Biol 2002;22(6):1947-60.

263. Lee CM, Hickey MM, Sanford CA*, et al.* VHL Type 2B gene mutation moderates HIF dosage in vitro and in vivo. Oncogene 2009.

264. Iliopoulos O, Kibel A, Gray S, Kaelin WG, Jr. Tumour suppression by the human von Hippel-Lindau gene product. Nat Med 1995;1(8):822-6.

265. Jiang BH, Zheng JZ, Leung SW, Roe R, Semenza GL. Transactivation and inhibitory domains of hypoxia-inducible factor 1alpha. Modulation of transcriptional activity by oxygen tension. The Journal of biological chemistry 1997;272(31):19253-60.

266. Nickerson ML, Jaeger E, Shi Y*, et al.* Improved identification of von Hippel-Lindau gene alterations in clear cell renal tumors. Clin Cancer Res 2008;14(15):4726-34.

267. Foster K, Prowse A, van den Berg A*, et al.* Somatic mutations of the von Hippel-Lindau disease tumour suppressor gene in non-familial clear cell renal carcinoma. Human molecular genetics 1994;3(12):2169-73.

268. Kondo K, Yao M, Yoshida M*, et al.* Comprehensive mutational analysis of the VHL gene in sporadic renal cell carcinoma: relationship to clinicopathological parameters. Genes Chromosomes Cancer 2002;34(1):58-68.

269. Rathmell WK, Chen S. VHL inactivation in renal cell carcinoma: implications for diagnosis, prognosis and treatment. Expert Rev Anticancer Ther 2008;8(1):63-73.

270. Hu CJ, Iyer S, Sataur A, Covello KL, Chodosh LA, Simon MC. Differential regulation of the transcriptional activities of hypoxia-inducible factor 1 alpha (HIF-1alpha) and HIF-2alpha in stem cells. Molecular and cellular biology 2006;26(9):3514-26.

271. Le Bras A, Lionneton F, Mattot V*, et al.* HIF-2alpha specifically activates the VE-cadherin promoter independently of hypoxia and in synergy with Ets-1 through two essential ETS-binding sites. Oncogene 2007;26(53):7480-9.

272. Sanchez-Elsner T, Botella LM, Velasco B, Langa C, Bernabeu C. Endoglin expression is regulated by transcriptional cooperation between the hypoxia and transforming growth factor-beta pathways. The Journal of biological chemistry 2002;277(46):43799-808.

273. Elvert G, Kappel A, Heidenreich R*, et al.* Cooperative interaction of hypoxia-inducible factor-2alpha (HIF-2alpha) and Ets-1 in the transcriptional activation of vascular endothelial growth factor receptor-2 (Flk-1). The Journal of biological chemistry 2003;278(9):7520-30.

274. Brusselmans K, Bono F, Collen D, Herbert JM, Carmeliet P, Dewerchin M. A novel role for vascular endothelial growth factor as an autocrine survival factor for embryonic stem cells during hypoxia. The Journal of biological chemistry 2005;280(5):3493-9.

275. Alvarez-Silva M, Belo-Diabangouaya P, Salaun J, Dieterlen-Lievre F. Mouse placenta is a major hematopoietic organ. Development (Cambridge, England) 2003;130(22):5437-44.

276. Voss AK, Thomas T, Gruss P. Mice lacking HSP90beta fail to develop a placental labyrinth. Development (Cambridge, England) 2000;127(1):1-11.

277. Guenet JL. Chemical mutagenesis of the mouse genome: an overview. Genetica 2004;122(1):9-24.

278. Anderson LM, Diwan BA, Fear NT, Roman E. Critical windows of exposure for children's health: cancer in human epidemiological studies and neoplasms in experimental animal models. Environmental health perspectives 2000;108 Suppl 3:573-94.

279. Miller MS. Transplacental lung carcinogenesis: molecular mechanisms and pathogenesis. Toxicol Appl Pharmacol 2004;198(2):95-110.

280. Carmeliet P, Dor Y, Herbert JM*, et al.* Role of HIF-1alpha in hypoxia-mediated apoptosis, cell proliferation and tumour angiogenesis. Nature 1998;394(6692):485-90.

281. Covello KL, Simon MC, Keith B. Targeted replacement of hypoxia-inducible factor-1alpha by a hypoxia-inducible factor-2alpha knock-in allele promotes tumor growth. Cancer Res 2005;65(6):2277-86.

282. Williams-Simons L, Westphal H. EIIaCre -- utility of a general deleter strain. Transgenic Res 1999;8(4):53-4.

283. Kearney JB, Kappas NC, Ellerstrom C, DiPaola FW, Bautch VL. The VEGF receptor flt-1 (VEGFR-1) is a positive modulator of vascular sprout formation and branching morphogenesis. Blood 2004;103(12):4527-35.

284. Mansfield KD, Guzy RD, Pan Y*, et al.* Mitochondrial dysfunction resulting from loss of cytochrome c impairs cellular oxygen sensing and hypoxic HIF-alpha activation. Cell metabolism 2005;1(6):393-9.

285. Abramoff MD, Magelhaes PJ, Ram SJ. Image Processing with ImageJ. Biophotonics International 2004;11(7):36-42.

286. Gordan JD, Lal P, Dondeti VR*, et al.* HIF-alpha effects on c-Myc distinguish two subtypes of sporadic VHL-deficient clear cell renal carcinoma. Cancer Cell 2008;14(6):435-46.

287. Whitaker GB, Limberg BJ, Rosenbaum JS. Vascular endothelial growth factor receptor-2 and neuropilin-1 form a receptor complex that is responsible for the differential signaling potency of VEGF(165) and VEGF(121). The Journal of biological chemistry 2001;276(27):25520-31.

288. Bautch VL, Redick SD, Scalia A, Harmaty M, Carmeliet P, Rapoport R. Characterization of the vasculogenic block in the absence of vascular endothelial growth factor-A. Blood 2000;95(6):1979-87.

289. Kearney JB, Ambler CA, Monaco KA, Johnson N, Rapoport RG, Bautch VL. Vascular endothelial growth factor receptor Flt-1 negatively regulates developmental blood vessel formation by modulating endothelial cell division. Blood 2002;99(7):2397-407.

290. Roberts DM, Kearney JB, Johnson JH, Rosenberg MP, Kumar R, Bautch VL. The vascular endothelial growth factor (VEGF) receptor Flt-1 (VEGFR-1) modulates Flk-1 (VEGFR-2) signaling during blood vessel formation. Am J Pathol 2004;164(5):1531-5.

291. Carmeliet P, Ferreira V, Breier G*, et al.* Abnormal blood vessel development and lethality in embryos lacking a single VEGF allele. Nature 1996;380(6573):435-9.

292. Ferrara N, Carver-Moore K, Chen H*, et al.* Heterozygous embryonic lethality induced by targeted inactivation of the VEGF gene. Nature 1996;380(6573):439-42.